Characterization of Conical and Elliptical Fuel Spray Nozzles using Non-Intrusive Laser Diagnostic Methods

KHALID KORAITEM

A Thesis

In

The Department

Of

Mechanical and Industrial Engineering

Presented in Partial Fulfillment of the Requirements

For the Degree of Master of Applied Science (Mechanical Engineering) at

Concordia University

Montreal, Quebec, Canada

July 2011

CONCORDIA UNIVERSITY

School of Graduate Studies

This is to certify that the thesis prepared

By: Khalid S. Koraitem

Entitled: Characterization of Conical & Elliptical Fuel Spray Nozzles using Non-intrusive Laser Diagnostic Methods

and submitted in partial fulfillment of the requirements for the degree of

Master of Applied Science (Mechanical Engineering)

complies with the regulations of the University and meets the accepted standards with respect to originality and quality.

Signed by the final examining committee:

Dr. Hoi Dick Ng _____ Chair

Dr. Lyes Kadem _____ Examiner

Dr. Amir G. Aghdam_____ Examiner

Dr. Ali Dolatabadi _____ Supervisor

Approved by _____

Chair of Department or Graduate Program Director

_____

Dean of Faculty

Date _____

Abstract

Characterization of Conical and Elliptical Fuel Spray
Nozzles using Non-Intrusive Laser Diagnostic Methods
Khalid Koraitem

Spray nozzles and atomizers have several applications in many forms of industry such as aerospace, automotive, combustion, pharmaceutical, and spray coating industries. These nozzles vary in design and performance depending on the application they are used in. Nevertheless, the primary objective for all atomizers is to disperse liquids in a controlled and uniformed manner while minimizing the amount of energy needed in the breakup process to achieve high quality atomization.

Air-assist and air-blast atomizers are fuel injector nozzles commonly used in gas turbine engines in the aerospace, and power generation industries. The flow in these atomizers is considered to be two-phase flow since a portion of air taken from the compressor is also used to assist in the breakup of the fuel inside the combustion chamber. These nozzles play a critical role in determining the efficiency of gas turbine engines as their ability to disperse liquid fuel into fine droplets allows for better mixture and evaporation rates; therefore, improving engine performance, reducing emissions, and maximizing fuel efficiency.

The objective of this study is to experimentally analyze two gas turbine fuel injector nozzles. The first nozzle is a standard hollow cone nozzle currently used in gas turbine engines, whereas the other is a hollow elliptical nozzle designed to offer greater control over fuel distribution as well as improve overall atomization. The nozzles are investigated under varying gas to liquid ratios (GLR) where key spray parameters such as droplet diameter, velocity, volume flux, as well as spray angle are measured to characterize the nozzles using methods such as Shadowgraph, Optical Patternation, Phase Doppler Particle Analyzer (PDPA), and Particle Image Velocimetry (PIV).

Acknowledgments

This thesis would not have been possible without the support and guidance of several individuals who have contributed their time and effort in the preparation and completion of this study.

First I would like to thank Dr. Ali Dolatabadi, his moral support and inspiration was instrumental in guiding me through the obstacles and hurdles in the completion of this research work.

Second, I thank my friends and colleagues Hadi Alaee, Jordan Lafrenière, Mohsen Najafi, Ehsan Farvardin, Percival Graham, and everyone else from the Multiphase Flow Laboratory at Concordia University for putting in the time and effort in assisting me in this study. Many thanks to Jeff Verhiel and John Hu at Pratt & Whitney Canada for giving me the opportunity to work on this project. I would also like to extend my gratitude to Dan Troolin and Tyson Strand at TSI inc. for their support in overcoming technical issues encountered throughout this study.

A great deal of gratitude goes out to my parents for their hard work in razing me and guiding me from to achieve my goals, as well as teaching me the values of honesty, integrity, and self respect.

In addition, I would like to express my sincere gratitude to His Majesty King Abdullah Bin Abdul Aziz, and members of the Saudi Arabian Cultural Bureau in Ottawa for supporting me and other fellow students throughout my graduate studies.

Table of Contents

List of Figures

Notations

D	diameter
GLR	Gas to Liquid mass flow Ratio
m	mass
t	time
V	volume
PMT	Photo Multiplier Tubes
SMD	Sauter Mean Diameter
F	Volume Flux

Greek letters

θ	Phase angle
μ	Dynamic viscosity
ρ	Density

Subscripts and superscripts

g	gas
l	liquid

1. Introduction

1.1. Background & Motivation

Atomization is a surface dispersion process in which a bulk liquid such as a jet or sheet is disintegrated into small droplets, by the kinetic energy of the liquid itself or by exposing the liquid to high gas velocities, or through mechanical energy by means of rotation or vibration. In our world, atomization is found and applied in many forms of nature itself and industry. For example, sprays may be found in nature such as water falls, rain, mist, or ocean sprays caused by the crashing of waves against rocky seashores. The industrial application of atomization is vast and extensive where sprays are considered commonplace if not crucial to the industry they are used in. Typical applications of the atomization process may be found in industries such as the aerospace, automotive, agriculture, and pharmaceutical. (1)

Sprays may be used in agricultural industry for the purpose of spreading water or chemical pesticides over farm crops. They are also used for coating processes such as painting, or as part of corrosion prevention in which sprays are used to uniformly apply a protective layer over materials that are sensitive to the ambient environments they are used in. Atomization is also used extensively in combustion engines and plays a vital role in the process where virtually every type of combustion engine is dependent on some method of spray atomization. A few general applications of spray atomizers are show in Figure 1. (1)

(a)

(b)

(c)

(d)

(e)

Figure 1: Examples of spray atomizer applications such as (a) Agricultural Spraying (b) Drug Coating (c) Diesel spray injector (d) Fire sprinkler system (e) A P&W JT15D Turbofan engine (2)

There is also a growing worldwide effort to reduce overall fuel consumption and improve energy efficiency in many industrial applications. The aerospace industry has been a leader in a drive towards meeting and exceeding strict environmental standards set out by federal regulators such as the International Civil Aviation Organization (ICAO) (3) (4) (5). Therefore more research and development has focused on ways to improve the method of distributing fuels within a gas turbine engine's combustion chamber.

A typical gas turbine engine operation such as the one shown Figure 2 forces air through a series of compressors where pressure and temperature begin to rise. Most of the compressed air is then taken into a combustion chamber similar to the one shown in Figure 3, where fuel is injected into the chamber in a highly turbulent environment in order to allow the air and fuel to properly mix. The mixture in the chamber is then lit with an igniter which causes the fuel air mixture to burn releasing a great deal of thermal energy. The thermal energy caused by the combustion is then converted to kinetic energy using turbines at the end of the engine where part of the turbine's kinetic energy is used to drive the compressor and the remaining is accelerated out to the ambient environment through the exhaust in order to create thrust.

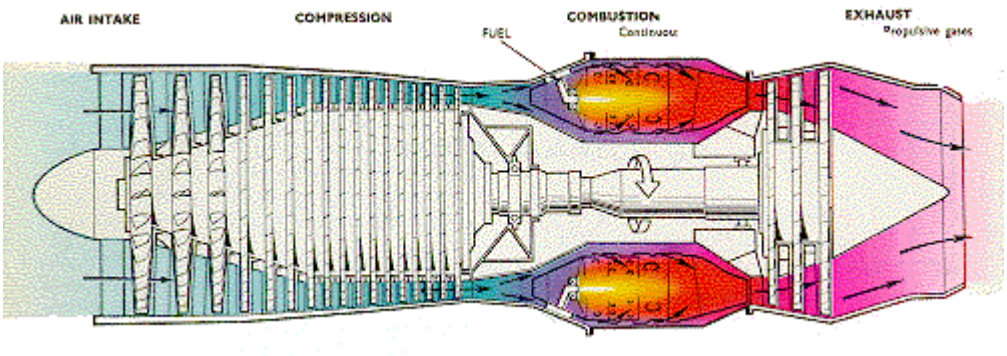

Figure 2: An example of a gas turbine engine (turbojet) (6)

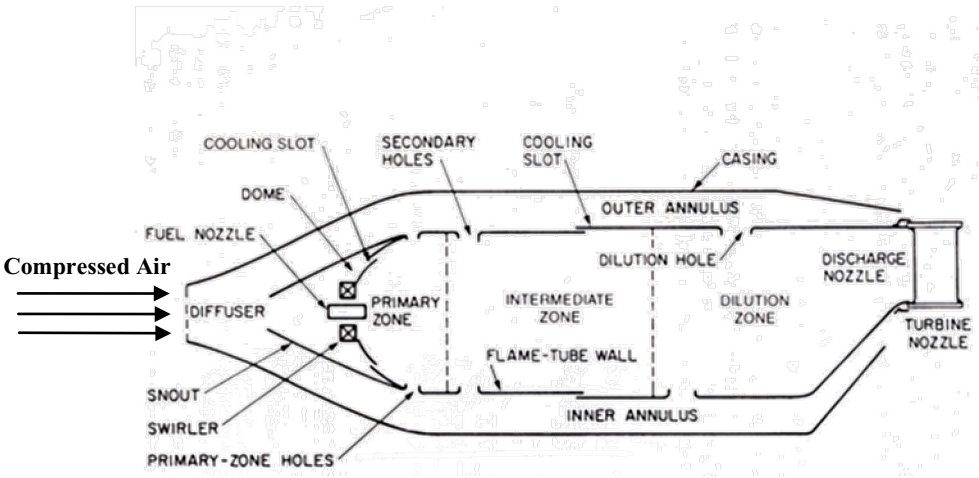

Figure 3: Diagram of a gas turbine combustion chamber. Air enters the chamber from the compressor via the diffuser, while fuel enters through the injector and mixes with the surrounding air. (7)

Courtesy of Hemisphere Publishing Corp.

An area of particular importance in ensuring optimal combustion efficiency lies within the way fuel is injected into the combustion chamber. Fuels used in gas turbine engines are liquids that must be converted into small fine droplets when entering the combustion zone. The main principal to this process is to produce a high surface to mass ratio of liquid fuel so that better evaporation rates are obtained resulting in improved performance in the engine, fuel efficiency, as well as reduction of emissions (7). Several types of fuel spray atomizers used in combustion applications are discussed in this study; however a general understanding of atomization fundamentals are first described.

Since the application of sprays is extensive, it is natural to assume that several types of spray atomizers need to be designed according to the different applications they are used in. The simplest form of spray atomizer that has been extensively studied and analyzed is the plain orifice atomizer. A simple circular hole is used to inject liquid into the surrounding gas environment where the liquid's own pressure is converted into kinetic energy to drive the

breakup process in creating small droplets. A general schematic of plain orifice atomizers is shown in Figure 4.

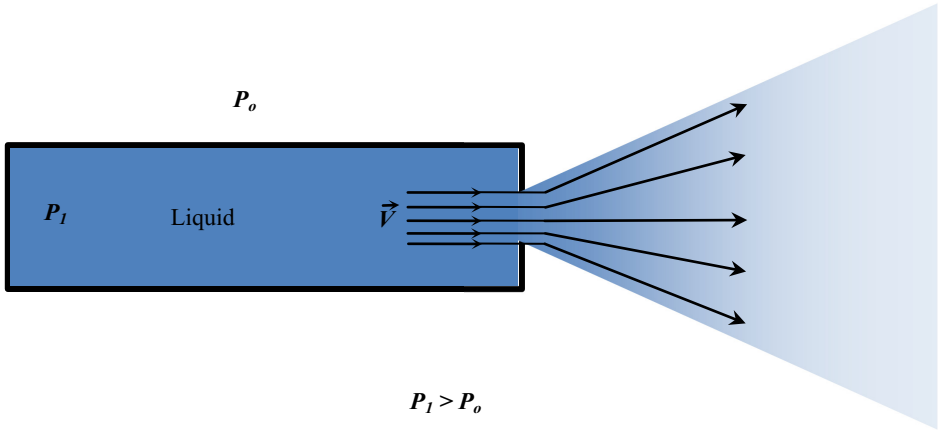

Figure 4: A simple orifice atomizer in which the kinetic energy of the liquid is the driving force behind the breakup

Lord Rayleigh first developed the fundamental theory to liquid jet breakup in simple orifice nozzles such as this and categorized the different breakup regimes for liquid jets exiting simple circular orifices (8). In his experiments Rayleigh identified surface tension as the driving force behind liquid breakup at low flow rates such as the flows seen in Figure 5. The surface tension force is the liquid's tendency to maintain energy conservation. When a liquid jet leaves a circular orifice, perturbations create disturbances in the liquid jet causing it to oscillate. At the same time however, surface tension attempts to pull back on the liquid resulting in liquid breakups seen in (a) and (b). Higher jet velocities in (c) and (d) are known as first and second wind induced sprays, where liquid turbulence and aerodynamic forces begin to have greater influence on the breakup of the liquid. (9)

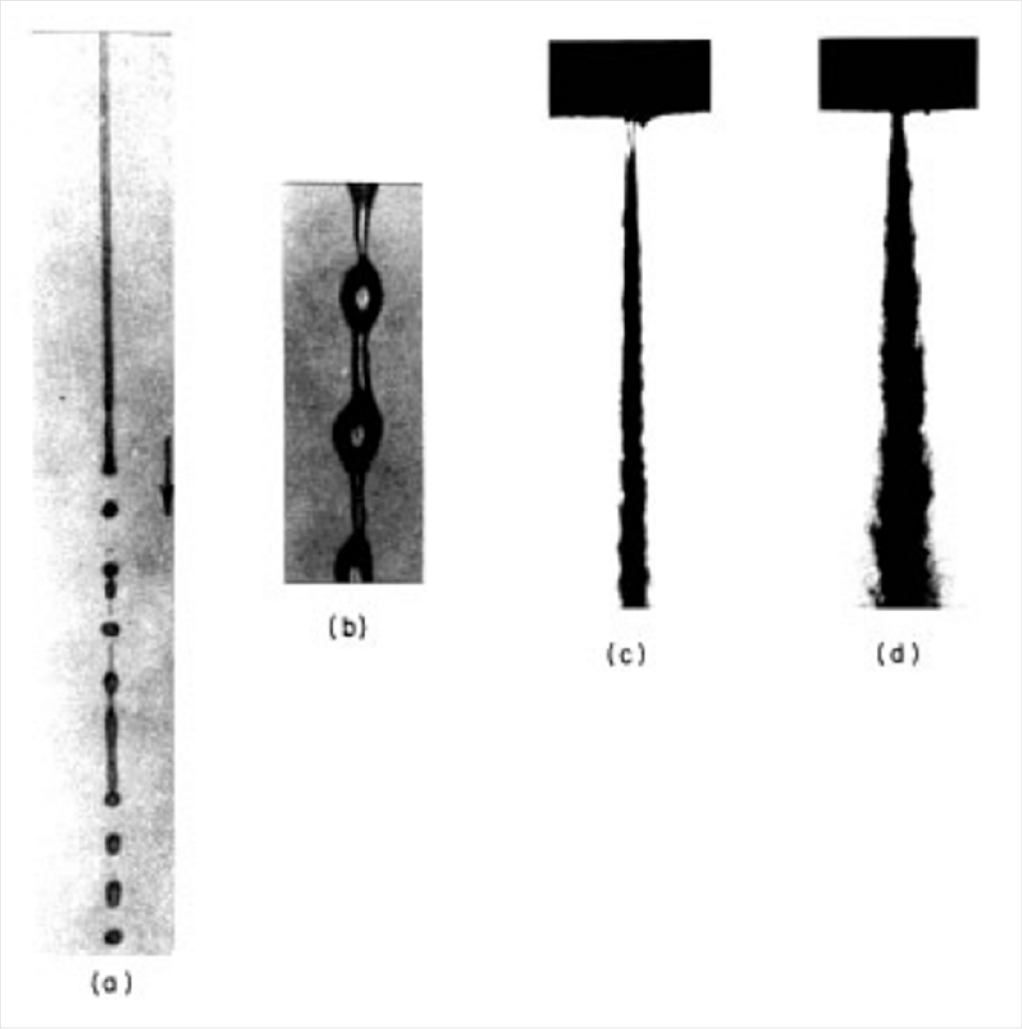

Figure 5: Breakup regimes for plain orifice atomizers (a) Rayleigh breakup, (b) First wind induced, (c) Second Wind induced, (d) Full atomization (9)

Generally with plain orifice atomizers, fine atomization is achieved when the orifice diameter is made as small as possible and the flow rate is as high as possible. This however is considered impractical in most applications due to the increased likelihood of blocking the orifice with debris or particles when using small diameters, as well as limitations on how much pressure can be provided to the atomizer (10). Therefore, other types of atomizers where developed in order to cope with the shortcomings of simple orifice atomizers. Two of the more commonly used atomizers are discussed in the following section.

1.2. Swirl Atomizers

Swirl atomizers use internal tangential slot or plates to impose a centrifugal acceleration onto the liquid as it leaves through an annulus which causes breakup to occur more readily than in simple orifice atomizers. Figure 6 shows some of the basic designs used in swirl atomizers.

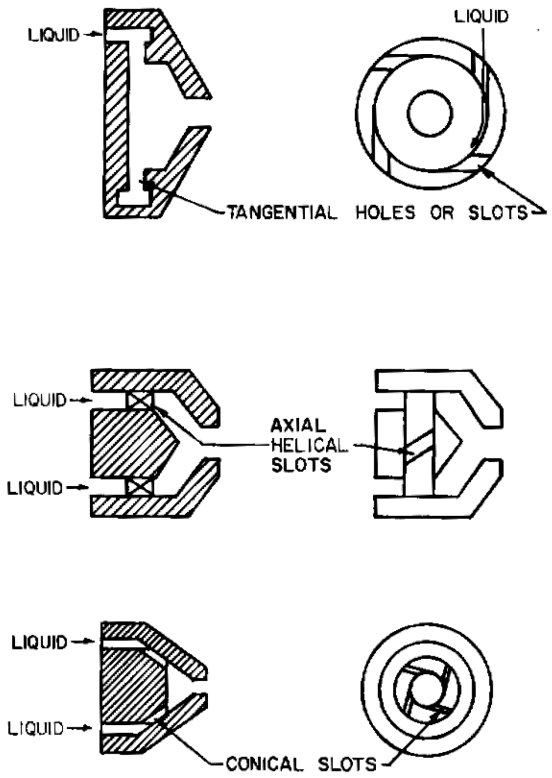

Figure 6: Common swirl atomizer designs (10)

Courtesy of Hemisphere Publishing Corp.

The centrifugal acceleration causes the spray to take on a hollow cone shape rather than the solid cone shapes seen in simple orifice atomizers. In this matter, swirl atomizers are more efficient since the centrifugal acceleration causes the liquid sheet to breakup more readily than in simple orifice designs. This means that less injection pressure is required to achieve the same level of atomization. The centrifugal acceleration in swirl atomizers also allows for better radial distribution than simple orifice atomizers.

The hollow cone spray is known to have a unique development when increasing liquid flow rates from zero and goes through several stages as shown in Figure 7. The figure shows how the hollow cone spray first begins in the dribbling stage in (a) at very low pressures, where surface tension alone causes the liquid to neck and break up into a drop. At higher injection pressures (i.e. higher flow rates) such as in (b), the liquid takes on a closed cone or onion like shape. The tangential slots the impose a centrifugal acceleration onto the liquid causing it to spread out into a hollow cone shape; however the kinetic energy of the liquid is still not strong enough to overcome the surface tension forces that pull back on the liquid resulting in the onion like shape. In (c) the flow rate is further increased causing the liquid to take on a tulip shape where a clear liquid sheet is now visible, and perforated holes due to disturbances begin to appear. At the final stage in Figure 7 (d), the increased kinetic energy of the spray begins to overcome the effects of surface tension where full atomization is achieved. At this point the liquid sheet is experiencing wave instabilities caused by other factors that oppose surface tension. These wave instabilities cause the liquid to breakup into small ligaments which then undergoes secondary atomization where spherical droplets are formed.

The appearance of waves within the liquid sheet is the result of sheering caused by the difference in velocity, density, and other properties of the exiting fluid and the surrounding ambient fluid (i.e. gas). This wave sheering effect is known as the Kelvin-Helmholtz Instability, and is a fundamental theory in determining liquid sheet breakup characteristics, which in turn also relates to droplet formation and their sizes (8) . Recent work by Martottant and Villermau (11) showed that liquids under the influence of the Kelvin-Helmholtz instability produce waves whose wavelengths are controlled and proportional to the boundary layer thickness of the gas flowing parallel to a liquid jet.

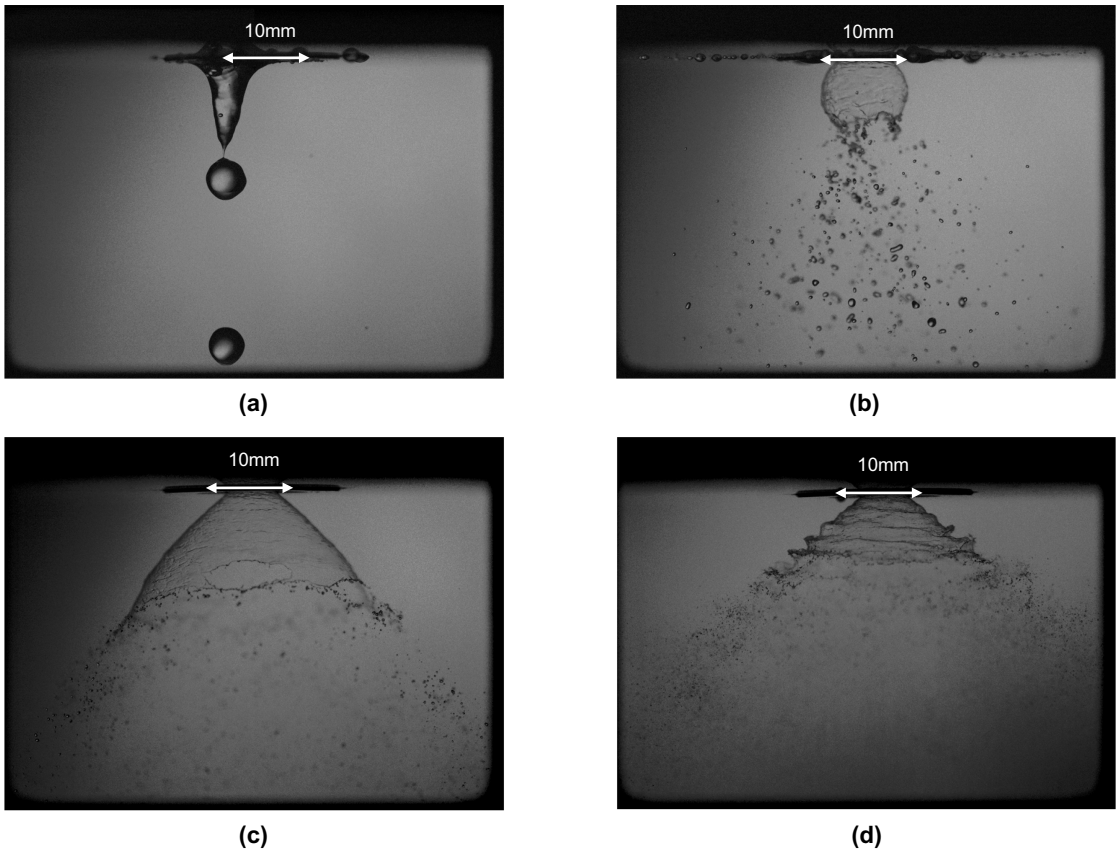

Figure 7: Swirl atomizer development as liquid flow rate is increased from (a) dribble stage, (b) onion stage, (c) tulip stage (d) fully developed spray

One drawback to swirl atomizers is that their flow rate is dependent on the square root of the liquid's injection differential pressure; therefore, a doubling of the flow rate would require four times higher injection pressures. Another disadvantage to swirl atomizer is that they can cause soot formation and poor combustion quality since part of the spray is still intact in a liquid sheet (10). One way to overcome this problem is by using other sources to assist in the breakup of the liquid sheet cone. This then lead to the creation of the air-assist or air-blast atomizer.

1.3. Air-blast atomizers

The atomizers used in this study are referred to as air-blast atomizers because they are built to use high volume flow rates of gas to further assist in the breakup of liquids. These nozzles should not be confused with air-assist atomizers although they do share many similarities. The main difference between an air-assist atomizer and an air-blast atomizer is that the latter uses far more gas flow to breakup liquids. Air-blast atomizers are extensively used in aircraft engines for the many advantages they have over other spray atomizers. There are various subcategories of air-blast atomizers that use different configurations and methods of dispersion such as the ones displayed in Figure 8. However, one commonly used type of air-blast atomizer uses a similar liquid swirl atomizer configuration coupled with an air swirler to further assist in the breakup process.

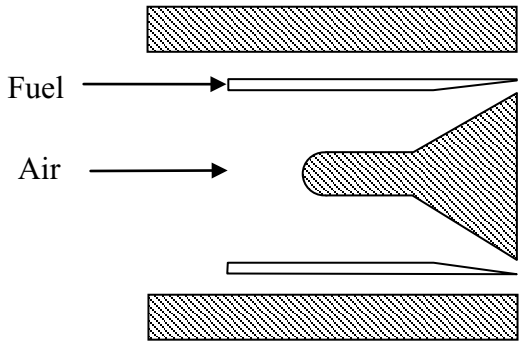

Figure 8: Common air-blast atomizer design configuration

One of the defining advantages of air-blast atomizers is their ability to be used in high gas pressure environments. This makes them ideal for aircraft gas turbine engines as these nozzles require vast amounts of air flow rate that is readily available and abundant. Generally, a portion of air is taken from the engine's compressor and used to assist in the atomization of the fuel. The air is then injected back into the combustion chamber with the fuel along with the original air from the compressor stage. In this case, the air is not

considered to be wasted since it will be remixed in the combustion chamber before ignition. In addition, air-blast atomizers offer very fine sprays and much more thorough mixtures with air and fuel resulting in a highly efficient combustion, which in turn reduces soot and exhaust smoke (7).

Some air-blast atomizers have geometrical designs similar to pressure swirl atomizers in which a hollow cone spray pattern appears when no air is being used to assist in the atomization. Figure 9 shows the swirl atomizer that was previously presented in Figure 7; however, air has been added to assist in the breakup process.

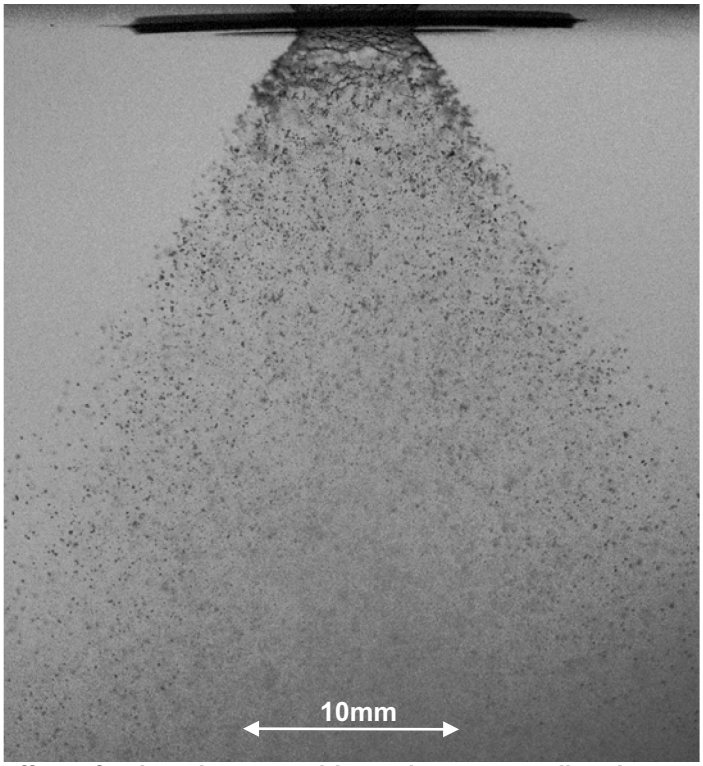

Figure 9: The effect of using air on a swirl atomizer causes disturbances to the hollow cone spray that offer better atomization than simple swirl atomizers

The characteristics that cause the air-blast atomizer to take on these shapes are discussed in the following section of this study. In addition, tests on air-blast atomizer nozzles have shown volume distributions in which two peaks appear to correspond to the higher liquid

concentrations near the edge of the spray that makes up the hollow cone structure. Other tests have shown that once air is added to the swirl atomizer, the liquid distribution narrows and contracts. This characteristic will be addressed in the upcoming results section of this study (10).

1.4. Spray Characteristics

The atomization process in gas turbine engines is achieved by injecting liquid fuel into a thin sheet where instabilities are induced to promote breaking the liquid into smaller droplets. Sheet spraying may be achieved through specially shaped passages, injection through narrow slots, spreading over metal plates, and other methods. In either case, the end result is to distribute the liquid fuel into the combustion zone in a controlled manner. Therefore, it is necessary to study and understand the key spray characteristics that define gas turbine fuel spray nozzles.

Sheet Breakup

Certain types of spray nozzles inject liquid into the ambient environment by imposing a centrifugal acceleration onto the liquid causing the spray to take on the shape of a thin hollow cone sheet. The liquid sheets themselves disintegrate into ligaments which turn into smaller droplets, and there are three main types of sheet breakups that have been studied. The three types of sheet disintegration are rim, perforated, and wave sheets.

In rim breakup, surface tension forces cause the liquid at the edge of the sheet to contract into a thick rim which then breaks up in a manner similar to what was seen in Rayleigh's experiments. This type of sheet breakup is associated with liquids that have high viscosities and surface tensions and result in large droplets followed by smaller satellite droplets. In

perforated mode, holes begin to appear within the sheet itself where the holes expand rapidly and coalesce with other holes resulting in ligament breakup and drops of varying sizes such as what was seen earlier in Figure 7 (c). In wave mode, the instability of the liquid sheet itself causes it to oscillate in which breakup may occur at half or full wavelengths similar to what was seen in Figure 7 (d). The wave is partially the result of surface tension forces causing the liquid to contract rapidly; however other factors may even include disturbances such as the ambient gas environment or even turbulence within the liquid itself. The combination of all these sources of instability are studied and referred to as the Kevin-Helmholtz instability (12). Furthermore, one characteristic of wave breakup is that the drop size distribution tends to vary due to the instability of the waves.

Mean Drop Size & Distribution

In gas turbine engines it is important to calculate the evaporation rates of atomizers as part of determining atomizer performance. In order to do so, it is necessary to obtain droplet diameters which are statistically determined by taking significant sample measurements of data and obtaining an overall mean diameter size. One such statistical parameter that is widely used in sprays is the Sauter Mean Diameter (SMD). The SMD is calculated as the diameter of a drop having the same volume to surface ratio as the entire spray itself as depicted in equation 1

$$\mathbf{SMD} = \frac{\sum \boldsymbol{nD^3}}{\sum \boldsymbol{nD^2}} \qquad 1$$

Diameter measurements can be achieved using non-intrusive methods such as Phase Doppler Particle Analyzers (PDPA) that uses laser beams and the concept of phase Doppler shifts to determine the size of a droplet passing through the beam at localized points within the spray. The details of PDPA are discussed later in the experimental setup. Another important parameter in atomizers is to know the extent at which sprays disperse liquids. The advantage of good dispersion is that it allows for better mixing of fuels with the surrounding gas which in turn lead to better evaporation rates. In addition to mean droplet size; spray angle and penetration also govern the liquid dispersion.

Penetration

Penetration is defined as the maximum distance a spray reaches when injected into still air. The two primary forces responsible for penetration are the kinetic energy of the spray itself and the aerodynamic forces of the surrounding gas. Knowing the penetration depth of a spray is very important especially when using relatively small combustion chambers. Excessive penetration would cause fuel to deposit onto the chamber walls resulting in inadequate and incomplete burning of the fuel (10).

In most cases, the initial velocity of the spray is high and the trajectory of the droplets is dictated by their own momentum. However, the velocity magnitude of the spray and its droplets quickly begin dissipating due frictional losses with the surrounding gas. Once the droplets lose their kinetic energy their trajectory is then governed by the movement of the surrounding gas and gravity.

Cone Angle

As mentioned earlier, dispersion is an important characteristic of spray atomizers and knowing the spray cone angle of an atomizer further enhances one's understanding of dispersion. They are also of particular importance in combustion chambers as they have strong influences on pollutant emissions. There is no set standard for measuring spray cone angles as there are difficulties in determining the boundaries of the spray. Many atomizers also have liquid sheets that are curved and unstable rather than straight and most practical application of atomizers operate under high pressure and momentum causing the atomization of the liquid to occur almost instantly resulting in a silhouette of liquid droplets with no clearly defined boundaries. For this study shadowgraph photography is used to capture still images of the spray angle. The details of this method are explained later in the experimental setup.

Patternation

Patternation is another parameter linked to a spray nozzle's ability to disperse liquid. In this case, the symmetry of the cross sectional spray pattern itself is of importance. Clogged or malfunction sprays can lead to poor performance in sprays. In turbine combustors, symmetric sprays are important because uniformly distributed fuel can have a direct effect in obtaining high efficiencies, reduced pollutant and longer turbine blade life (13) (14) (15). More importantly, patternation is used to give researches a visual understanding of the spray's cross sectional profile. Methods of determining spray patterns include mechanical and optical patternation which is discussed later in this study.

1.5. Objective

The objective of this study is to conduct an experimental analysis on two types of air-blast atomizers used in aircraft gas turbine engine. One is a standard hollow cone air-blast atomizer and the other is a hollow elliptical atomizer. The study uses tools and methods such as Shadowgraph, Optical patternation, PIV, and PDPA to characterize and compare both nozzles in order to asses the performance of the elliptical spray the commonly used conical spray. The outline of this study is as follows

- Chapter 2 discusses the equipment and operating conditions used in this study. An overview of the nozzles used and their differences are discussed. The chapter also covers details on the experimental methods used in this study. Details on their conceptual use and how they are implemented in this study are discussed. The methods include Shadowgraph, Optical Patternation, Phase Doppler Particle Analyzer (PDPA), and Particle Image Velocimetry (PIV).
- In Chapter 3, validation of the experimental methods and results are discussed. Information on possible sources of error is addressed along with methods of reducing and eliminating error is described.
- Chapter 4 presents the experimental results of both nozzles. First, data from the conical spray nozzle is presented as a benchmark to compare with the elliptical nozzle. The data is presented in the same order used in Chapter 2. The elliptical spray results are also presented in a similar manner. The chapter ends with a one-to-one direct comparison of the spray nozzles where results will show that the elliptical spray exhibits better atomization quality

through improved distribution of the spray flow; whereas, the conical spray exhibits better penetration.

- In Chapter 5, a summary of the works conducted for this study and conclusions on the obtained results are discussed. The chapter will also discuss suggestions for future works and methods that may help improve the analysis based on the current results.

2. Experimental Setup

2.1. Nozzle Apparatus & Tools

The approach taken for this study looks at comparing two different air-blast swirl atomizers. The first nozzle is a standard air-blast atomizer that is commonly used in gas turbine engines. Both the liquid and air make use of internal slots to impose centrifugal accelerations on the fluids resulting in a hollow cone spray. The purpose of testing the nozzle is to gather experimental data that may be used as a benchmark to compare its performance with other experimental nozzles, and is therefore referred to as the "conical" nozzle. The second nozzle is an asymmetric nozzle designed to offer greater distribution in one direction than the other and is referred to as the elliptical nozzle. The elliptical nozzle is referred to it as such because it is an air-blast atomizer that also sprays in a hollow cone profile; however, this nozzle incorporates a different design feature where the air injector used to assist in the atomization of the liquid forces the spray to take on more of a hollow elliptical pattern rather than a typical hollow circular pattern. The ability to control the spray's distribution is due to the unique air holes that cause the hollow cone nozzle to contract in one direction while increase in the other. Due to the proprietary nature of the work, details on the nozzle designs themselves are withheld. Nevertheless, Figure 10 shows a simple schematic representation of the asymmetric nozzle and how it alters the hollow cone spray.

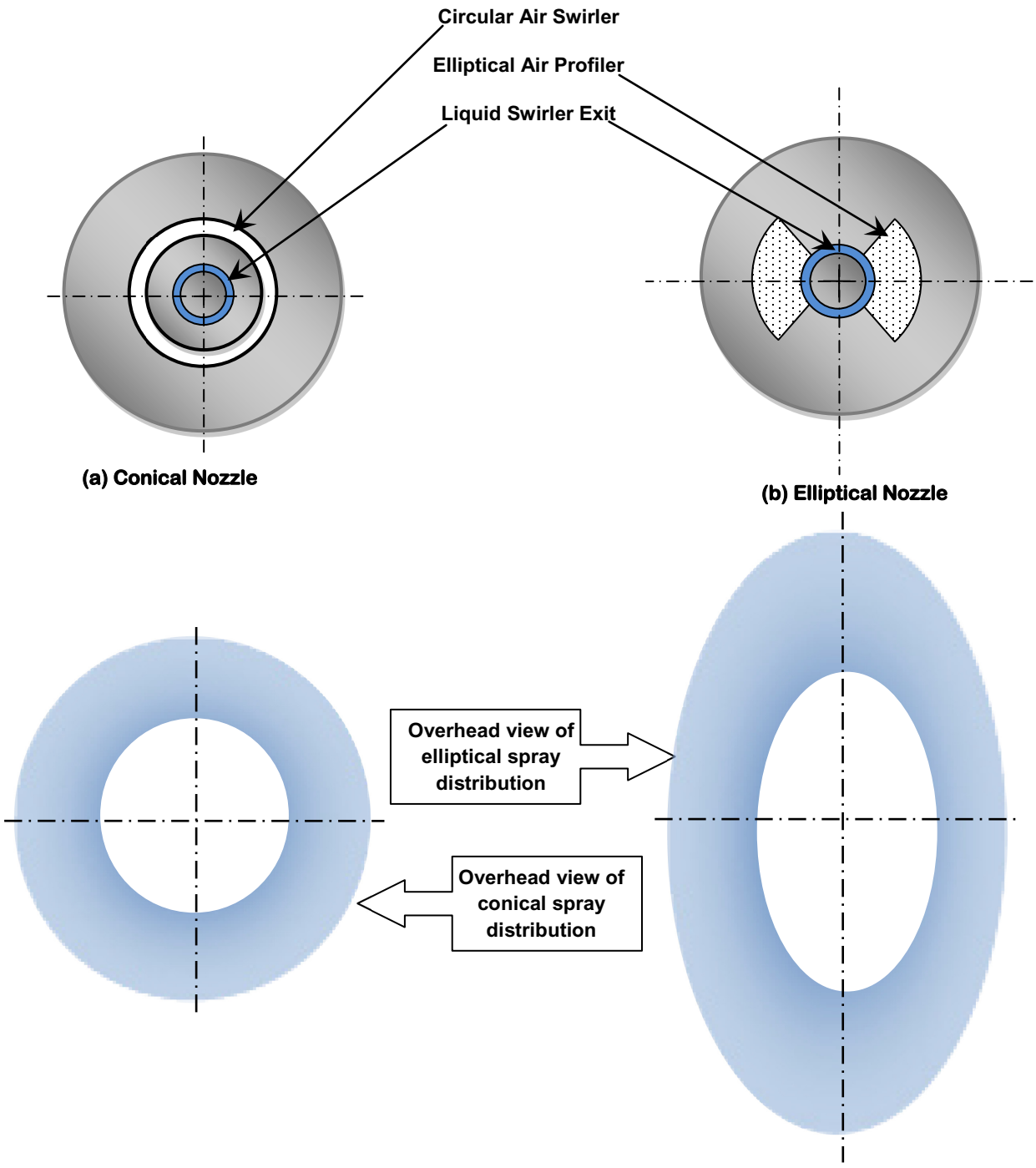

Figure 10: Schematic representation of asymmetric nozzle showing the effect air has on the cross sectional spray pattern

As mentioned earlier, the liquid of the elliptical nozzle exits the nozzle via tangential swirlers that are located within the nozzle's structure through an annulus orifice that has a hydraulic diameter $D_o = 5.7mm$. The air exit is also composed of two sections. One section is an air annulus exit designed to cause a tangential swirl to the air itself as it exists the nozzle and is referred to as the *gas swirler*. The other air injection section known as the *profiler* is the primary driving force behind the nozzle's elliptical pattern. Perforated holes are strategically placed so that the air imposes an aerodynamic force on the liquid spray that causes it to contract in one axis and expand in another axis, resulting in a hollow ellipse with a major and minor axis. The types of fluids used in this study and their respective properties and operating conditions are discussed in following section.

2.2. Fluid Operating Parameters and Properties

The testing fluids used were distilled water as the primary liquid source and air supplied externally to the laboratory through the building's air supply system where it is brought to ambient conditions. **Table 1** shows the general properties of both fluids used in the experiments.

Table 1: Testing fluid properties for air and water

	Distilled Water	Air
T (°C)	20	20
ρ (kg/m^3)	998	1.20
μ (N.s/m^2)	1.002×10^{-3}	1.98×10^{-5}
σ (N/m)	7.34×10^{-2} (water-air contact)	

With most air blast atomizers it is the air that plays a dominant role in determining the performance and behavior of the spray profile. Therefore, both nozzles were operated at constant liquid flow rates of 30.5 lb/hr of distilled water and had the air flow varied according to the volume flow rate measured in the system. The air flow is varied from 0 to 16 ft^3/min of air which is the nominal design condition for the conical nozzle. The variation of air flow is tabulated and converted to a mass based gas-to-liquid ratio ($GLR = \dot{m}_g/\dot{m}_l$) in Table 2. Details on the flow metering devices are shown in Appendix A. In the following section, experimental methods used to analyze the sprays are discussed.

Air Flow Rate (SCFM)	No Air	5	10	16
GLR	0	0.75	1.47	2.35

Table 2: List of various air flow rates used to test both baseline and asymmetric nozzles

2.3. Shadowgraph

Shadowgraph is a background illuminating photographic method used to capture detailed images of spray flows that reveal more detail than conventional photography. In most cases, the spray flow is moving at velocities that are far too great to capture in conventional camera setup because the continuous ambient light illumination results in blurred or streaked images. To overcome this effect, an image is taken by illuminating the background with a stroboscopic light source that is synchronized to the camera's capture settings. In this study, the strobe light source is high repetition rate (14.5 Hz) Nd:YAG laser. The laser light flashes onto a light diffuser as presented in the schematic of Figure 11. The laser's optics is modified to emit a laser cone. The laser cone shape is created by having two cylindrical lenses placed behind each other while having their longitudes at 90° angles. Normally, a

single cylindrical lens is used to collimate light into a sheet which may be horizontal or vertical. On the other hand, placing two cylindrical lenses back to back while keeping their longitudinal axis at 90° would cause light to collimate in both directions creating a diffused laser cone.

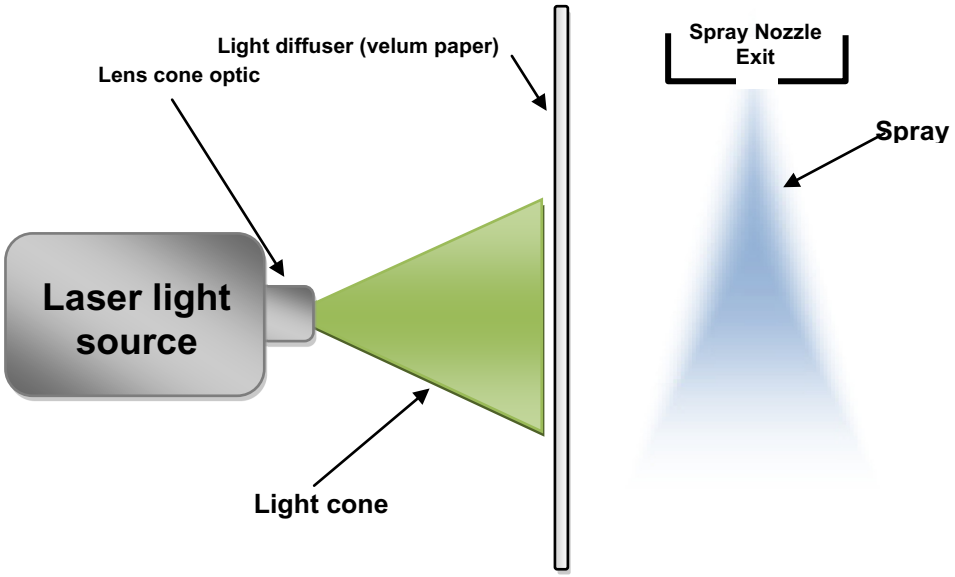

Figure 11: Shadowgraph setup in which background is illuminated using a stroboscopic light source

The laser cone illuminates the background and gives a sharply contrasted image of the spray revealing details such as wave instabilities, ligaments, and droplets that are not seen by the naked eye. Figure 12 is a sample shadowgraph image of the conical spray that will be discussed in detail later on.

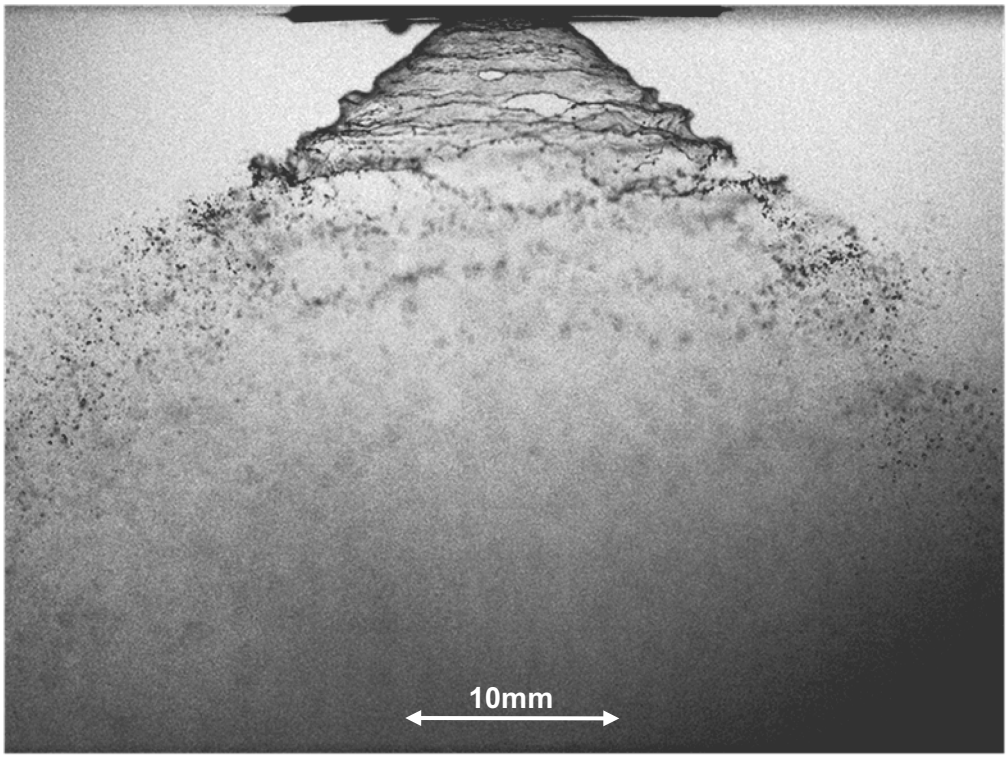

Figure 12: A sample shadowgraph of the conical spray

2.4. Optical Patternation

Optical patternation is a laser based photographic method used to obtain horizontal cross sectional images of spray patterns. Optical patternation is considered as a non-intrusive form of mechanical patternation where spray distribution patterns are determined by the volume of liquid accumulated in tubes placed at specified heights below the spray nozzle. The development of optical patternation came as a result of the disadvantages of mechanical patternation. First, mechanical patternation is intrusive since the accumulating tubes are directly obstructing the spray flow's natural path and would alter the intended spray flow pattern. The second disadvantage of mechanical patternation is the lack of spatial resolution where the size of the accumulating tubes may not yield enough information about liquid concentrations with sufficient detail.

Optical patternation on the other hand is considered to be non-intrusive and posses good spatial resolution. The reason for these advantages is because optical patternation uses mie-scattering laser light to illuminate the cross-sectional spray pattern without interfering in the natural flow of the spray. Over the years, several works have used optical patternation as a reliable method in evaluating spray performance and characteristics (16) (15) (17).

Figure 13 shows how the optical patternation system is set up. The PIV's YAG laser has its optics setup to fire a horizontal laser sheet. Any liquid from the spray that intersects the laser sheet is illuminated and captured by a CCD camera. The CCD camera is oriented at an angle since capturing images from the top or bottom is not practical due to the visual obstruction of the nozzle and testing apparatus. Naturally, any images captured at an angle will be distorted; therefore, a de-warping algorithm that corrects the distortion caused by the angular placement of the camera is used. A sample image of circular spray profile is shown in Figure 14 (a) taken at an angle of approximately 45°. Note that capturing the image at such an angle causes the image to distort and appear elliptical. However, once the de-warping algorithm is implemented, the image is corrected and shows the true spray pattern to be circular as in Figure 14 (b).

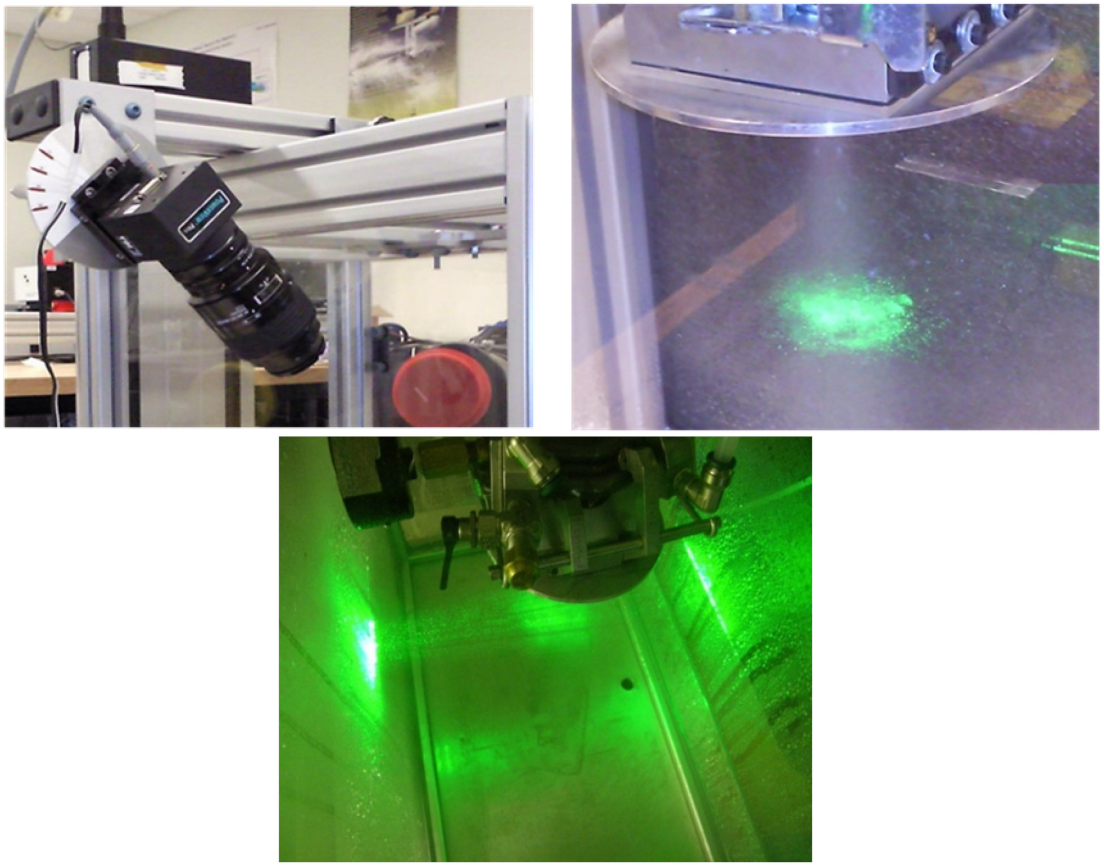

Figure 13: General setup of on optical patternation capture (a) Camera directed towards spray at an arbitrary angle, (b) cross sectional spray pattern illuminated by laser light

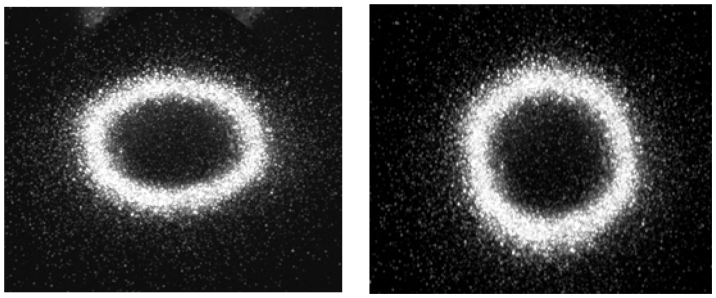

(a) **(b)**

Figure 14: A sample patternation image showing the cross sectional spray pattern (a) before dewarping, (b) after dewarping

2.5. Particle Image Velocimetry

Particle Image Velocimetry is a non-intrusive laser diagnostic technique used to obtain vector velocity information of fluid flows in a 2-D or 3-D viewing fields. The PIV system was first developed in the early 1980s and has become an indispensible tool for

experimentally analyzing many types of fluid flow experiments. They are also sometime used to validate and improve on numerical simulations of fluids flows (18).

The general PIV system setup used in this study for capturing droplet velocities of the spray flow is illustrated in Figure 15. The 2D PIV system is made up of an Nd:YAG laser, a CCD camera, pulse synchronizer, and a PC for processing PIV data. Details on the equipment and components used to setup the PIV system are listed in Appendix B.

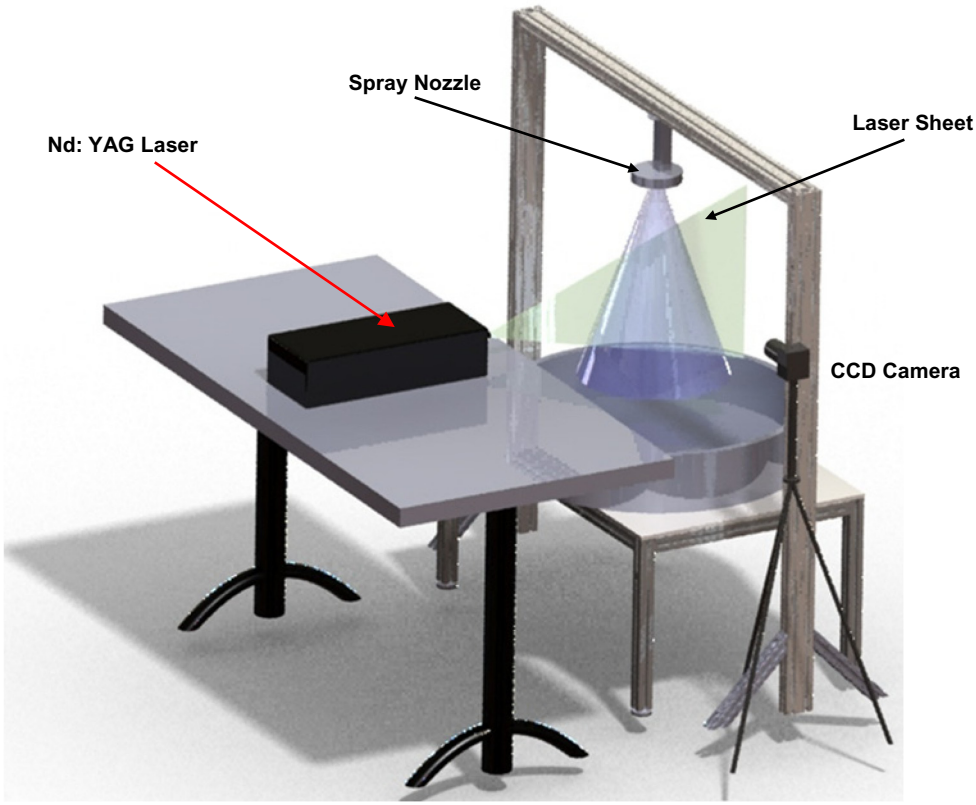

Figure 15: General PIV system setup for capturing 2D velocity profile of spray nozzle

The PIV system's fundamental concept involves capturing two successive images using a CCD camera and high power YAG laser. The illustration of Figure 16 shows an example of the velocity of droplets determined by the PIV's algorithm. The camera and laser are controlled via a synchronizer that controls the timing of when the laser and camera are

triggered. At first the laser fires a single pulse at t_0 to illuminate the droplets within the flow. A short time later (in the order of a few microseconds), the camera opens for a short duration as shown in its iris to capture the first image of the flow (frame A). A second pulse of laser light is pulsed at $t_0+\Delta t$ and again the camera opens its iris to capture the second image of the flow (Frame B). In all, only a few milliseconds have passed and two images have been captured.

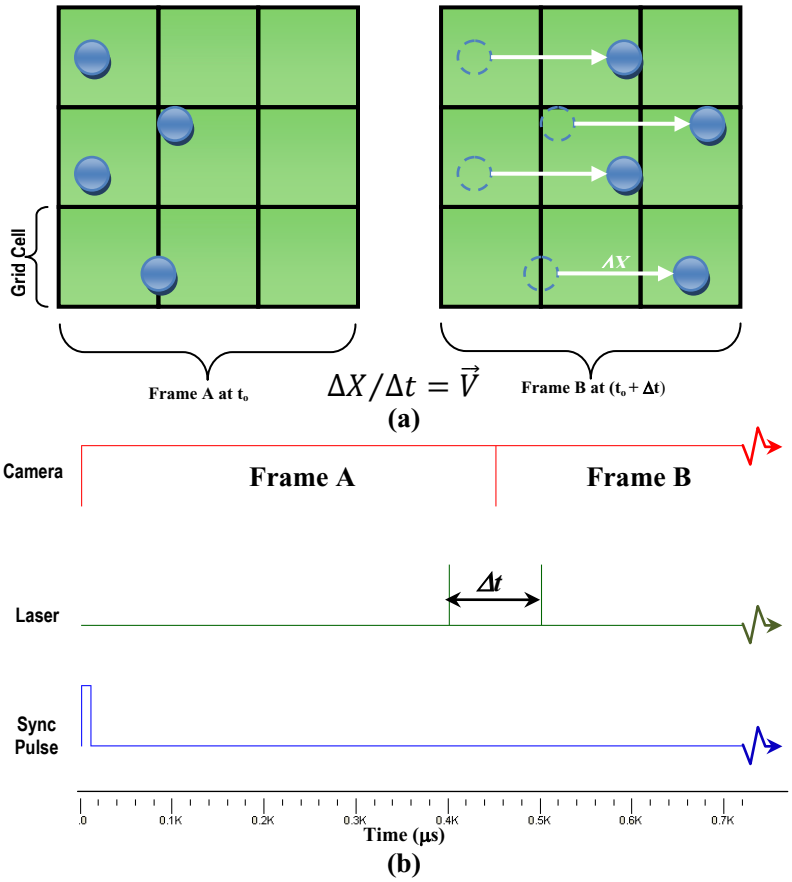

Figure 16: (a) an illustration showing how PIV uses a cross correlation method to determine droplet velocities, (b) a sample timing diagram used to synchronize the camera and laser pulses of the PIV system

These images are stored in the computer's memory and referred to as frame A and frame B for the first and second image, respectively. Each frame is divided into cells known as interrogation regions. The frames are then processed as digital signals whereby the illuminated droplets are displayed in their respective greyscale intensities.

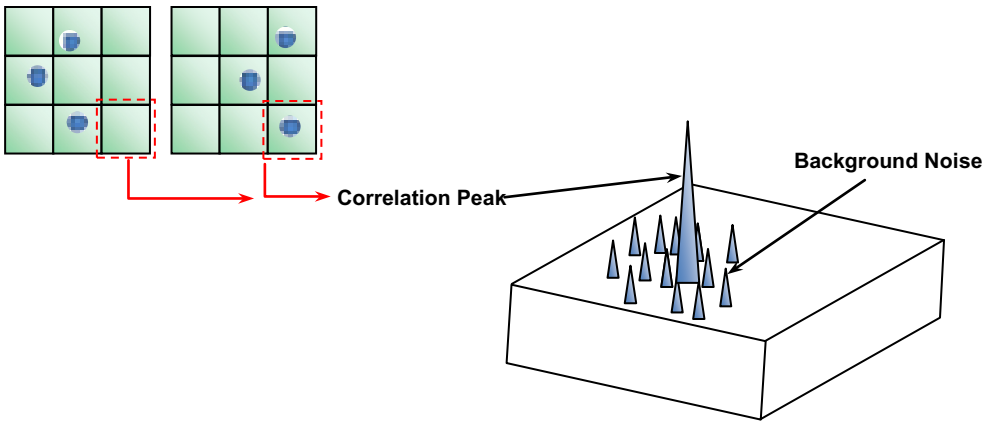

Figure 17: The PIV's Cross-correlation creates signal peak corresponding identifying common particle displacements

The light intensities in Figure 17 shows how the droplets are interpreted as a Gaussian light signal where the FFT cross correlation algorithm creates a signal peak that identifies common particle displacements. This calculation is then carried out and repeated in cells within the rest of the image to obtain a 2-D velocity profile of the flow thereby giving a visual representation of the particle's speed and trajectory. The image of Figure 18 shows a sample spray flow image captured by the PIV system and processed to show the velocity of the spray flow. The details on the algorithm and methods used for validating the PIV results are described in Chapter 3 as part of the data validation.

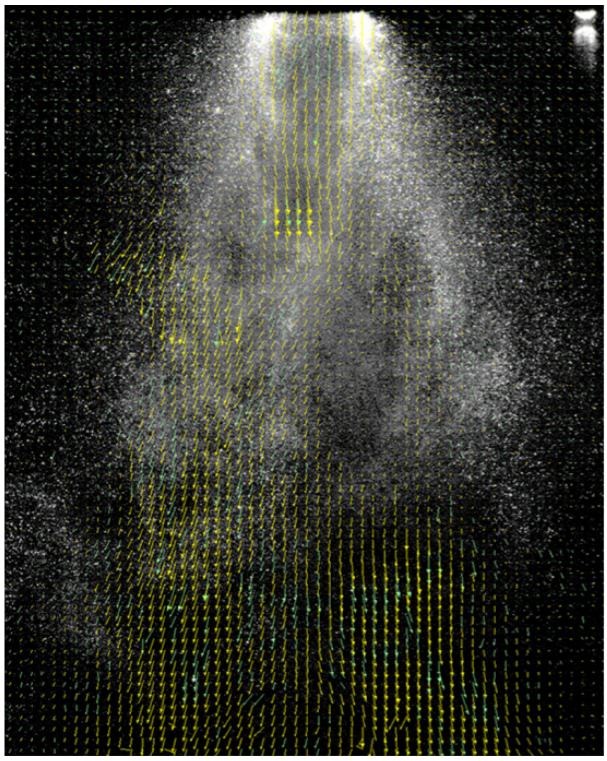

Figure 18: A sample PIV post processed image showing the instantaneous velocity profile

The PIV settings used in this study are varied according to the flow rate. Changes were made to the camera aperture setting, laser power, and time sequence depending on the experiment and are tabulated in Table 3.

Table 3: Setup of the PIV system

GLR Setting	0	0.75	1.47	2.35
Δ t *(μs)*	80	60	40	20
Lens Focal Length *(mm)*	50	50	50	50
Lens Aperture *(F#)*	8	11	11	16
Camera Distance *(mm)*	890	890	890	890
Grid Size	32x32	32x32	32X32	32x32
Spatial Resolution (mm)	2.8x2.8	2.8x2.8	2.8x2.8	2.8x2.8

In addition, several rules of thumbs are implemented to ensure accurate and precise measurement of the flow in question. First, the size of the interrogation regions (i.e. cells) is set to as small a size as possible in order to capture detailed flow displacements such as areas

of vortices, and recirculating flow. There is however a limit to the size of the cells. Size reduction of cells may cause some cells to have very few seed particles (i.e. droplets) that would create difficulty in obtaining valid correlations. Several works have suggested using cell sizes that ensure at least 5-10 or more particles are present in the cells (19). For this study cell size of 32x32 pixels (2.8x2.8mm) was used in all PIV images.

Another important setting is the time step Δt which is crucial in ensuring correct velocity estimates. If a relatively short time is selected then this would falsely estimate lower velocity magnitudes. Selecting too large a time step on the other hand would cause the PIV's correlation algorithm to lose track of the particles moving through the interrogation region and may even allow for out of plane particles to pass through the illuminated region. Studies into proper time step selection suggest that tracer particles in the area of highest velocity gradients should travel approximately ¼ of the interrogation region. For example, if a 32x32 cell is used then a time step should be selected to ensure that the particles only displace by approximately 8 pixels (20). The time steps used for this study are presented in Table 3.

2.6. Phase Doppler Particle Analyzer

Phase Doppler Particle Analyzer (PDPA) is also a non-intrusive laser diagnostic tool that uses the fundamentals of the Doppler Effect to determine the velocity and size of droplets (particles). The origin of the PDPA system is evolved from of Laser Doppler Velocimetry (LDV). The only difference between LDV and PDPA systems is that the latter has the ability to determine both the velocity and diameter of the droplets being measured; whereas LDV

can only measure droplet (particle) velocity. PDPA systems are also sometimes referred to as Phase Doppler Anemometry (PDA).

The general setup for the PDPA system is shown in Figure 19 and is made up of several components. The laser transmitter and receiver make up the optical components, and a signal processor and standard personal computer to analyze and display the measured data. The PDPA is considered an Eularian system where the system focuses on a specific point in space and measures any particles that move through its point of interest (converging laser beams). Therefore, the PDPA is coupled with a programmable 3-Axis traverse that scans regions of the spray giving the PDPA a minimum spatial resolution of 0.125mm where accuracy and repeatability are enhanced.

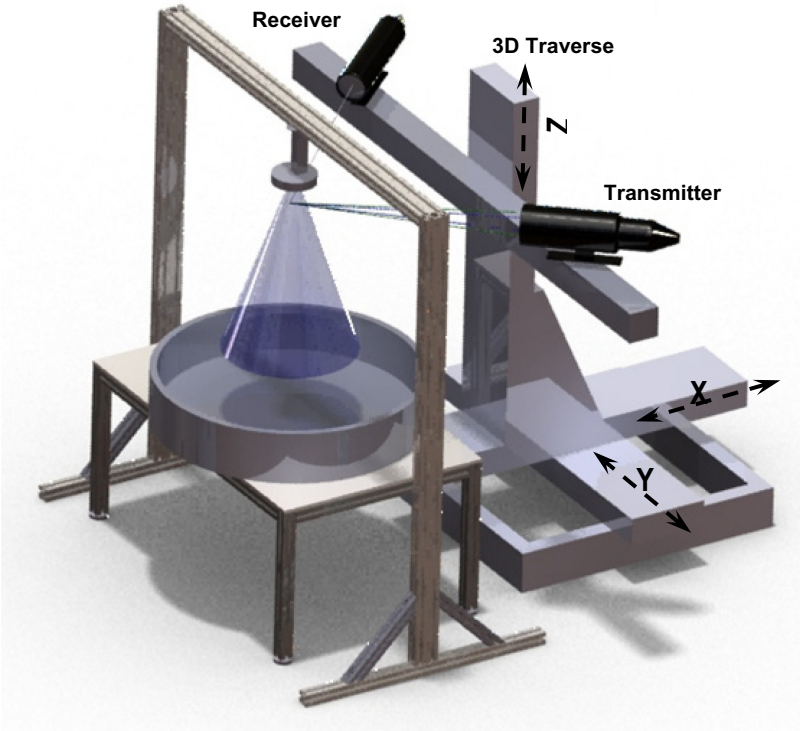

Figure 19: PDPA Setup using a programmable 3D traverse system to scan multiple locations of the spray

In its simplest form, PDPA/LDV transmitter uses monochromatic coherent laser light for the data measurements. Essentially, two laser beams are emitted from the laser transmitter where the beams converge onto a single point known as the Probe Volume. This volume of converged laser light creates a zone of light and dark lines known as the fringe pattern. A light sensitive receiver made of Photomultiplier Tubes (PMT) is positioned normal to the plane of the fringe pattern in order to detect reflections or refractions of any particle passing through the probe volume. The reflected signal is processed using a multibit digital processor that converts the light signal into a digital signal before being displayed as velocity and size data on a computer processor.

In Figure 20 the fringe pattern is calibrated so that the light rays posses a specific wavelength λ which is on the order of a few nanometers. The PDPA's processor measures the time it takes for a particle to pass through the probe volume by detecting the pulse of light reflections when the particle passes through. Since both the time and distance are known, then it is possible to determine the velocity of the particle that passed through.

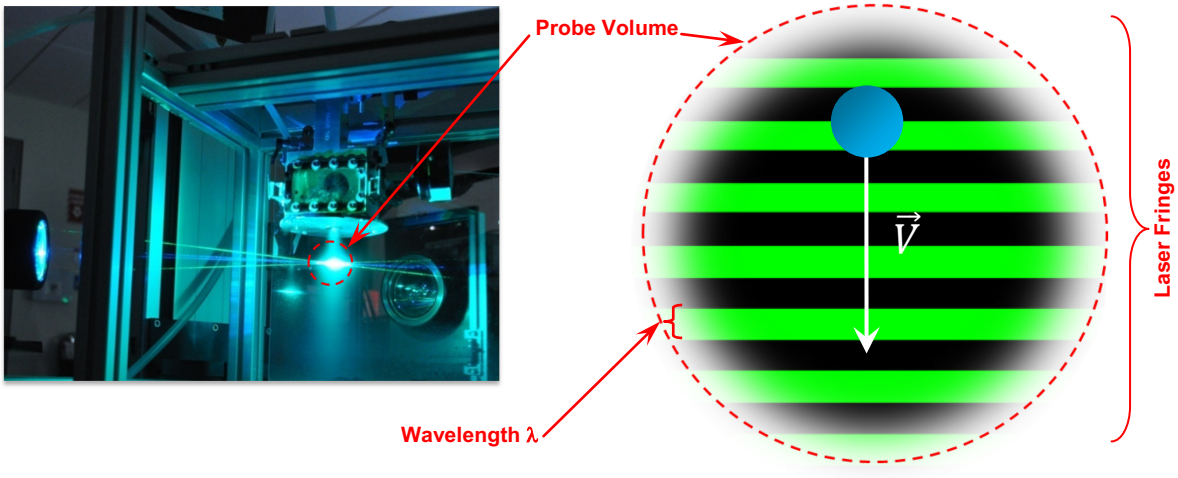

Figure 20: A schematic depicting a droplet passing through the PDPA's fringe pattern. Knowing the wavelength and frequency of the reflections from the droplet determine the droplet's velocity

The diameter measurement of the PDPA is done differently. The diameter is determined based on the phase angle of the received light signal. The illustration of Figure 21 shows an exaggerated example of a large and small droplet sending refracted laser light to the receiver. The receiver is made up of three PMT face plates. The plates are placed at specific distances from each other where each plate will detect the refracted light at a slightly different angle. In the first example, a large droplet passes through causing the laser light to deviate from its original path. Notice in Figure 21 (a) that a large droplet has shallow curvature causing the angle between each ray to deviate slightly. On the other hand, the smaller droplet in Figure 21 (b) has a very sharp curvature that causes the rays to deviate substantially. The difference in their angle is known as the phase angle and the face plates detect the degree of shift in phase angle in order to determine how large or small a droplet is. The properties of the laser settings used for this experiment is presented in.

As mentioned earlier, the PDPA is a point-wise measuring system that can only investigate a small point in space at a time. The 3-Axis traverse is used to scan both spray nozzles in increments of 2.5mm, where the conical spray is scanned across one axis (assuming axisymmetric spray), and the elliptical spray is scanned in the major and minor axes as depicted in Figure 22.

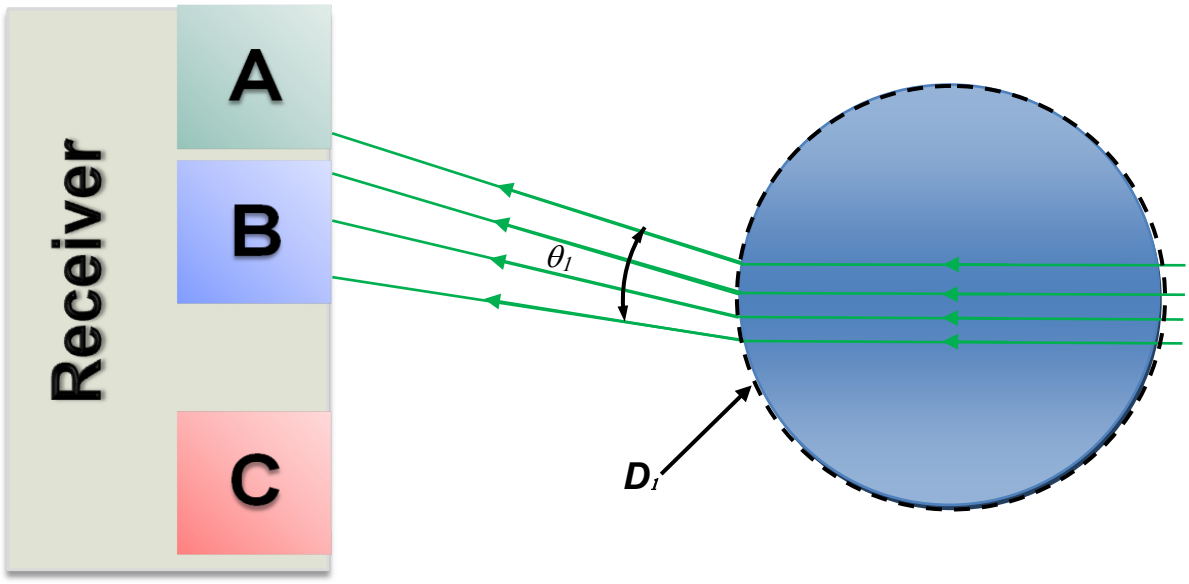

(a) Large droplet with less curvature results in less phase angle difference

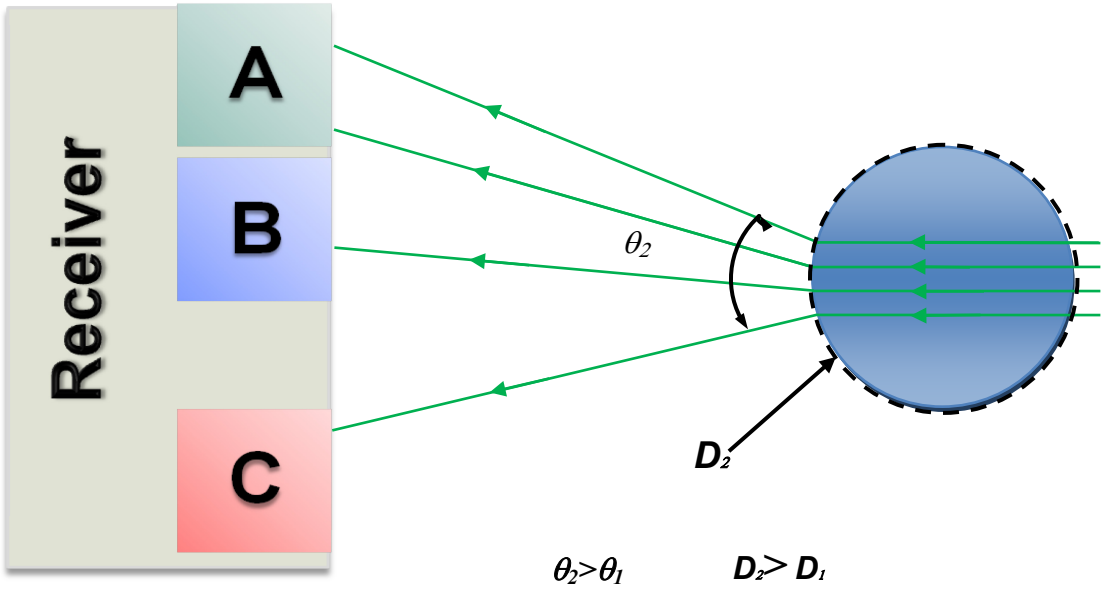

(b) Small droplet with sharp curvature results in greater phase angle difference

Figure 21: Determination of droplet diameter of PDPA systems using radius of curvature

	Channel 1 (Green Laser)	Channel 2 (Blue Laser)
Laser Power (mW)	500	
Transmitter Focal Length (mm)	512	
Max Diameter Difference	7%	
Beam Expander (ratio)	1.0	1.0
PMT Voltage (V)	525	525
Max Number of Samples	10,000	10,000
Band Pass Filter (MHz)	2-20	1-10
Downmix Freq (MHz)	38	37
Time Out (s)	30	30
Burst Threshold (mV)	200-300	200-300
Wavelength (nm)	514.15	488
Focal Length (mm)	512	512
Laser Beam Diameter (mm)	2.65	2.65
Fringe Spacing (μm)	3.7441	3.7441
Beam Waist (μm)	84.93	80.55
Bragg Cell Frequency (MHz)	40	40
Scattering Mode	Refraction	
Polarization	Normal to beam	
Scattering Off Axis Angle (deg)	60	
Droplet Refractive Index	1.33	

Table 4: Laser beam properties of PDPA system

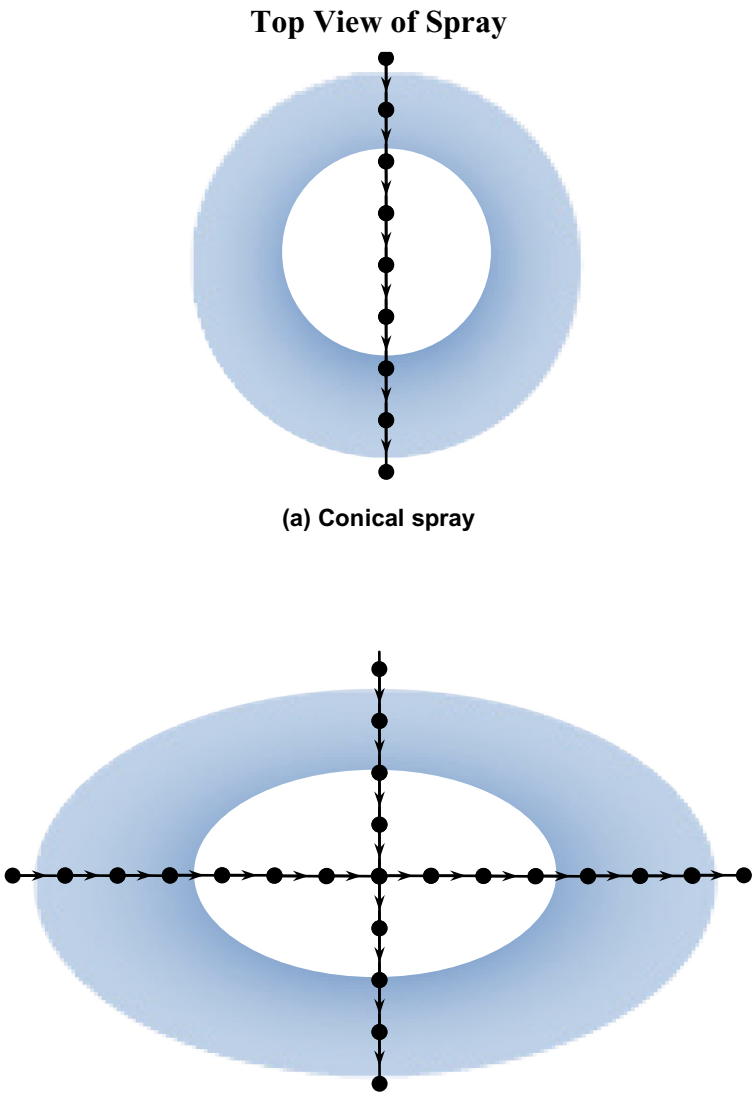

(a) Conical spray

(b) Elliptical spray

Figure 22: An illustration of the PDPA's scanning path for (a) Conical spray (b) Elliptical spray

3. Validation of Results

3.1. PDPA Validation

The PDPA is an accurate and precise point-wise measurement; however it is subject to errors that need to be taken into consideration. The errors associated with the PDPA are both random and biased; however, bias errors tend to have a greater influence on the outcome of the results. One of the factors that affect the accuracy of the PDPA results is in PMT Voltage. PMT voltage is the signal setting used to determine the receiver's sensitivity to light signals. Generally, for a given spray, a high PMT voltage setting will cause the PDPA to become more sensitive to light from smaller droplets. This indicates that mean diameter measurements such as SMD are dependent on PMT settings. However, a certain method was taken to ensure that the measured mean diameters are made independent of PMT setting.

In order to determine the proper PMT setting required for this study, the PDPA laser had to be directed at the densest and most complex region in the spray to measure. Therefore, the conical spray running under its nominal operating conditions (GLR 2.35) was used. A height of 12.7mm distance from the nozzle's exit was chosen because it was the densest and most complex region to measure in the spray.

Figure 23 shows a plot of the PMT voltage signal versus the mean diameter (D_{10}) measured by the PDPA. The PMT voltage was first set to its default setting of 375 V and the mean was measured. The measurement is repeated by incrementally increasing the PMT voltage signal (increments of 25 V) resulting in smaller D_{10} measurements. The decrease in mean diameter continued until a point was reached where any increase in PMT voltage resulted in no change in diameter. Therefore the test showed independence from PMT voltages was achieved at

525V and was selected as the nominal PMT setting for all experiments carried out in this study (21) (22) (23).

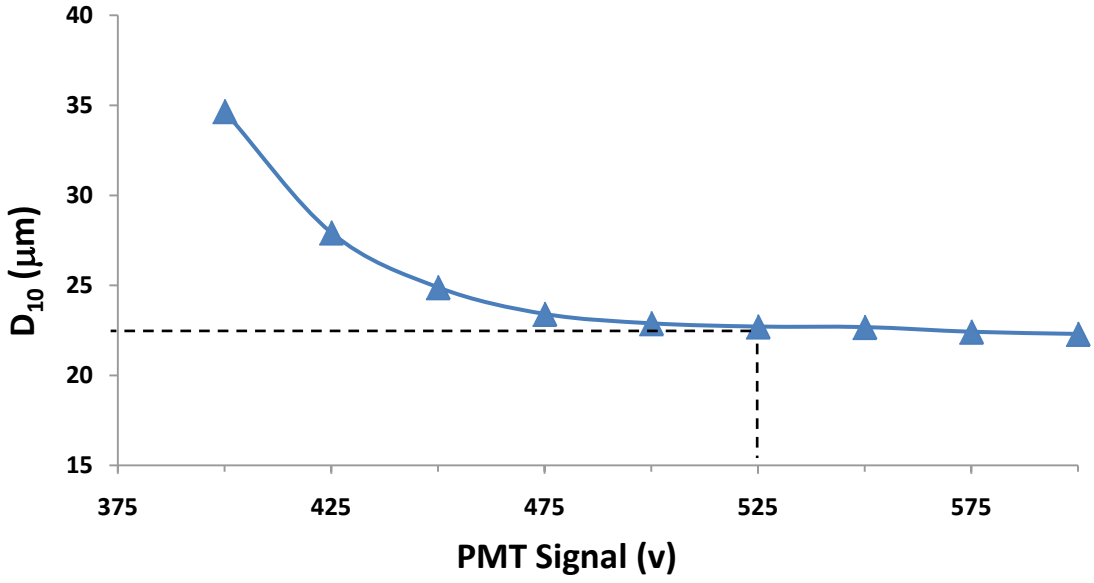

Figure 23: Droplet diameter in PDPA systems are dependent on the PMT settings used. Therefore, the PMT voltage signal is increased until no change in mean diameters is noticed

One of the characteristics in PDPA operations is that the fringe pattern of the converging laser beams takes on a Gaussian distribution where the light beams are somewhat thicker in the center and thinner at the outer edge. This in turn indicates that good strong reliable signals can only be picked up when passing through the center of the fringe pattern. The issue that arises in many spray applications is that larger droplets may be passing at the outer edge of the fringe pattern, and although signal detection is weak, large droplets tend to reflect stronger signals than smaller droplets passing through the center. This ends up causing a bias error in which large droplets are being detected even though they are not part of the flow passing through the point of interest resulting in larger mean diameters that are incorrect. Furthermore, some dense spray atomizers are subject to secondary laser light reflection

further increasing the error in diameter measurements in the PDPA. A criterion for filtering out unwanted bias from larger droplets known as Intensity Validation was used.

The intensity validation method establishes a criterion for selecting cut-off lines in which data beyond a certain limit are rejected and not taken into consideration as part of the mean. For example, Figure 24 shows an extracted image from the PDPA's software showing a plot of all the data detected by the system for a single point within the spray. The graph plots the individual diameter measurements of the droplets that passed through versus their respective intensity signal in mV. Notice in Figure 24 that there is a cluster of data that naturally corners itself within a certain average size, and that the data creates a natural parabolic curve. The concentrated cluster of droplets is the droplets that passed directly through the center of the fringe pattern. However, there is also some scattered data of larger droplets that passed through the outer edge of the fringe pattern with faint intensity signals that were also picked up. The user is required to set the curves in such a way as to isolate the natural tendency of the data to lie within a certain diameter range and reject larger diameters. In this example, the SMD when not using intensity validation was taken to be 30.04μm; however, once intensity validation was implemented the SMD was estimated to be 24.19μm resulting in a 19.47% difference in Sauter mean diameter.

Intensity validation in PDPA measurements requires great emphasis since this type of data validation will not only affect droplet diameter measurements but other parameters such as volume flux measurements.

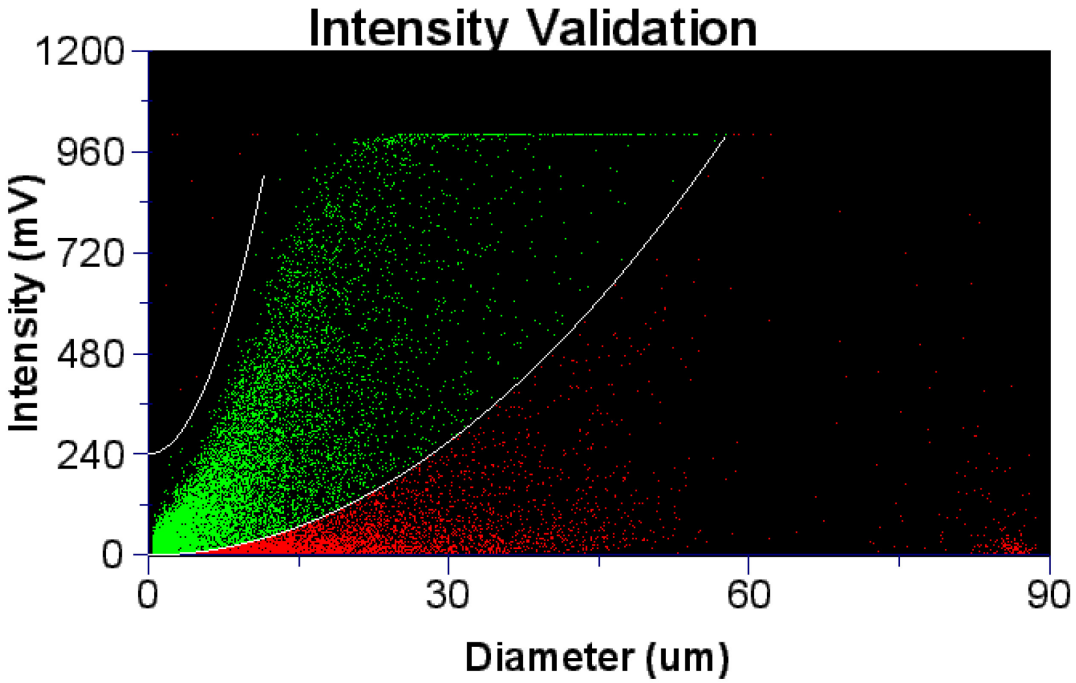

Figure 24: Example of good intensity validation where the cluster of data creates a natural curve and larger data seems to be spread further out resulting in their rejection

Schwarzkopf et al. (24) carried out PDPA tests on pressure swirl atomizer using a similar intensity validation method. The tests showed that intensity validation not only improved droplet diameter measurements but that volume flow rate estimated from volume flux data also improved. However, the work carried out by Schwarzkopf et al. showed that the best possible flux measurements were only within 30% of the actual volume flow rate. The cause for the large inaccuracy was due to the increased amount of uncertainty inherit in volume flux measurements because volume flux is estimated based on other inputs which have their own uncertainty (24).

Another important aspect in validating data is related to diameter-velocity bias. Some sprays have characteristics in which a faint mist occupies the spray region apart from the larger core of the spray. The mist usually has droplet diameters that are significantly smaller than the mean diameter of the flow in question. The smaller mist droplets tend to float or remain

stationary in the ambient environment and do not contribute significantly to the overall behavior and performance of the spray. Nevertheless, these fine mist droplets may sometimes be detected by the PDPA system and bias the results. Figure 25 shows the PDPA's software plotting the data according to their respective velocities and diameters. In this case, the data shows that the majority of the droplets create a normal distribution where the mean velocity is approximately 15m/s.

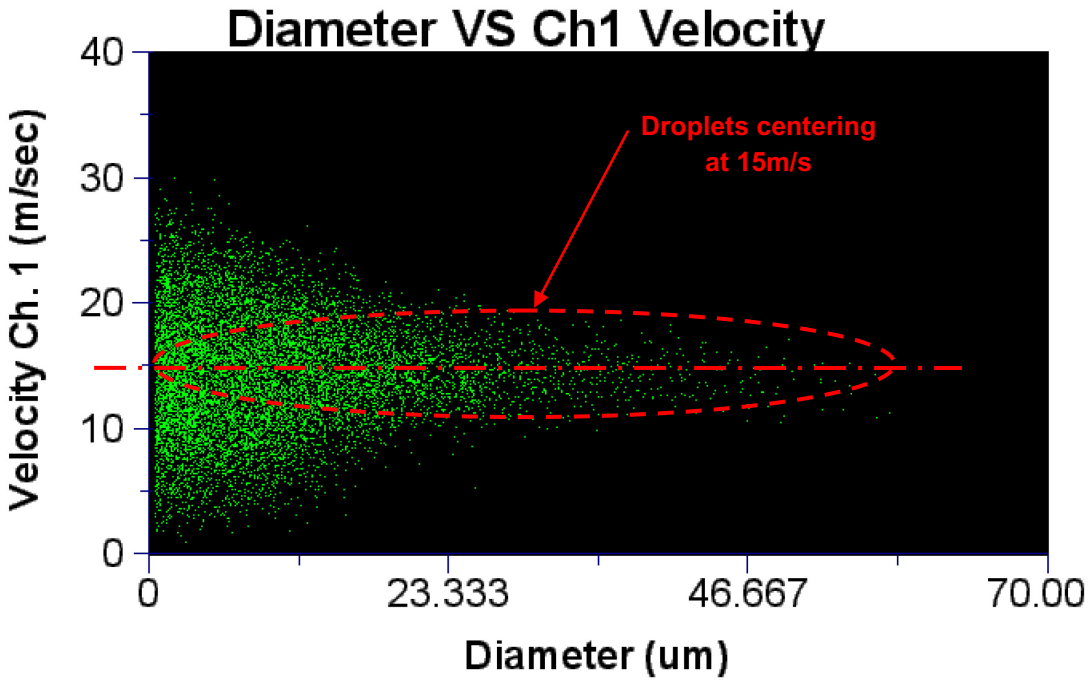

Figure 25: A graph plotting the droplet velocity VS diameter in an ideal spray where velocities take on a normal distribution about a mean velocity of 15 m/s.

On the other hand, Figure 26 shows a scan from the elliptical spray where two velocity peaks were detected. In this case, a smaller peak corresponded to smaller diameters that hovered near lower velocity magnitudes. This in turn caused the PDPA to underestimate the mean velocity of the flow. For example, isolating and eliminating the slower droplets gave a mean velocity of 9.2 m/s, whereas a mean velocity of 2.5 m/s was measured when taking in all the

data. The difference in velocity means corresponded to a 27.72% difference. Therefore, elimination of the slow flowing droplets was necessary in order to correct for the bias towards slower moving droplets but it was also important to determine if the droplets where representative of the overall flow or not. By inspecting smaller slower droplets, the volume flux was estimated to be 0.0004 $cm^3/cm^2.s$ and the total volume flux was estimated at 0.0190 $cm^3/cm^2.s$. This meant that the slower droplets represented only 2% of the total flow of data detected by the PDPA and should therefore be neglected as the slower droplets did not represent a significant volume of the overall flow.

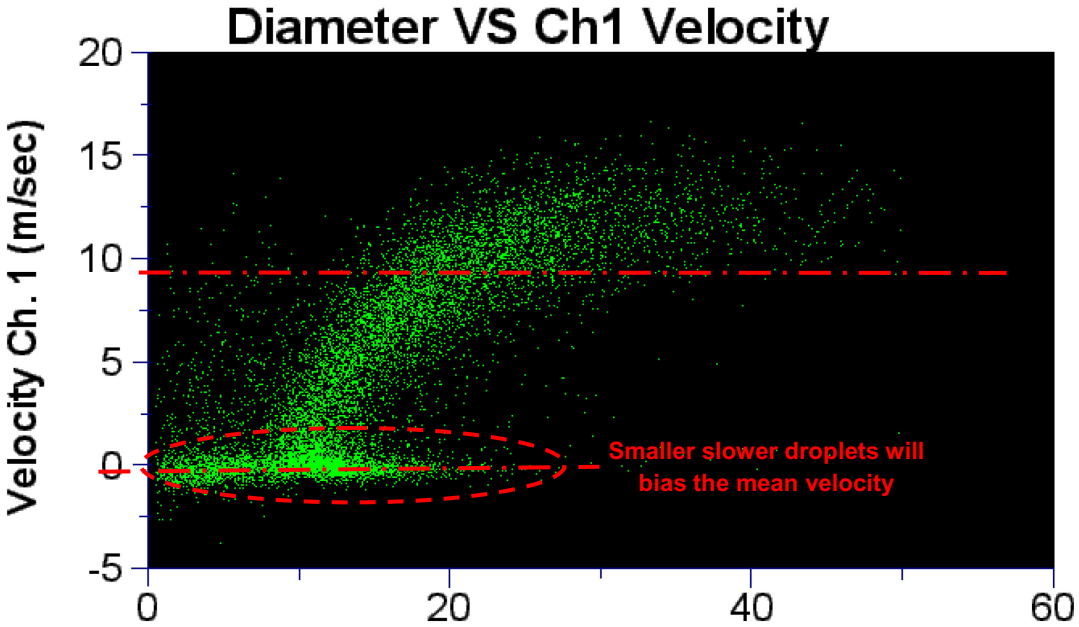

Figure 26: A sample plot from the elliptical spray showing evidence of a mist of droplet hovering in mid air since their velocity is nearly 0 m/s

Throughout this study, the conical spray showed no signs of double velocity peaks. On the other hand, the elliptical spray did have some areas of double velocity peaks where smaller droplets were drifting at magnitudes ranging 0-5 m/s. The PDPA is capable of isolating and eliminating such velocity bias; however no attempt was made to correct for this bias. No

attempt was made because each point measured by the PDPA system showed double velocity peaks at different ranges of magnitudes, making it impractical to apply a uniform filtering scheme onto the data due to the sheer number of data points taken. This method so far has addressed issues regarding the spray characteristic itself; however, other factors such as changes in operating conditions also contributed to the overall error in PDPA measurements.

In some cases the sudden change in flow operating conditions may have altered the data. The consequence of a change in flow condition would be that the diameter and velocity of the droplets would also suddenly change leading to erroneous data being captured. A criterion is setup so that the PDPA system rejects any droplet whose diameter exceeds 7% of the recorded mean diameter. The diameter difference plot may also serve as an indicator to how wide spread the diameter measurements are. In this case, the diameter difference in Figure 27 (a) is fairly small which indicates a narrow distribution in droplet diameters. In other cases such as in Figure 27 (b), the diameter difference plot showed sudden changes in the flow of the spray caused by air flow fluctuations from the lab's own air supply. In this study, any signs of data fluctuation were discarded and the test was repeated.

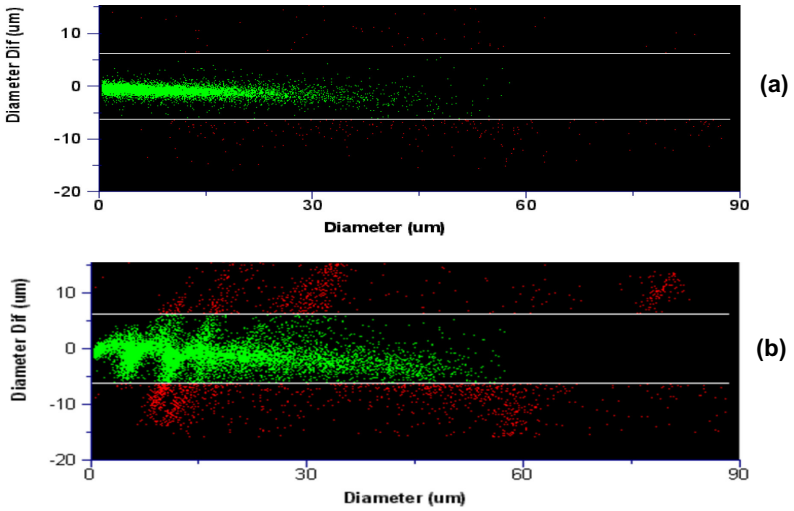

Figure 27: The diameter difference plot shows how wide the data distribution is where in (a) the data is fairly narrow and, (b) shows evidence of flow fluctuations caused by the change in air pressure from the supply line

3.2. PIV Validation

The overall measurement accuracy in PIV is dependent on a combination of several factors that contribute to the total error in PIV. Therefore, it is difficult to isolate individual source of errors, however, there are several methods that can help reduce the overall error that help improve the accuracy of a PIV analysis. In addition, several rules of thumbs must be implemented in order to ensure that the resulting PIV data is a valid representation of the flow.

One of the issues encountered with analyzing PIV images stems from background noise. In many cases, the noise constitutes a major source of error that if not taken into consideration can greatly affect the accuracy of a PIV analysis. Noise error in PIV images appear as faint low intensity particles that create low frequency peaks in the peak correlation. Some of the noise within a PIV image can be the result of electronic noise coming from the PIV equipment such as the camera; however, the majority of the noise is background illumination caused by secondary reflection of the PIV's laser light onto reflective surfaces. This

secondary reflection can cause faint images of the background environment to appear which in turn weakens the peak correlation detection in the PIV.

One method of eliminating background noise is through the Background Subtraction method. This method is used to eliminate background noise caused by secondary light reflection. Figure 28 shows sample raw PIV images of the conical spray in various stages of the background subtraction process. Figure 28 (a) is a sample of what a PIV image would look like if no noise removal processing was implanted. The procedure itself requires that several images (up to 100) be taken of the experiment without using seed particles (spray droplets) such as in Figure 28 (b). The processor then computes the average intensity of each image and creates a new image in which the total average intensity of all the images is placed onto one image. The background image is then subtracted from the actual experimental images that contain the spray flow which output a cleaner and more contrasted image making it easier for the processor to detect valid peaks such as the image in Figure 28 (c). Of course, not all noise has been removed from the image and other sources of error such as error in the correlation algorithm itself are also present. Therefore, further post-processing validation is required to ensure validity of the outputted results.

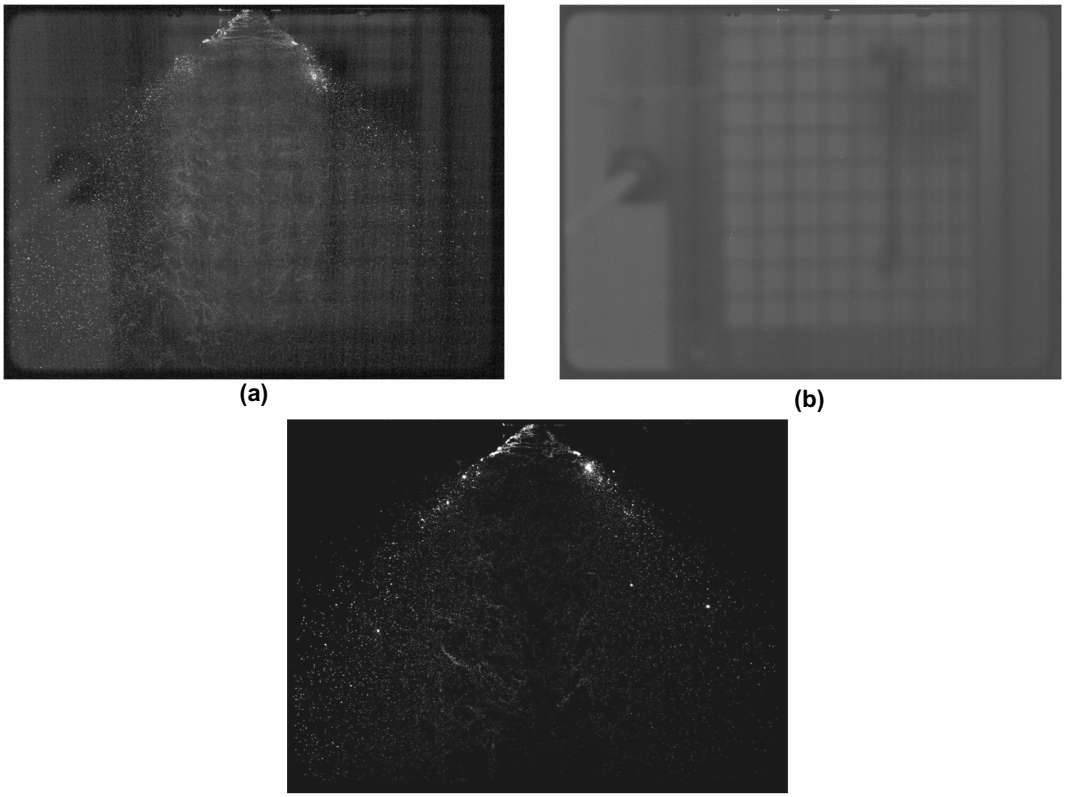

Figure 28: Implementing background subtraction reduces the effect of background noise caused by reflective surfaces. In (a) the raw image shows the spray along companied by the background, (b) Image capturing of the background only, (c) Subtraction of the background from the spray image

One of the post-processing validation methods used is median validation. The median validation looks to remove spurious vectors that arise as the result of errors in the correlation or noise. The validation scheme looks at individual vectors and compares them to neighboring vectors by ranking velocity magnitudes and removing spurious vectors. For example, a set of vector magnitudes of 3.5, 4, 5, 3.2, and 25 has mean value of 8.14. However, note that 25 is a significantly higher magnitude that most likely corresponds to a spurious vector. Median validation would eliminate values that differ dramatically from the other vectors resulting in a more reasonable mean value of 3.9 (25). The neighborhood size can be set by the user; however, care must be taken in the selection of neighborhood size. For example, a neighborhood size of 3x3 (compares vectors within 3 cells) may not be a

sufficient enough validation to eliminate spurious vectors when compared to a 5x5 or 7x7 neighborhood size.

One of the sources for spurious vectors in this study stems from laser light reflection of the spray nozzle's surface and face plate. These reflections cause may result in false signal detection that ends up being treated as a high velocity gradient. For example, Figure 29 is a spray flow generated by the elliptical nozzle at a GLR of 1.47. Notice that in Figure 29 (a) there is an area of moderate velocity gradients. In reality, there is no flow of droplets in that region and only reflections from the face plate are picked up by the PIV algorithm. In the case of Figure 29 (a), a 3x3 median validation was implemented to reduce the appearance of falsely detected data; however that was not as sufficient as a 7x7 median validation such as in Figure 29 (b) were the saturation is reduced. This study selected a 7x7 neighborhood size since smaller neighborhood sizes had no effect on the results. In addition, larger neighborhood sizes were avoided in order to prevent over processing data that would remove a significant portion of valid vectors. For this study, a median validation of 7x7 with secondary peak detection was used in all PIV images.

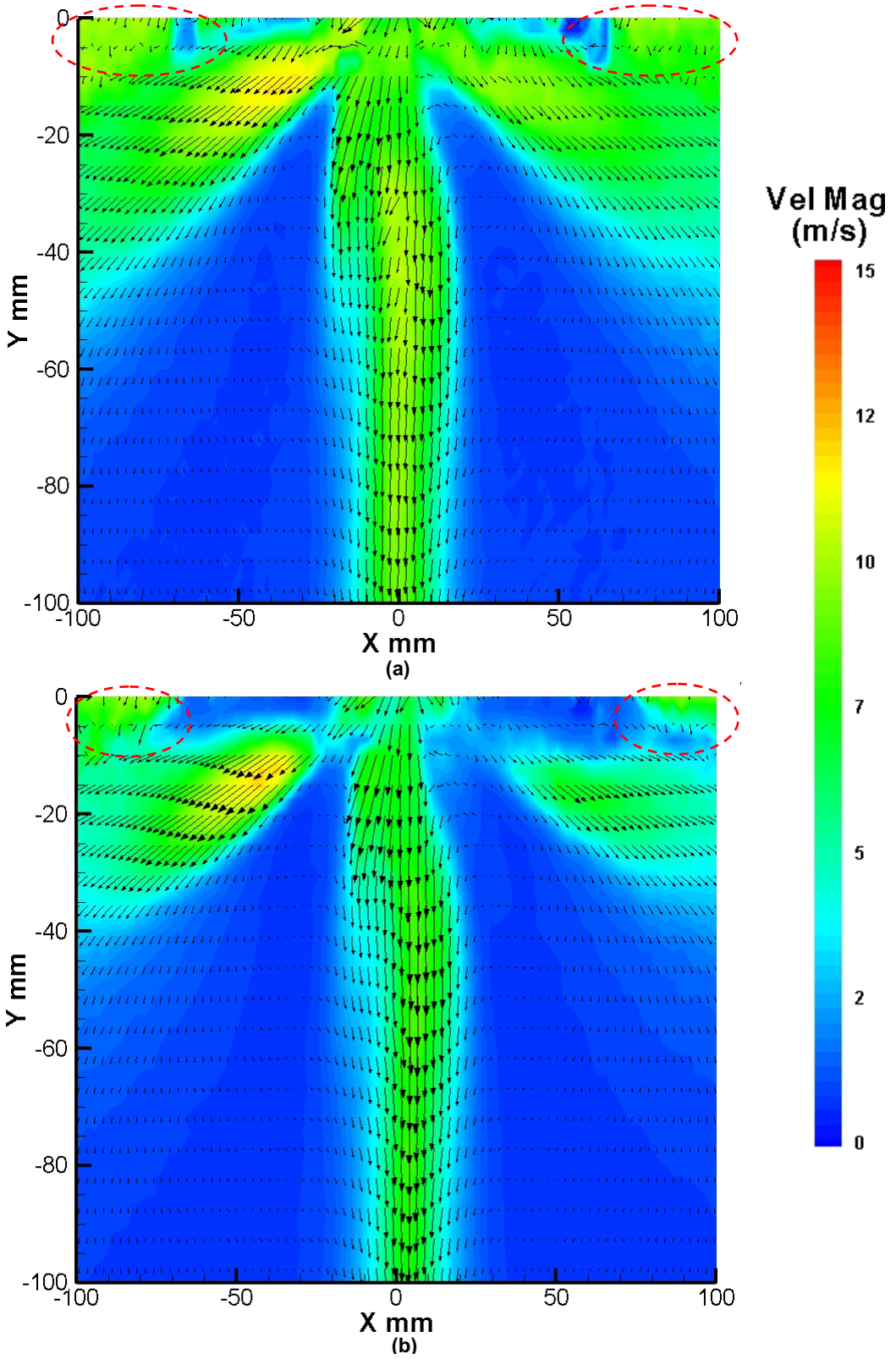

Figure 29: Velocity profiles of the elliptical spray comparing the difference between post processing and no post processing (a) Velocity profile with no post processing validation, (b) Velocity profile with a 7X7 median validation using secondary peak to replace bad vectors

4. Results

The results of the conical spray are first presented to establish a benchmark in order to compare the performance and behavior of the spray flow with the elliptical nozzle. Data from both nozzles are presented individually to see how they perform at different air flow conditions. The nozzles are then compared against each other to see what changes between both nozzles are observed.

4.1. Conical Nozzle

4.1.1. Conical Shadowgraph

The conical spray is run with water at a flow rate of 30.5 lb/hr. Figure 30 shows that the nozzle exhibited wave instabilities that were due to the combination surface tension, viscosity, and inertia of the liquid as well as properties of the surrounding gas.

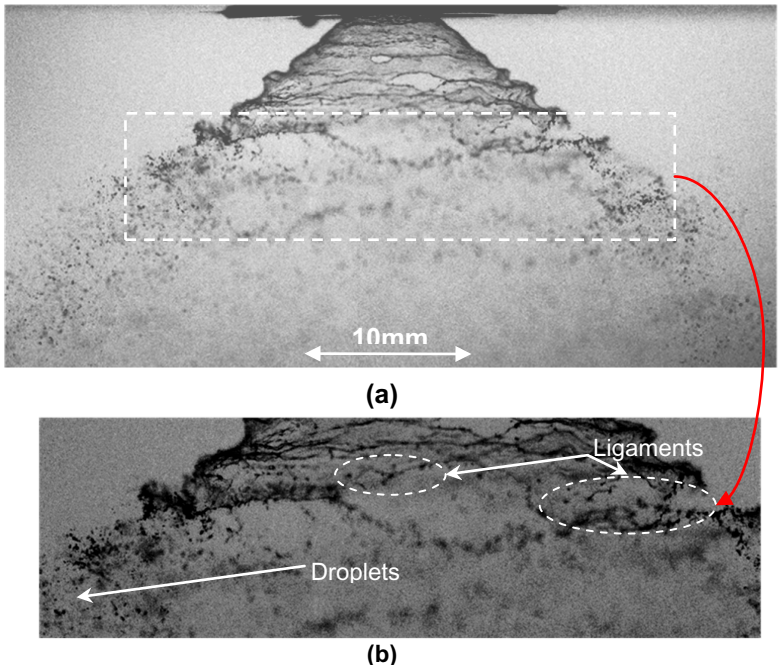

Figure 30: Shadowgraph of the conical spray at a GLR of 0. (a) No Air spray profile with a spray angle of 100° ±5°, (b) Closer inspection revealing sheet breakup where ligaments and droplets are formed.

The following shadowgraph image of Figure 31 shows the conical spray operating at a GLR of 0.75 in which some air was supplied to assist in the breakup of the spray. In this setting the spray still retains a liquid sheet near the nozzle exit; however, it is evident that the aerodynamic forces have changed the spray flow significantly. The spray cone angle has now contracted to 70° ±5°, the liquid sheet is more turbulent, and the wavelengths are also shorter with more perforated holes appearing in the sheet.

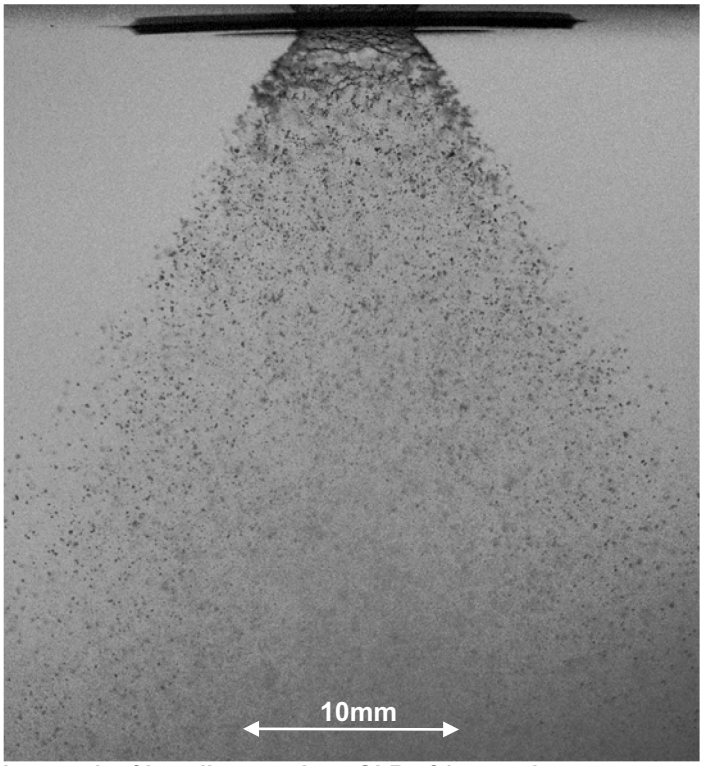

Figure 31: Shadowgraph of baseline nozzle at GLR of 0.75 and a spray cone angle of 70˚ ±5˚

In Figure 32, the air flow is increased to obtain a GLR of 1.47. Note that there was no major change in spray cone angle; however, the image appeared to show signs of increased turbulence in the structure of the spray with more numerous perforated holes appearing in the sheet.

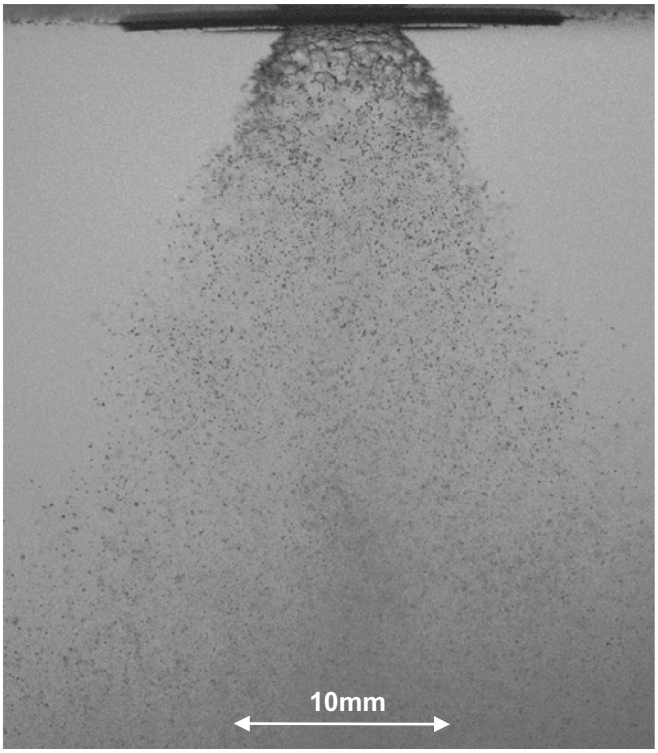

Figure 32: Shadowgraph of the conical spray at GLR 1.47 with a spray cone angle of 70˚ ±5˚

At a GLR of 2.35, the atomizer was running at its nominal setting as shown in Figure 33. Here, one can clearly see the change in spray cone angle where the bulk of droplets has contracted to define an angle of approximately 40° ±5°. Again, there was no significant change in the liquid sheet core other than an indication of a more turbulent sheet leaving the nozzle. The lack of change in liquid sheet breakup suggests that the air used to assist in the droplet breakup did not have a substantial effect on the water just as it left the nozzle. This introduced the possibility that parameters such as droplet diameters and their velocities were not exposed to the effects of the atomizing air until slightly further downstream from the nozzle. Also, the contraction of the spray cone angle showed an increase in droplet concentrations in the center of the spray that used to be relatively empty in previous settings. Tests using the Patternation, PIV, and PDPA will elaborate on this phenomenon in their respective sections.

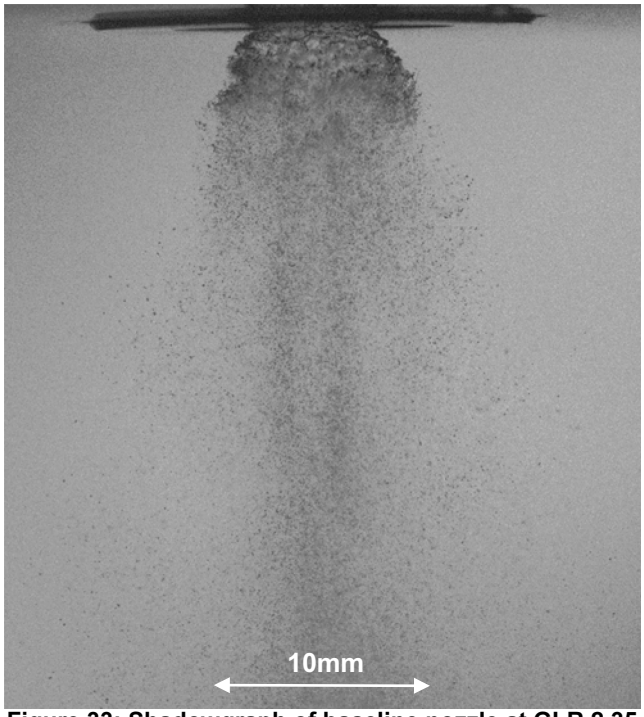

Figure 33: Shadowgraph of baseline nozzle at GLR 2.35 with a spray cone angle of 40˚ ±5˚

4.1.2. Conical Optical Patternation

The optical patternation images in Figure 34 showed cross sectional spray patterns of the conical spray taken at an axial distance of 12.7mm from the nozzle's exit at GLRs of 0, 0.75, 1.47, and 2.35. Initially, at a GLR of 0 the spray starts off as a simple hollow cone spray. Notice that the distribution was mainly focused around the periphery of the spray confirming the doughnut shaped pattern expected from a hollow cone swirl atomizer. Further increases in GLR resulted in a narrowing hollow cone spray as shown in Figure 34 (b), where at a GLR of 1.47 the hollow region is now filled with smaller droplets. On the other hand by increasing to a GLR of 2.35, the spray pattern appears as a solid cone spray and further reduced in size resulting in a more uniform droplet distribution.

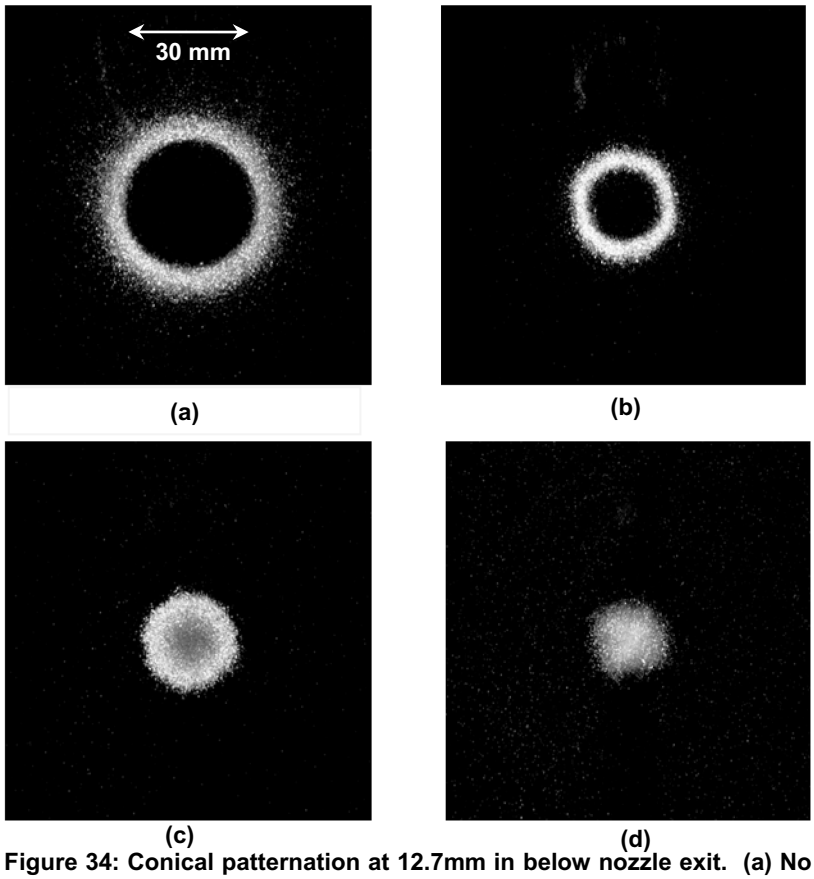

Figure 34: Conical patternation at 12.7mm in below nozzle exit. (a) No Air, (b) GLR 0.75, (c) GLR 1.47, (d) GLR 2.35

Patternation images at locations of 38.1mm (1.5in) in Figure 35 showed a similar repeating trend, only the size of the distribution had changed and the lower pattern intensities indicated a less dense spray cross section. The combination of the shadowgraph and patternation results indicated that the increase in GLR will contract the hollow cone spray, and finally at the nominal GLR of 2.35, a solid cone spray will be formed. This along with the shadowgraph images leads one to conclude that the conical spray penetrates more than it distributes.

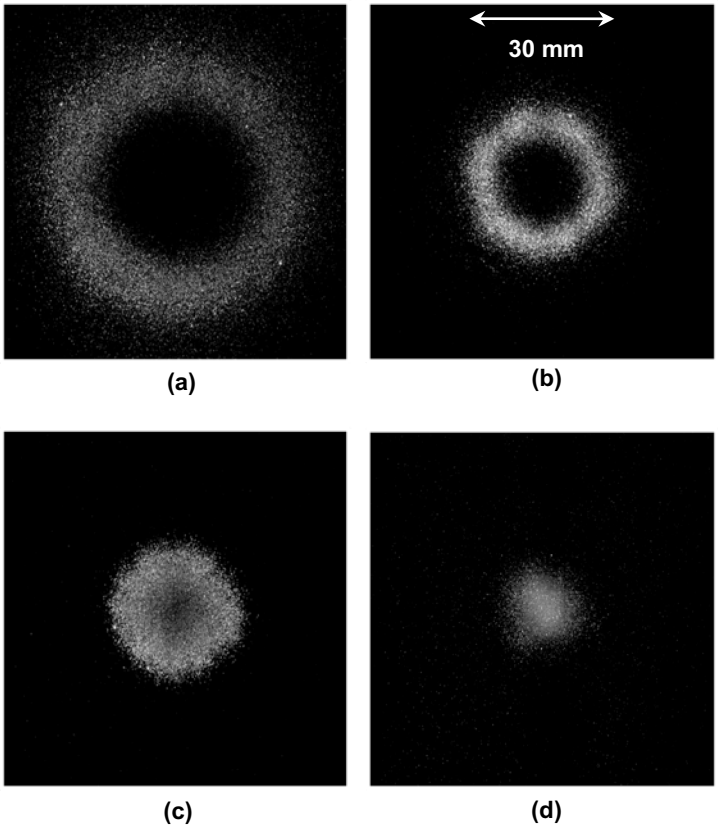

Figure 35: Conical patternation at 38.1mm below the nozzle's exit. (a) No Air, (b) GLR 0.75, (c) GLR 1.47, (d) GLR 2.35

4.1.3. Conical PIV Results

The shadowgraph and patternation methods provided a better understanding of the spray. The next step in spray characterization is to determine the spray velocity distribution. A 2D PIV system was used to determine the spray velocity profile.

First, a capture of the conical spray running at a GLR of 0 is shown in Figure 37. The contour plot of the velocity vectors showed an area of high velocity magnitudes of 10m/s stemming from the nozzle's exit extending downward to a distance of 40mm from the nozzle exit. Note that the central region within the spray showed low velocity magnitudes and the vectors experience a reversing tendency that corresponded to the reversing flow obtained by the PDPA system shown later in this study. In fact, a closer look at the GLR 0 PIV result in

Figure 36 near the hollow region of the spray showed vectors turning in the opposite direction of the exiting flow. The image did not fully capture the swirl since the velocity was low in which the averaging of several instantaneous PIV images dampened the reversing flow motion.

The lack of spatial resolution in the first PIV image serves as an indicator that PIV alone cannot sufficiently characterize the spray in certain areas. Recall that the shadowgraph image of Figure 30 showed a hollow cone spray. The PIV was only able to capture the main flow of the periphery where most of the droplets (seed particles) resided. There were droplets within in the center of the spray; however, they were small faint droplets that were under the effect of the ambient gas. Increasing laser intensity could have illuminated the smaller droplets; however, this would have lead to a saturation of the larger bright droplets. The saturated areas in the image would increase the risk of damaging the CCD sensor, as well as increase overall background noise. On the other hand, the PDPA results that are presented later will show more accurate and precise results in the areas that were considered too difficult for the PIV to capture.

Figure 38 shows the conical spray once air is supplied to it and run at a GLR setting of 0.75. In this figure one can observe the sudden increase of the velocity magnitudes to 15 m/s extending to a distance of 45mm from the nozzle exit, and that the area of high velocity magnitudes created an acute angle further indicating a contraction of the spray profile. In Figure 39 the spray was set to a GLR of 1.47. The maximum velocity magnitude has now risen to 20 m/s and has reached to a distance greater than 100mm. The image also shows how the central region possessed lower velocity magnitudes extending from the nozzle exit all the way towards the end of the image. Finally, the spray was set to a GLR of 2.35 in

Figure 40 where velocity magnitudes reached a maximum of 40 m/s. Unlike previous PIV results, the contour of maximum velocity magnitude did not start at the exit of the nozzle. The maximum velocity contour of 40 m/s starts at 25mm from the exit and extended all the way to the end of the image at 100mm.

The lack of any high velocity gradients near the nozzle indicated a velocity lag between the liquid and air. Recall, that the liquid leaves the nozzle at a lower flow rate than the air and that the atomizing air leaves from an annulus surrounding the liquid cone. Therefore, there is a zone in which the liquid is not directly affected by the atomizing air. In this zone, most of the breakup and movement of the droplets was due to its own momentum; however once passed this zone the aerodynamic forces of the atomizing air accelerate the droplets down even further. This acceleration is evident since the previous PIV images have shown that the velocity of droplets and the penetration depth based on the maximum velocity contours only increased when higher air flow rates were used. The main reason for this occurrence can be explained by the droplet size distribution along stream of the spray flow. Near the nozzle exit, the droplets are larger compared to the droplets further downstream (>40mm). The lower velocities associated with the larger droplets near the nozzle exit can be explained by inspecting the Stokes number. Stokes number represents how fast the droplets reach to the surrounding gas velocity. Near the nozzle exit due to the presence of many large droplets generated by primary atomization of liquid sheet the Stokes number will be larger. Downstream the spray on the other hand (>40mm), the secondary atomization results in smaller droplet sizes, hence smaller stokes number. These velocity characteristics seen in the PIV images are also presented in the PDPA data in the next section of this study where point-wise measurements are shown.

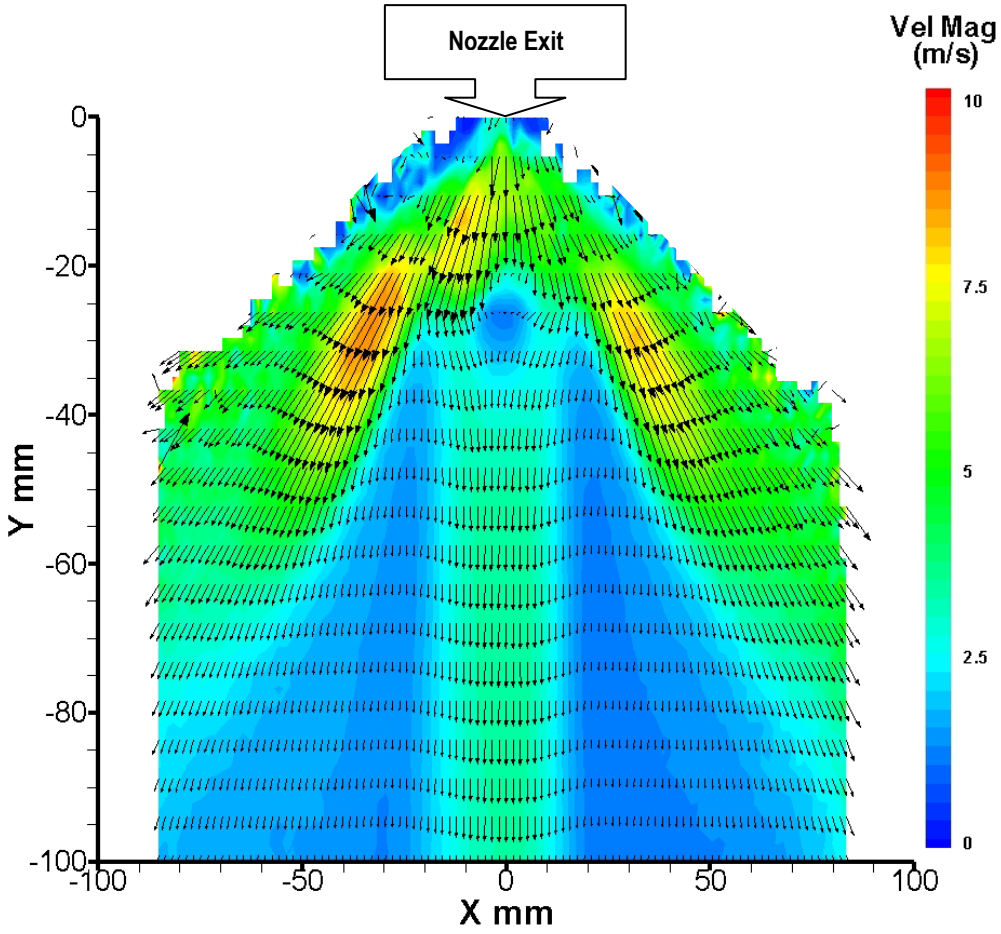

Figure 36: Conical spray velocity profile at GLR=0

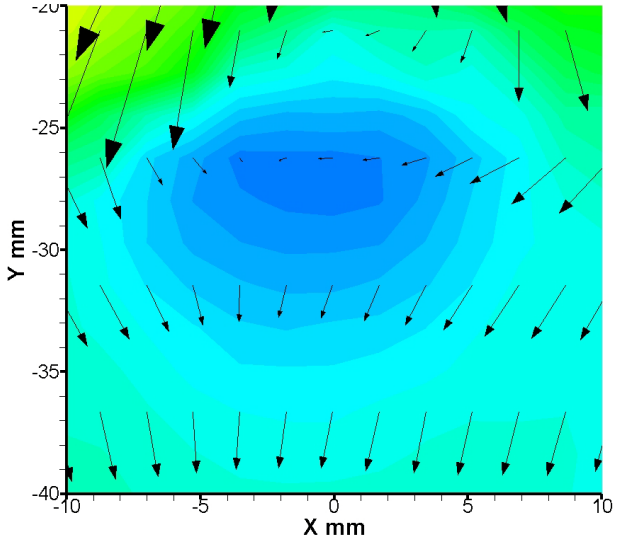

Figure 37: Closer inspection of the conical spray at a GLR of 0 that the center is experiencing a tendency to reverse flow

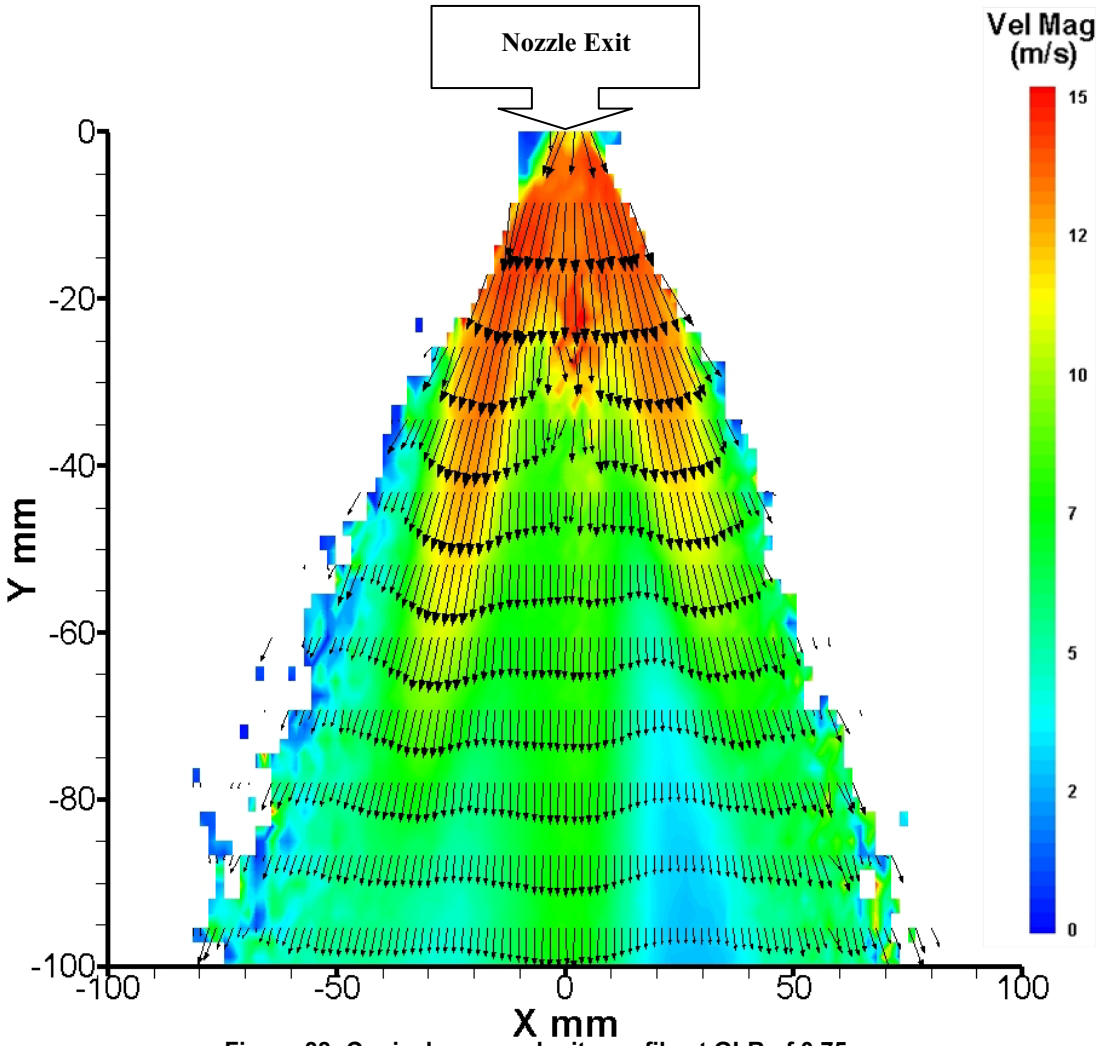

Figure 38: Conical spray velocity profile at GLR of 0.75

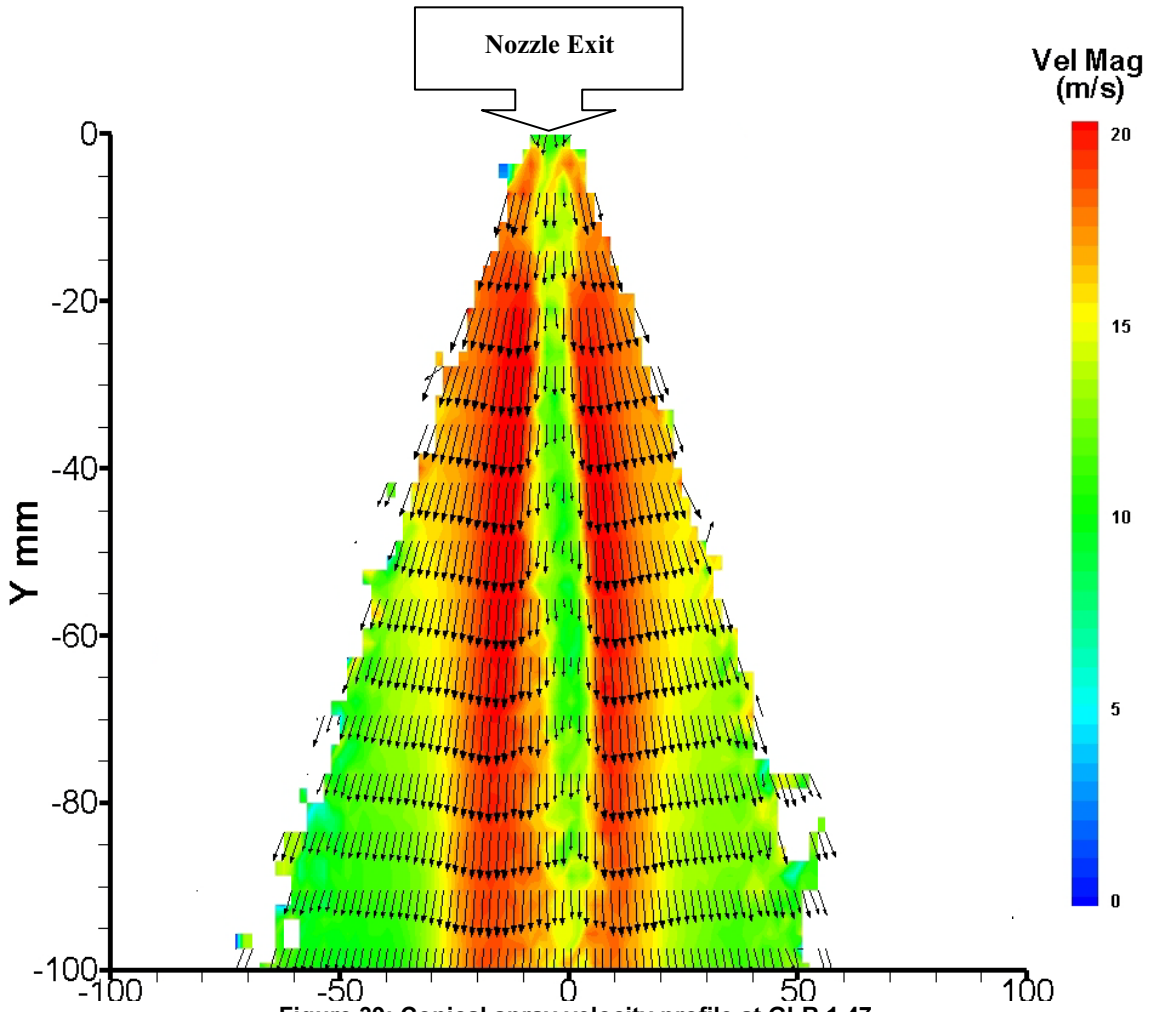

Figure 39: Conical spray velocity profile at GLR 1.47

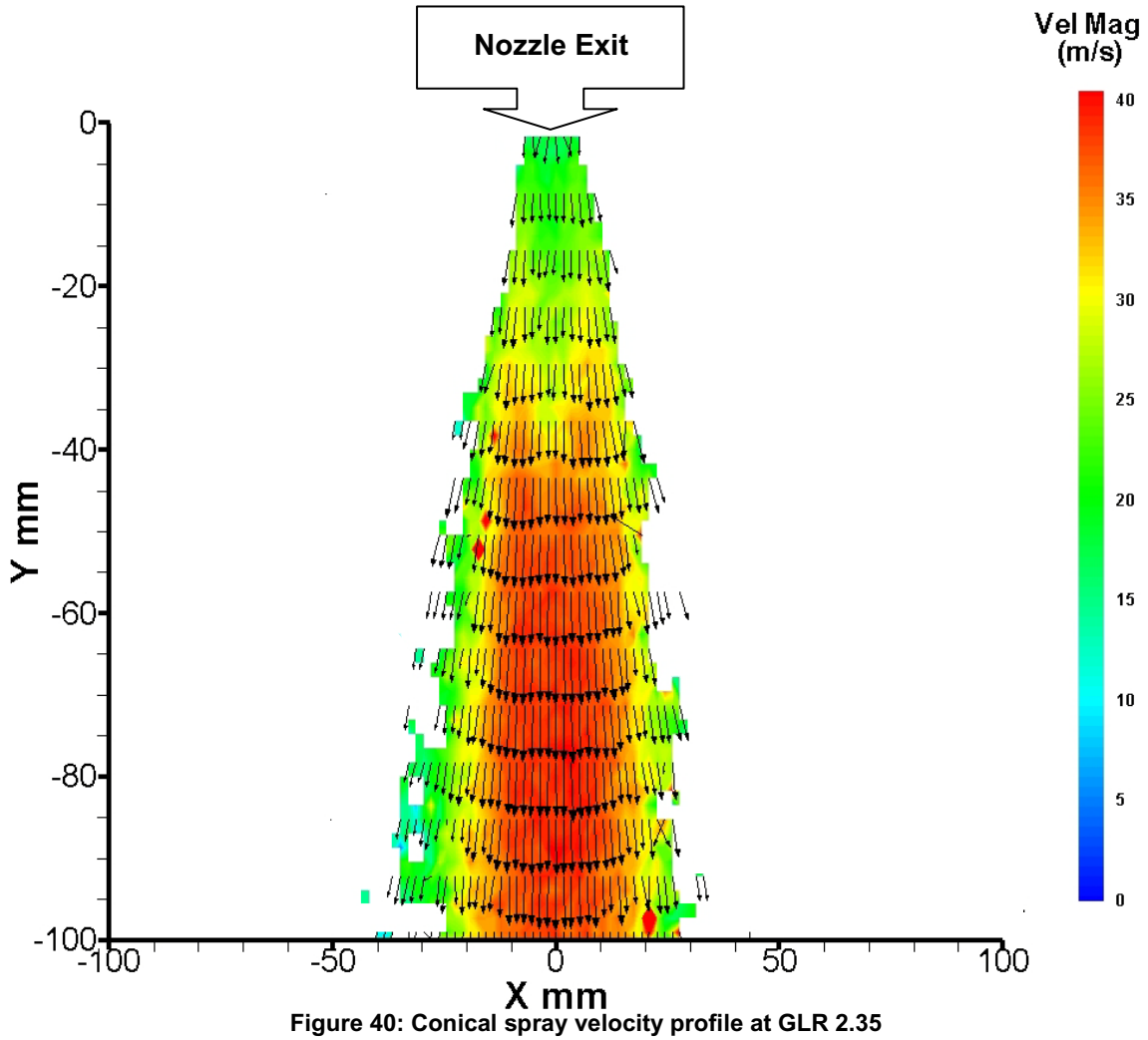

Figure 40: Conical spray velocity profile at GLR 2.35

4.1.4. Conical PDPA Results

The patternation images seen earlier showed that the conical spray was axisymmetric therefore PDPA scans were done across one line passing through the center line of the nozzle. The data presented here shows radial scans conducted at different distances from the nozzle's exit and at different flow rates to observe the variations in nozzle performance (e.g. diameters, velocity, flux…etc). Figure 41 shows the Sauter Mean Diameter (SMD) for each axial location from the nozzle's exit. First, notice that in Figure 41 (a) all the GLR settings showed two peaks of maximum SMDs being created. These maximum diameter peaks are a common occurrence in swirl type atomizers which corresponded to the densest parts of the spray's periphery where most of the liquid is present (26). In addition, note that the size distribution of the diameters varied from a bimodal distribution at a GLR of 0 to a less pronounced bimodal distribution at higher GLRs. The fluctuations in Figure 41 (a) at the 2.35 GLR were likely the result of visual obscuration of the PDPA receiver looking into a dense spray region.

At locations of 38.1mm and 76.2mm the PDPA was able to measure a larger radius due to the spray cone becoming wider at further axial locations as was seen by the patternation images. At the axial distance of 38.1mm, one can see that the SMD distribution widened substantially. Also note that the bimodal distribution at various GLRs still remained; however, the peaks diminished considerably compared to the peaks in the 12.7mm location.

The axial location of 76.2mm showed the widest distribution of SMDs and shows that the SMDs remained almost the same for all cases except at a GLR of 0. This indicated that the effect of the added air used to assist in the breakup of the droplets diminished at locations of 76.2mm and beyond.

The next set of graphs in Figure 42 shows the axial velocity distribution of the conical spray. In Figure 42 (a), GLRs of 0 and 0.75 shows a reversing flow tendency within the spray's central core where the smallest droplets occupied what is considered to be a hollow region. The reversing flow was the result of the aerodynamic forces of the liquid interacting with the ambient environment as well as the air swirler in the case of 0.75 GLR. Generally, higher ambient pressures resulted in greater shear forces being applied to the droplets as they left the nozzle. The reversing flow was the result of the shearing forces between the liquid and air (both ambient and injected air). The size of the droplets also played a role as smaller droplets were more susceptible to being driven by the air flow due to their lower momentum, whereas larger droplets tended to resist the air flow and move in accordance with their own high momentum when exiting the nozzle (26) (27).

Again two peaks are noticeable at GLRs of 0 and 0.75 where the high velocity magnitudes corresponded to the larger diameters shown previously in Figure 41. The reversing flow ceased to exist at locations further downstream of the nozzle where velocity profiles took on a Gaussian shape. The highest velocity peaks were recorded at a location of 38.1mm from the nozzle. The velocities were substantially lower at the 76.2mm locations; however the GLRs of 1.47 and 2.35 still showed significant magnitudes compared to the GLRs of 0.75 and 0. Recall that the SMD distribution in Figure 41 showed that added air had little effect on reducing droplet diameters at locations further away from the nozzle, yet the latest velocity data shows that the droplet velocities are maintained throughout the spray. This leads one to conclude that most of the air's energy is being used to transport the droplets rather than break the droplets into smaller diameters.

The next set of results from the PDPA show volume flux data obtained by the PDPA system. The volume flux is used as an indicator to determine where certain areas of the spray may have higher liquid concentrations and is compared to the shadowgraph observations made earlier.

The plots of Figure 43 show volume flux ratio based on the maximum flux recorded by the PDPA system. Initially, the volume flux at the 12.7mm location showed relatively low fluxes accompanied by the bimodal peaks pertaining to the spray cone's periphery. The widest peak recorded was for GLR= 0 (No Air) scenario, which indicated that the spray cone was widest when no air is used and narrowed when more air was added. At the location of 38.1mm the difference in flux ratios is apparent and the higher GLR setting of 2.35 showed the most significant increase, whereas other GLR settings remained relatively low. The volume flux taken at the 76.2mm location showed a substantial decrease since the data was taken at a relatively far away distance from the nozzle exit. In essence, the volume flux shows that higher liquid concentrations were found up until 38.1mm from the nozzle exit.

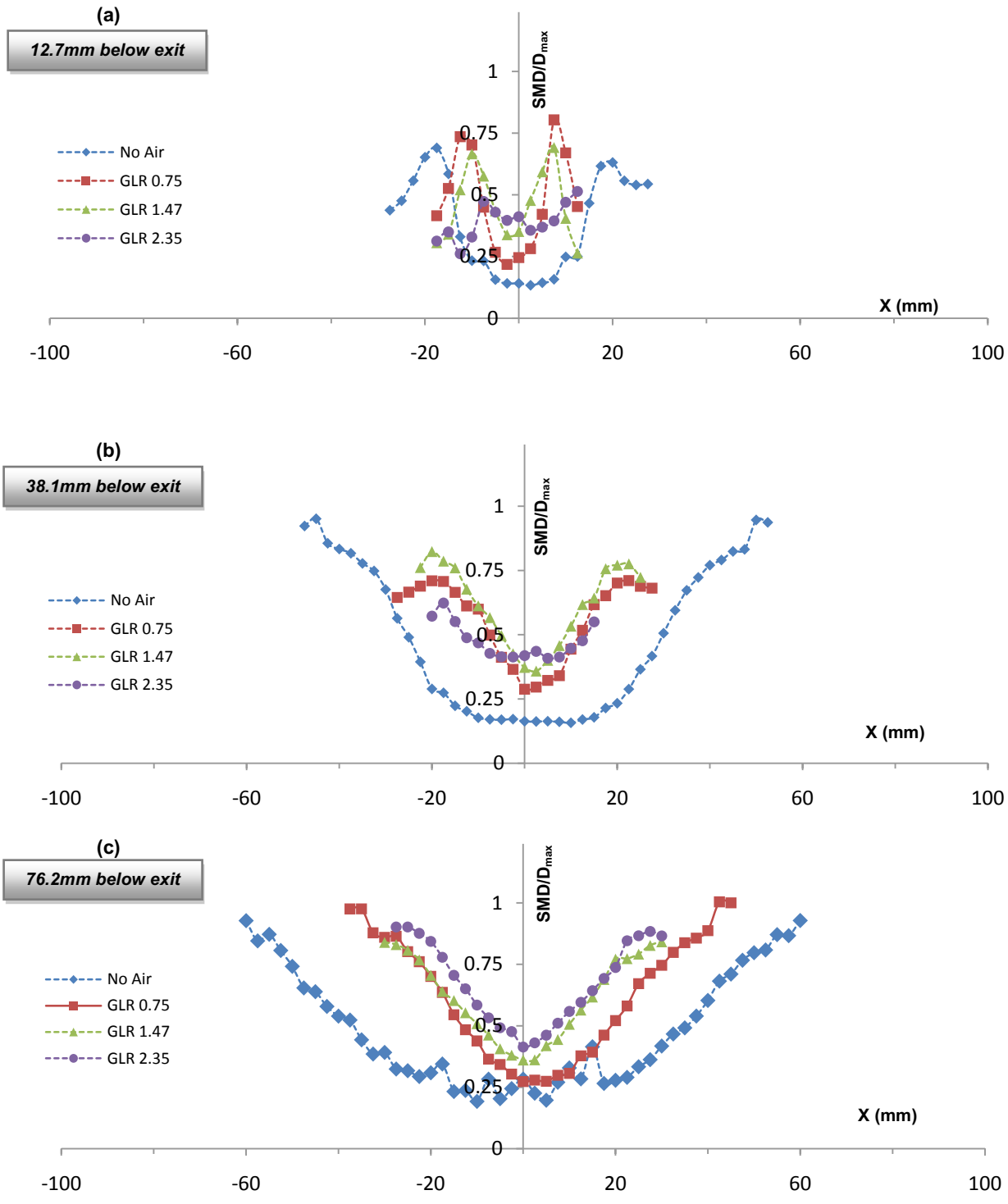

Figure 41: Conical spray SMD distribution taken at (a) 12.7mm below exit (b) 381.1mm below exit (c) 76.2mm below exit

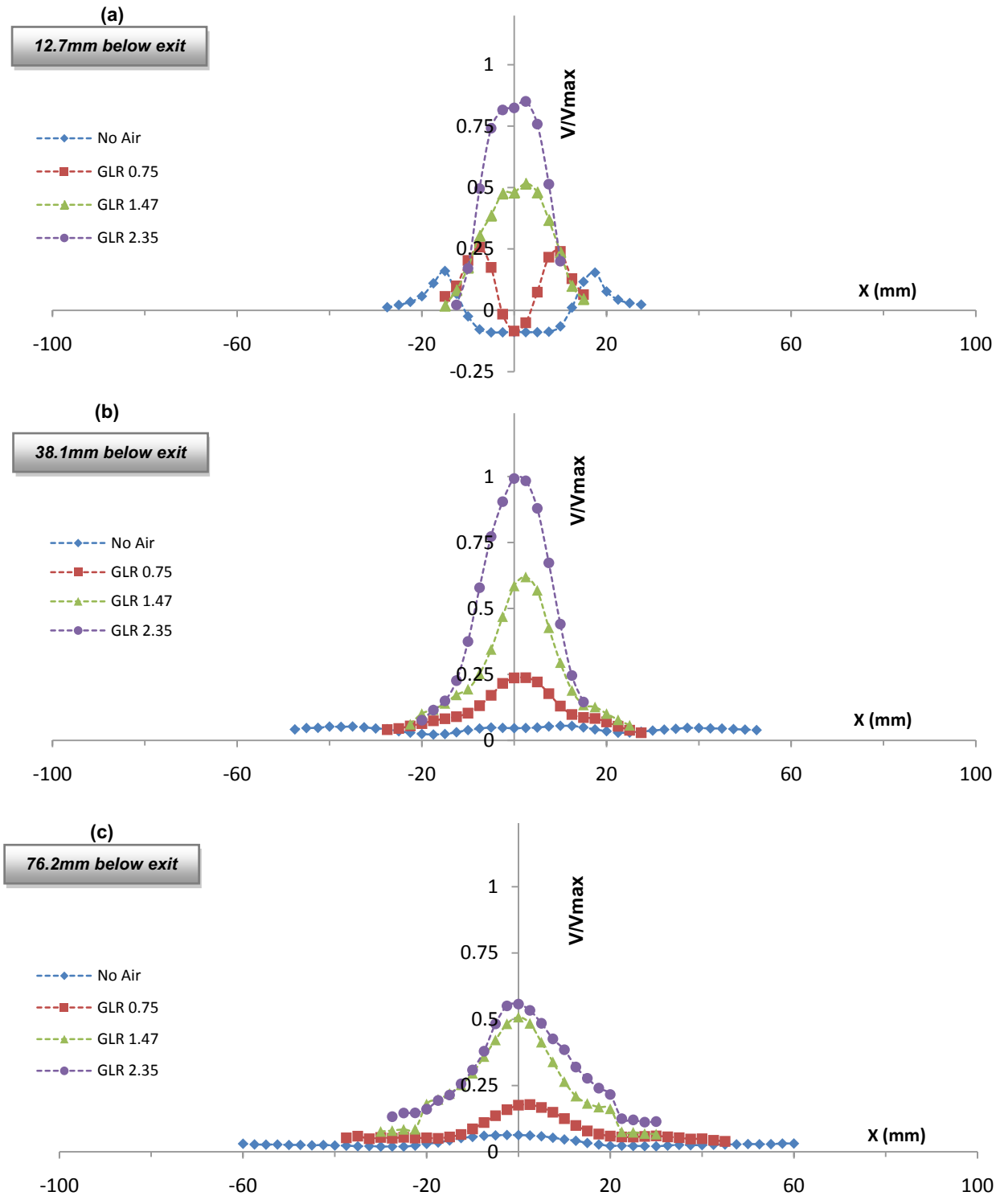

Figure 42: Conical velocity distribution taken at (a) 12.7mm below (b) 38.1mm below (c) 76.2mm below exit

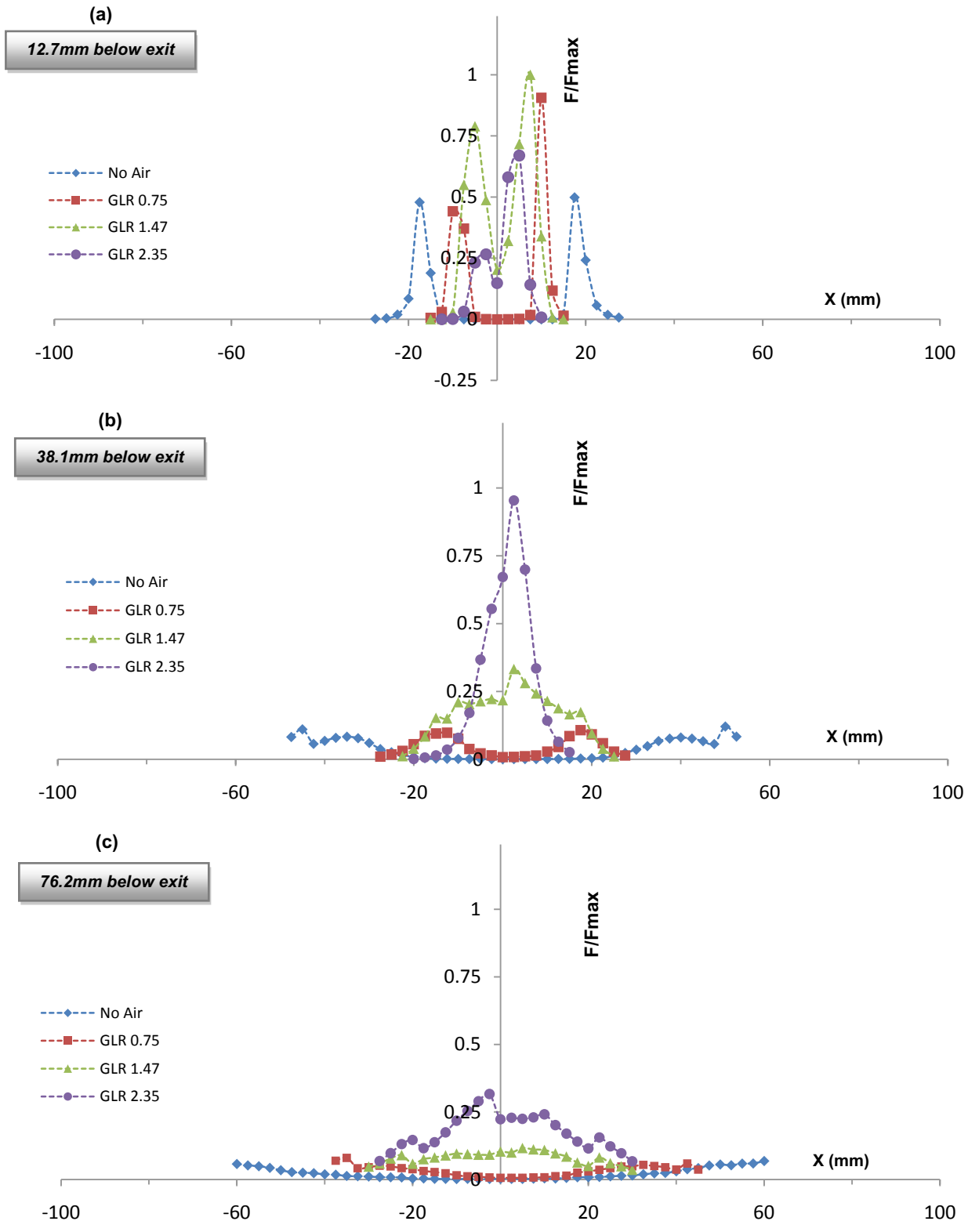

Figure 43: Conical volume flux distribution taken at (a) 12.7mm below exit (b) 38.1mm below exit (c) 76.2mm below exit

4.2. Elliptical Nozzle

4.2.1. Elliptical Shadowgraph

Shadowgraph images captured the elliptical spray in two different views. The left column images are for the major axis and the right column, the minor axis. Recall that the elliptical nozzle's liquid swirler is similar in design to the conical nozzle, and that the only difference between both nozzles is in the method of how air is issued to assist in the atomization process. The effect of the air profiler is clearly visible in Figure 44 (a) and (b) where the major axis view show a spray cone angle of 110º ±5º in (a), and an a narrow angle of 85º ±5º in (b). Worth pointing out is that the minor axis spray angle is also larger than the spray cone angle of the conical spray mentioned earlier when run at similar GLRs.

At higher GLRs in figures 44 (c) through (f), the elliptical spray shows a sign of higher quality atomization as the liquid sheet ceases to exist. This also however made spray angle determination impractical as only a silhouette of droplets remained making any spray angle determination highly subjective. Nevertheless, the silhouettes of droplets in the minor axis show a tendency of decreasing spray cone angle in the minor axis. The major axis silhouette was not as clear as the minor axis leading to the possibility that there is a higher liquid concentration in the view of the minor axis than there is in the major axis.

Shadowgraph analysis of the elliptical spray did not reveal distinguishable angles; however, the relatively high quality atomization of the elliptical spray showed signs that the spray is creating a much wider distribution of water droplets covering a larger area in the view of the major axis. Even the minor axis has shown signs of atomization being of a higher quality than what was observed in the conical spray earlier. The following section will show optical patternation images that further characterizes the elliptical spray's performance.

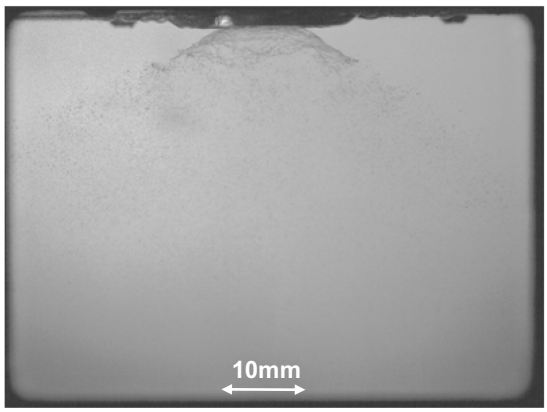

(a) GLR 0.75 Major Axis

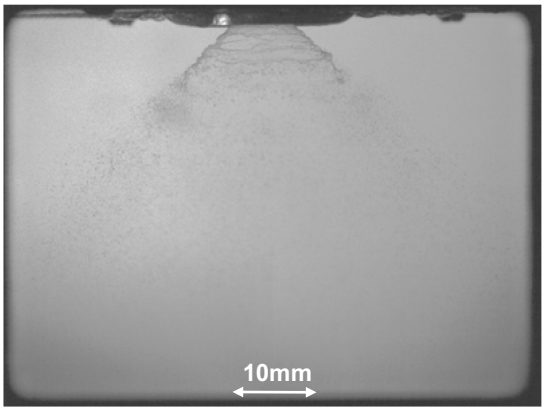

(b) GLR 0.75 Minor Axis

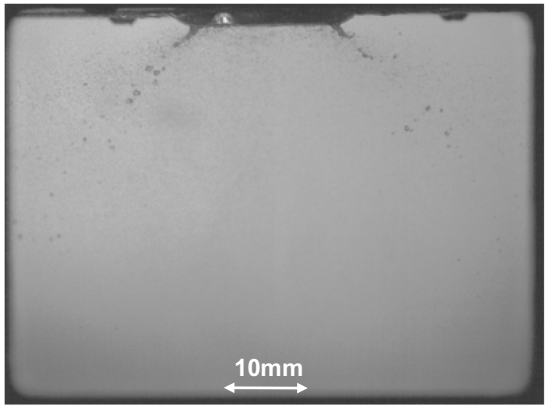

(c) GLR 1.47 Major Axis

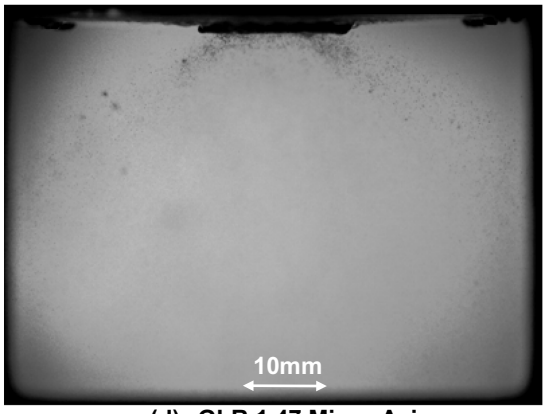

(d) GLR 1.47 Minor Axis

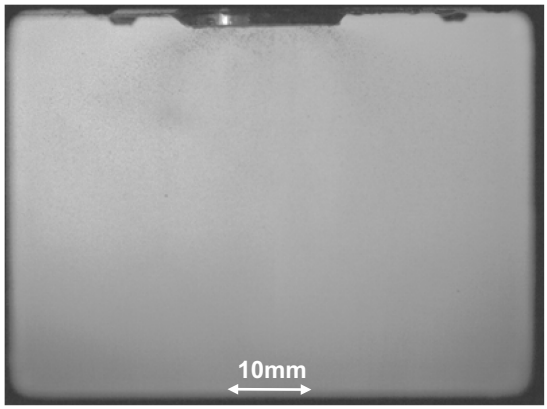

(e) GLR 2.35 Major Axis

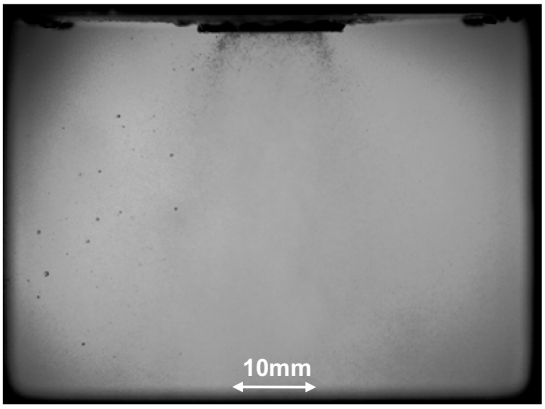

(f) GLR 2.35 Minor Axis

Figure 44: Shadowgraph imaging of the elliptical spray. The difference in spray angles is evident in (a) and (b), however it is difficult to determine the spray angle at higher air flows due to the high quality atomization.

4.2.2. Elliptical Optical Patternation

Figure 45 shows the pattern images of the elliptical spray spray taken at 12.7, 38.1, and 76.2mm below the nozzle's exit at GLRs ranging from 0 to 2.35. Initially, the spray pattern is a common circular hollow cone nozzle when no air is supplied to the air profiler. The addition of air flow to the nozzle causes a sudden change in the nozzle's spray pattern and shows interesting characteristics. First, the elliptical spray actually takes on a more rectangular or parallelogram form instead of the expected elliptical pattern. More importantly, the increasing of the GLR at 12.7mm causes the spray pattern to grow in size allowing for a greater distribution of the liquid. The GLR of 1.47 and 2.35 show what appear to be streaks that increase the area covered by the spray. It is also possible that the streaks are swirl streaks that will be discussed later. The other observation made on all GLR settings is that the spray has a wider distribution when moving downstream (i.e. 12.7 to 38.1mm).

At a location of 76.2mm from the nozzle exit the spray pattern becomes almost homogenous and the droplets effectively fill the images completely leaving a faint hollow region within the central core of the spray. The 76.2mm did however present an interesting phenomenon where the hollow region at various GLRs takes on helical shapes. These shapes along with the streaks the other images lead to the consideration of the swirl component of the spray.

Recall that the pattern images shown here are based on the superimposition of a hundred images that make up the overall spray pattern; therefore the appearance of a streaks and starbursts like images at higher GLRs may have been an indicator to a swirl motion that was sequentially captured by the patternation method. The individual spray images where studied separately to confirm the presence of any swirl motion, and the images of Figure 46 are samples of the elliptical spray showing swirling movement at 38.1mm and 76.2mm below the

nozzle's exit. The swirl motion present in the elliptical spray lead to the consideration that the droplet distribution of the elliptical spray has a transient characteristic. This type of swirl motion could therefore have an effect on the degree of error present in both the PIV and PDPA analysis which will be discussed in upcoming sections.

Figure 45: Optical patternation of the elliptical spray taken at various heights from the nozzle exit

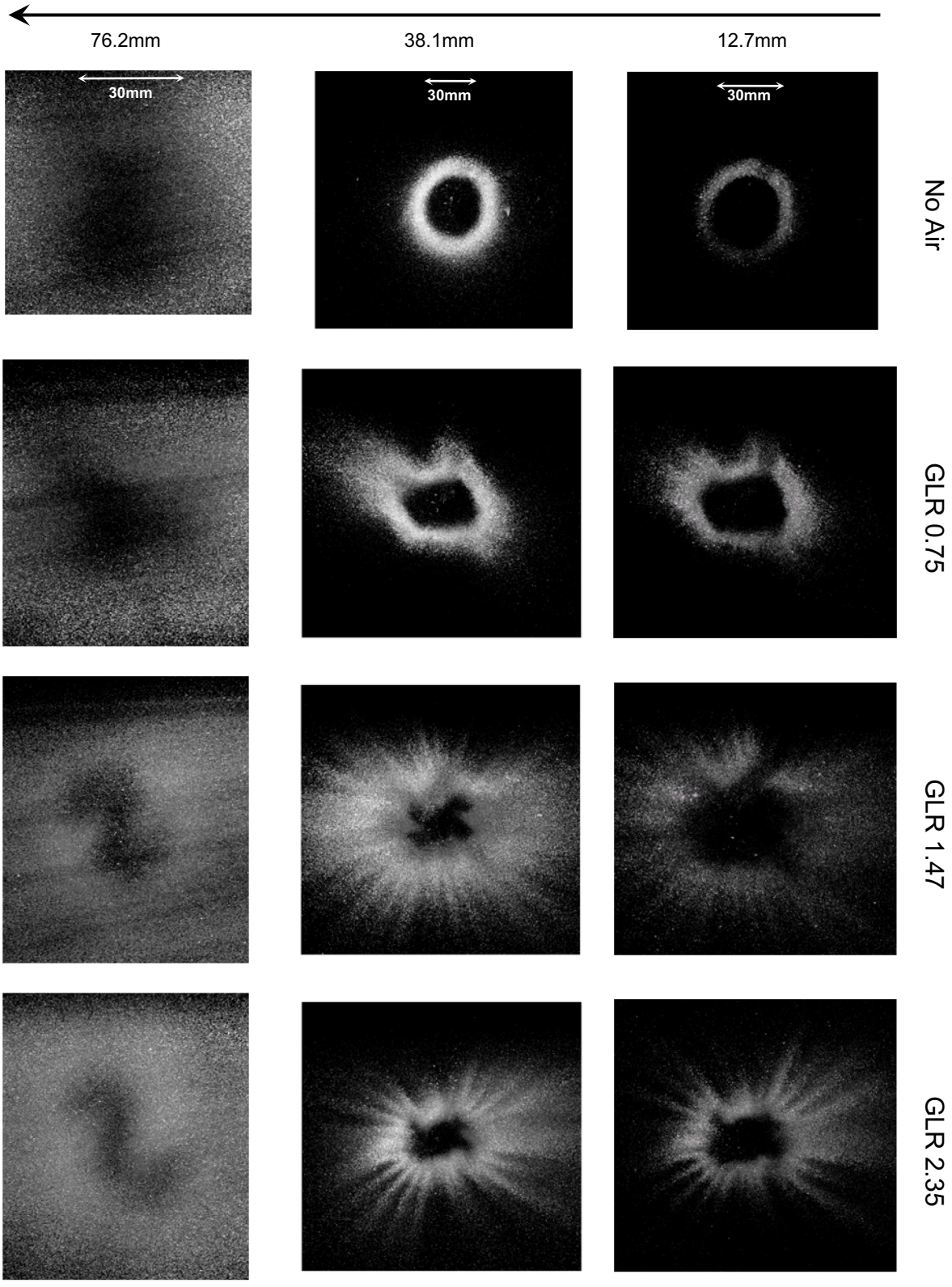

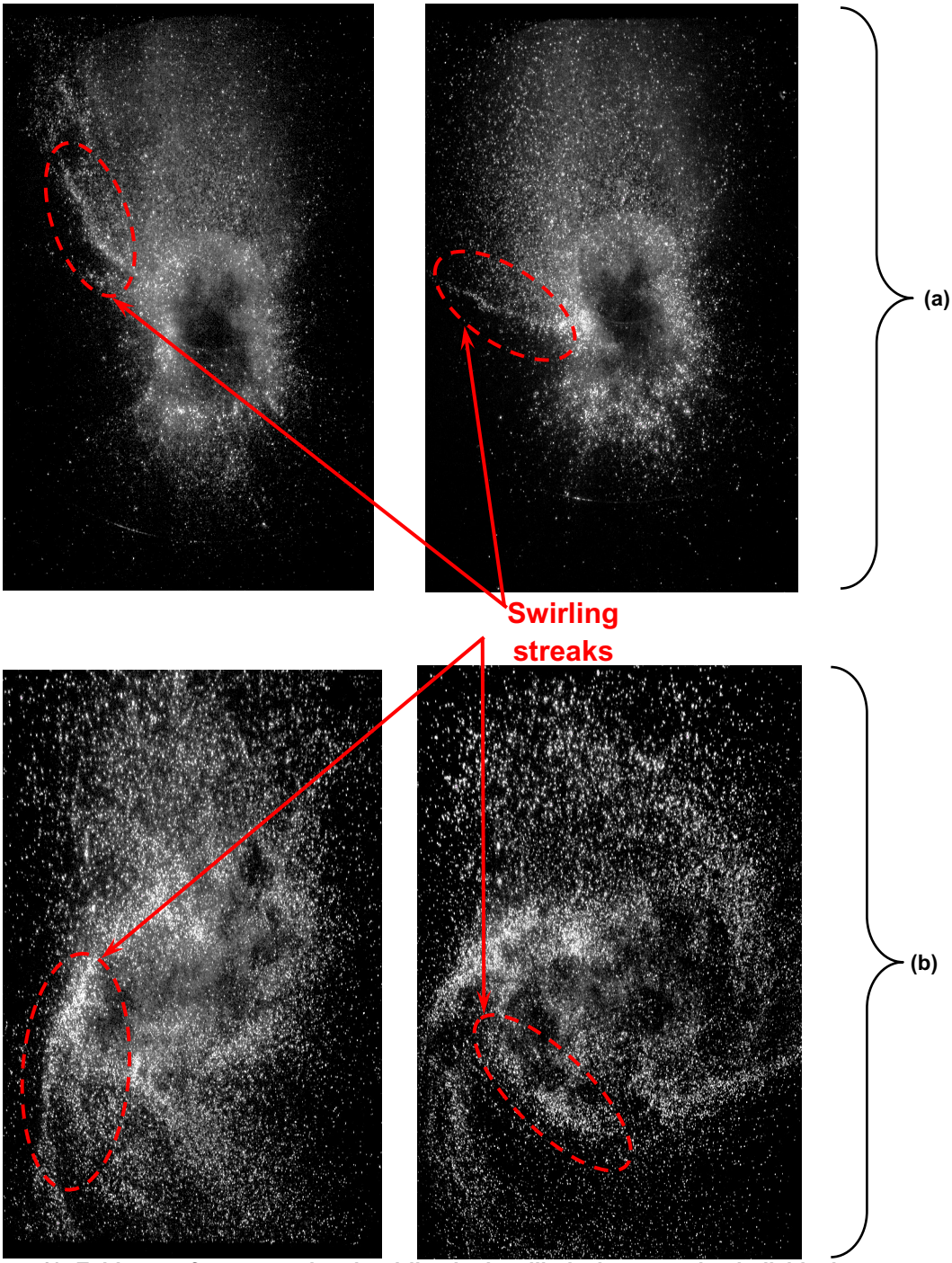

Figure 46: Evidence of cross sectional swirling in the elliptical spray using individual images taken from the optical patternation experiments (a) 1.5 in below exit (b) 3.0 in below nozzle exit

4.2.3. Elliptical PIV Results

The PIV analysis on the elliptical spray for GLRs of 0.75 to 2.35 is shown in Figure 47. The images in the left column represent the major axis view where one can imagine the laser sheet being emitted from the side of the paper. The first observation to note is that along major axis (Figure 47 a, c, and e) there is no significant change in the shape of the velocity profile. Overall maximum velocity magnitude determined by the PIV was at 12 m/s. There is a slight widening of the spray angle in (e) when the nozzle was running at a GLR of 2.35 and the image also appears to be nonsymmetrical. The lack of symmetry in Figure 47 (e) was likely the result of laser sheet being offset from the ellipse's plain of symmetry. Furthermore, Figure 47 (e) also shows area where the velocity contour near the exit of the nozzle has little or no velocity gradient. The likely cause for this again is possibly due to the saturation of liquid droplets and ligaments that increase the overall noise level in that particular area of the image making it difficult for the PIV to cross correlate any valid signals.

The minor axis velocity profile (Figure 47 b, d, and f) on the other hand tells a different story. Variation in GLR setting caused immediate and sudden changes in velocity profile. The significant change in the minor axis profile shows the direct effect the air profiler has on the minor axis when GLR is changed. At a GLR of 0.75 that velocity profile takes on an inverted V like formation with high velocity magnitudes of 12 m/s occupying the main spray periphery where most of the liquid is situated. The pattern is repeated at GLR of 1.47 where the magnitude of the velocity has increased to its maximum of 15 m/s. Issues regarding saturation of the image again arise in Figure 47 (f) where the GLR is set to 2.35. Again, the reduction in magnitude is likely the result of areas near the nozzle exit being oversaturated with droplets the hinder signal correlation for the PIV.

The PIV results of the elliptical spray did clearly identify two unique velocity profiles in the resultant spray. There were however some issues regarding image saturation that may have reduced the PIV's accuracy in this scenario. Furthermore, recall that the patternation images show signs of swirl motion being present in the elliptical spray. Droplet motion in and out of the PIV's laser sheet may have therefore reduced the accuracy in the analysis as this could have caused a droplet to appear in one image and disappear in the next image. Losing track of such droplets may result in an invalid detection (28). This setback proves how adding a point-wise measuring system such the PDPA can obtain valid results where the PIV had difficulties as will be seen in the next section.

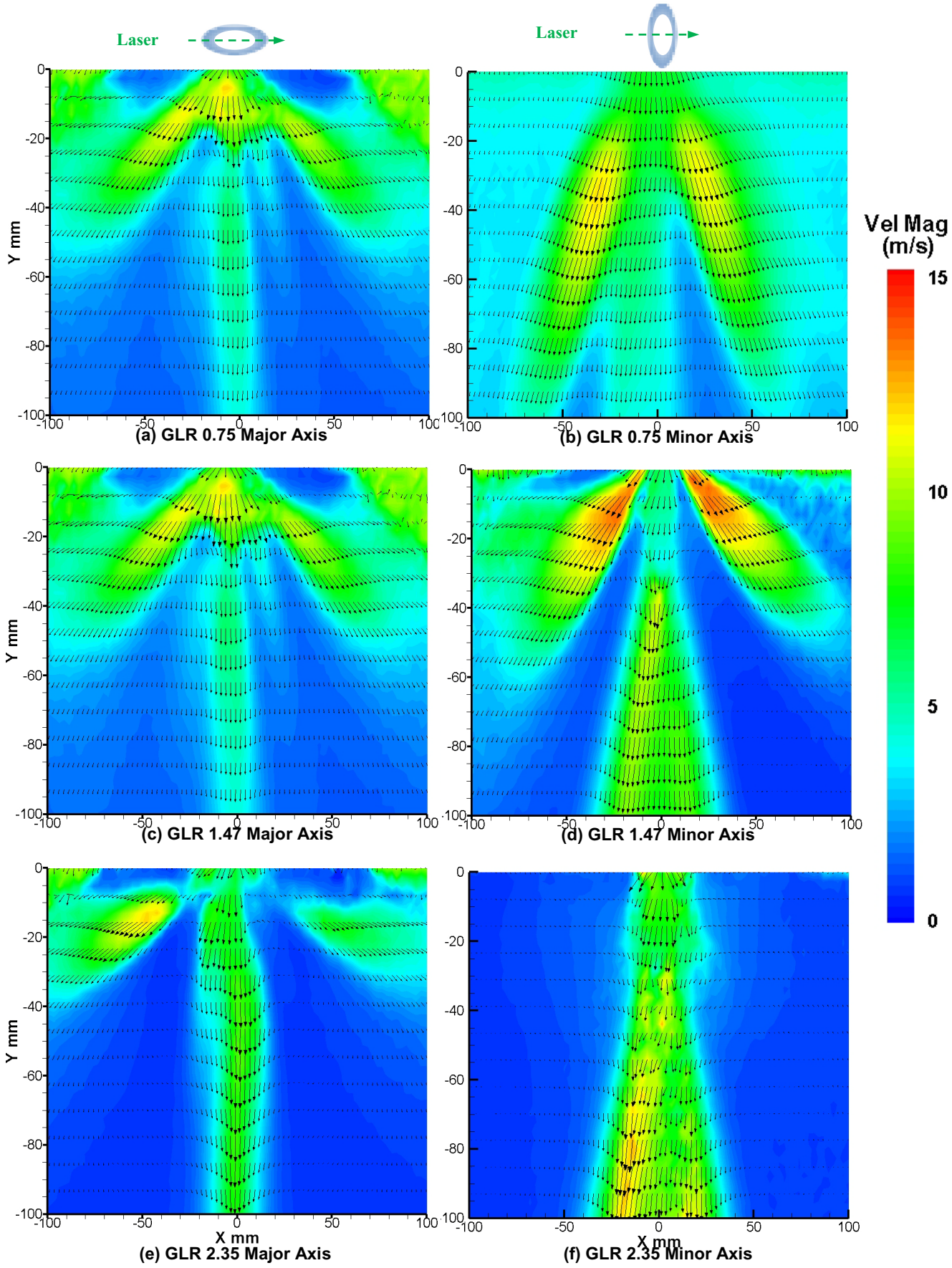

Figure 47: PIV image of the elliptical spray ranging from GLR 0 to GLR 2.35 (left) Major Axis (Right) Minor Axis

4.2.4. Elliptical PDPA Results

The imaging methods seen earlier have shown the unique characteristics of the elliptical spray. The results suggest that the quality of atomization in terms of droplet size is very fine and that atomization of water occurs almost instantly upon leaving the nozzle's exit. Additionally, the patternation images clearly showed that the elliptical spray posses a highly complex three dimensional pattern. Therefore, the PDPA measurements along the major and minor axis are expected to yield substantially different results with respect to each other. Figure 48 through 50 shows SMD distribution of the elliptical nozzle's spray captured at various GLRs mentioned earlier at axial distances of 12.7, 38.1 and 76mm from the nozzle's exit along major and minor axis planes. In Figure 48 through 50, the SMD distribution in all cases show a more uniform spread of droplets. Closer inspection of Figure 48 at 12.7mm below the nozzle exit shows signs of fluctuations; however, the trend of the distribution is more uniform than the conical spray. The measurement at 12.7mm is relatively close to the nozzle. It is therefore likely that 12.7mm is in a transition zone between primary and secondary atomization breakup mode in which not all of the liquid has been completely atomized. Therefore, the presence of non spherical droplets in this region may hinder the PDPA's ability to obtain valid diameter measurements of the droplets (28). In this case, the maximum deviation in diameter measurements was in regions of low data flow which are in hollow regions of the spray and its periphery resulting in a maxim standard deviation of 5.5 microns. Also, data was cut off from Figure 48 (b) because no data was detected by the PDPA in the central region.

The SMDs do not change significantly when GLRs are varied. This may in fact be the consequence of the air profilers responsible for creating an elliptical profile. The velocity distribution on the other hand showed greater changes. Figure 51 through 53 show the

velocity distribution taken at the same time as the SMD distribution measurements. The first note is the dramatic difference in spray velocity at the 2.35GLR when compared to other flow rates. In this case the maximum velocity distribution is recoded to be 21.67 m/s along the major axis and 26 m/s along the minor axis. Generally, the spray velocity is highest in the center of the spray where the peak velocity eventually begins to diminish when moving downstream to locations further away from the exit of the nozzle.

Looking back at the SMD distribution figures of the elliptical spray, one may come to the realization that most of the kinetic energy in the elliptical spray is consumed in uniformly breaking up the liquid into small finer droplets, rather than having deeper penetration such as that of the conical spray. This is evident in the fact that there was little change in the diameter distributions yet velocity magnitudes showed great differences along various axial locations and GLR settings. Volume flux measurements using the PDPA also reinforce the observation.

Looking back at the velocity profiles from the PIV results, it is evident that the maximum velocity magnitudes do not directly match between the PIV and PDPA. As mentioned earlier, one of the issues with the PIV is its lack of spatial resolution where it is unable to clearly distinguish individual droplets. Furthermore, the issue of oversaturation near the exit of the elliptical spray may have contributed to the discrepancy in the results.

The volume flux measurements in Figures 54 through 56 shed more information on the relationship between the droplet diameters and their velocities. In all cases, the GLR of 2.35 showed the highest volume flux. In addition, the GLR of 2.35 in all axial locations shows the greatest amount of flux compared to other GLR cases. The flux indicated that the spray

is far more wide spread and that more energy is spent on droplet dispersion than on transporting droplets further downstream (i.e. penetration). The combination of high velocity yet low volume flux accompanied with little change in droplets indicates that there is a high air velocity gradient in the center where liquid concentration is relatively less than areas further away from the center.

The flux measurements have also shown that the spray is empty in some areas; however there is evidence of some low volume flow rates in the center. It is possible that the elliptical spray entraps some droplets within the spray core; however, it is also possible that the PDPA scan did not pass directly through the centerline axis properly as this is subject to human error in determining the central axis line of the nozzle.

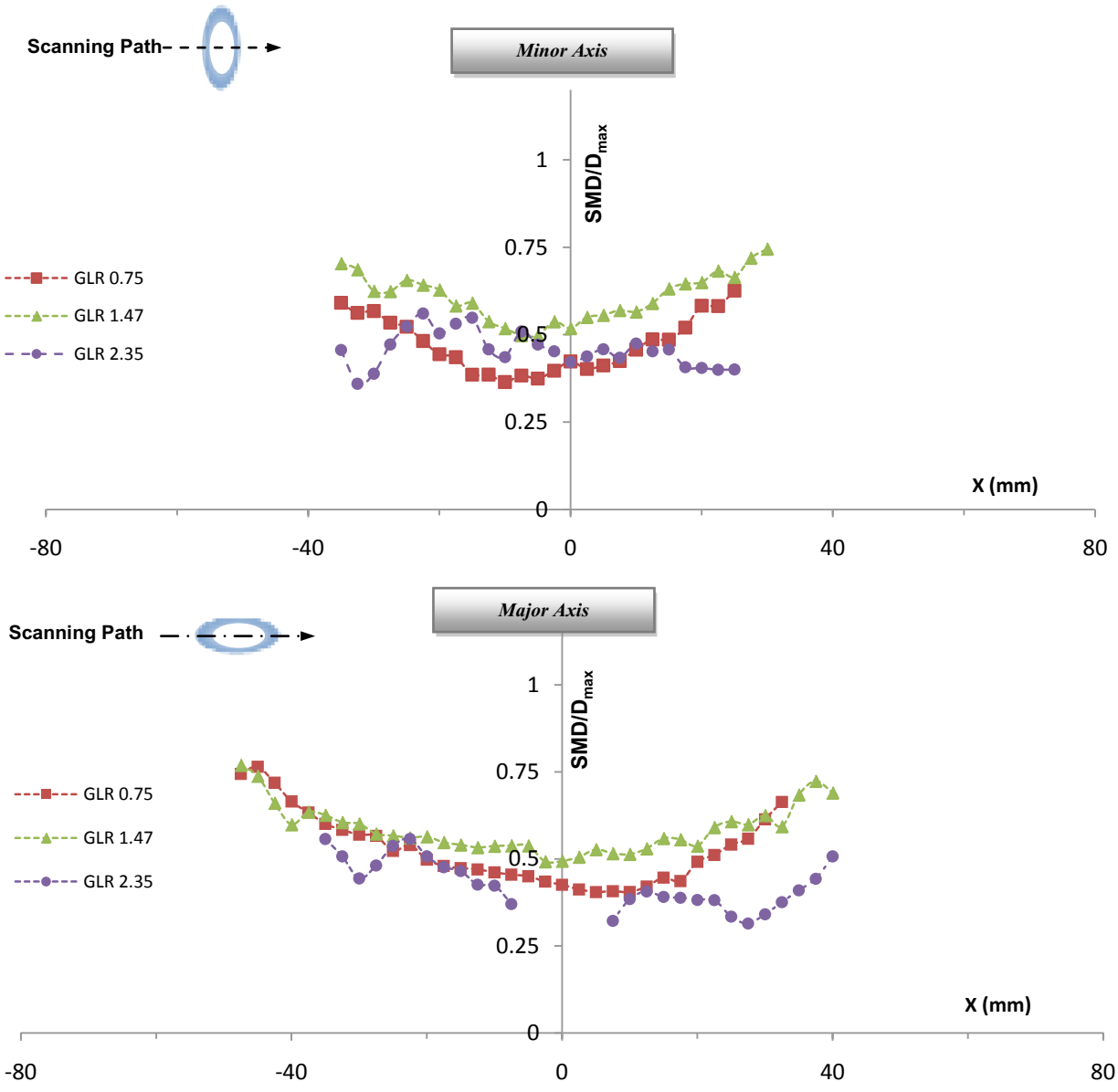

Figure 48: Elliptical SMD distribution at 12.7mm below exit

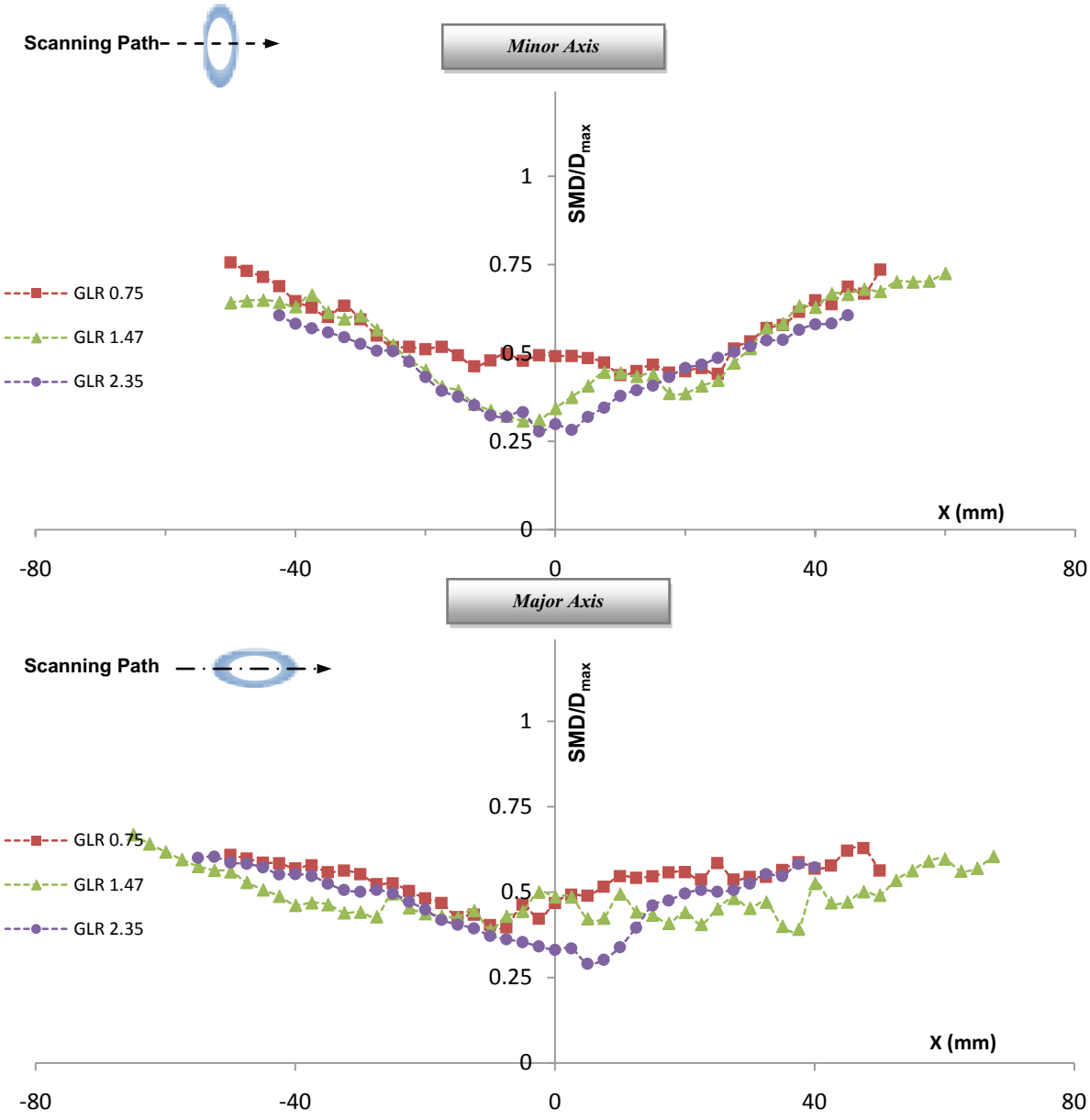

Figure 49: Elliptical SMD distribution taken at 38.1mm below exit

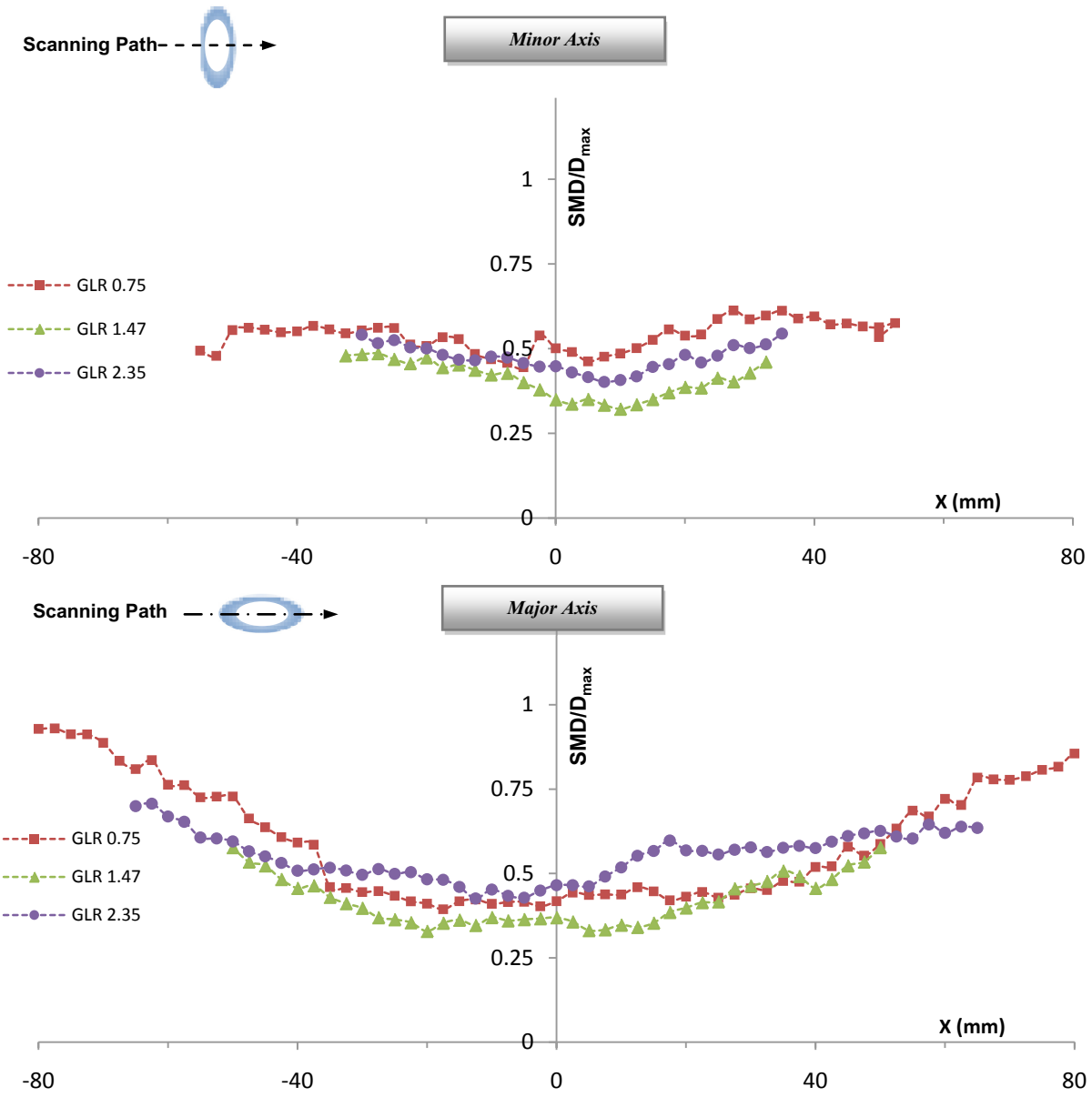

Figure 50: Elliptical SMD distribution taken at 76.2mm below exit

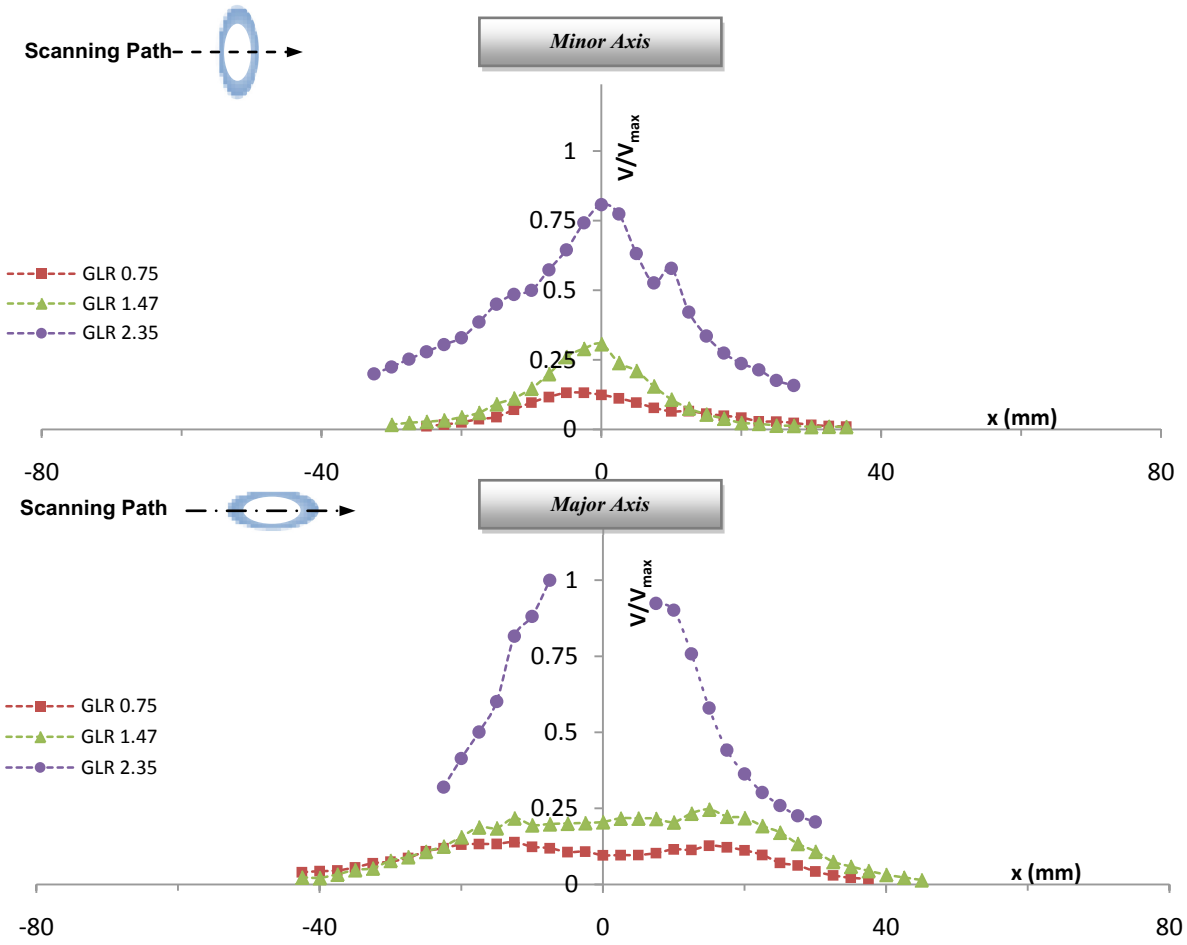

Figure 51: Elliptical velocity distribution taken at 12.7mm below exit

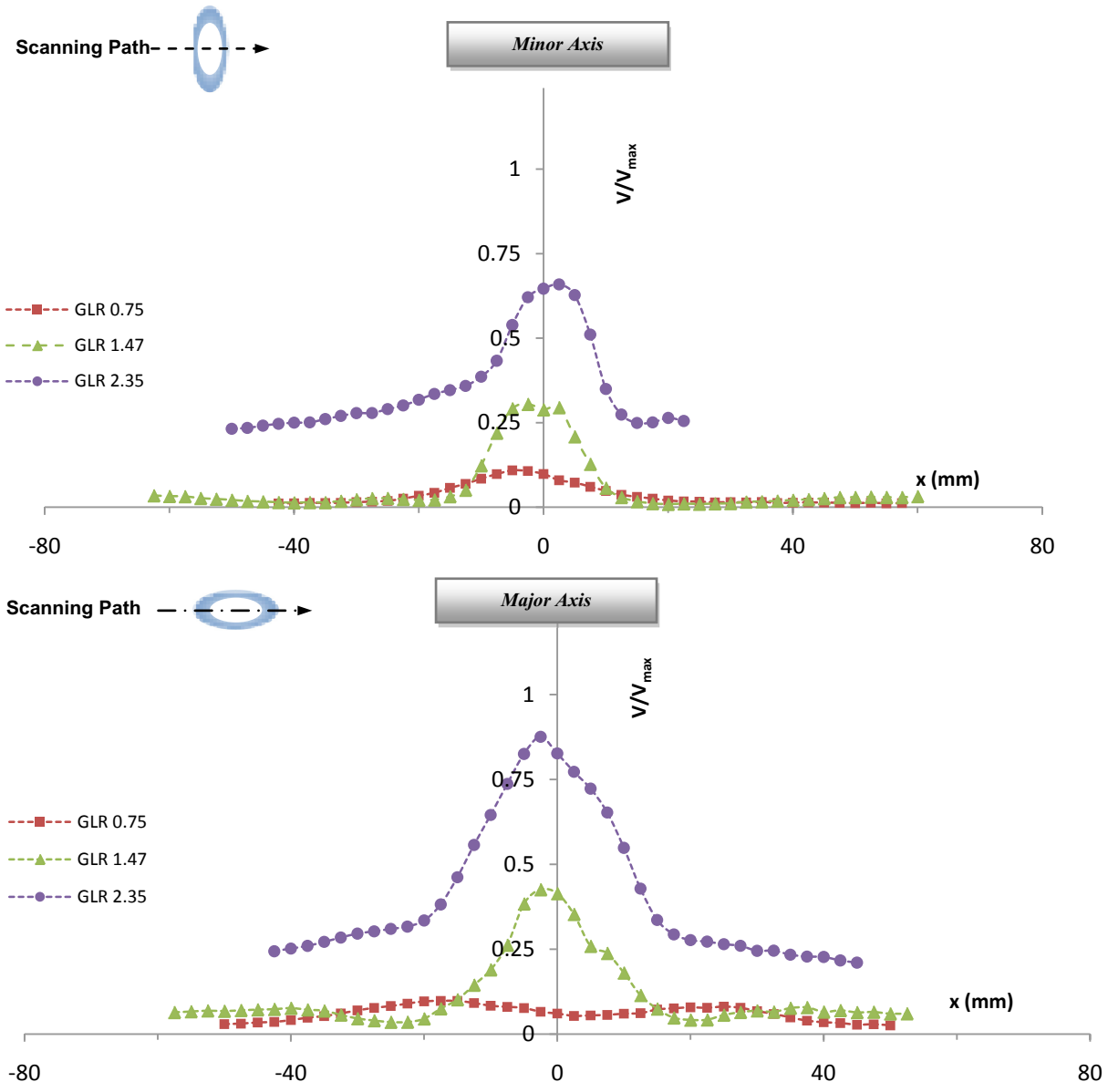

Figure 52: Elliptical velocity distribution taken at 38.1mm below exit

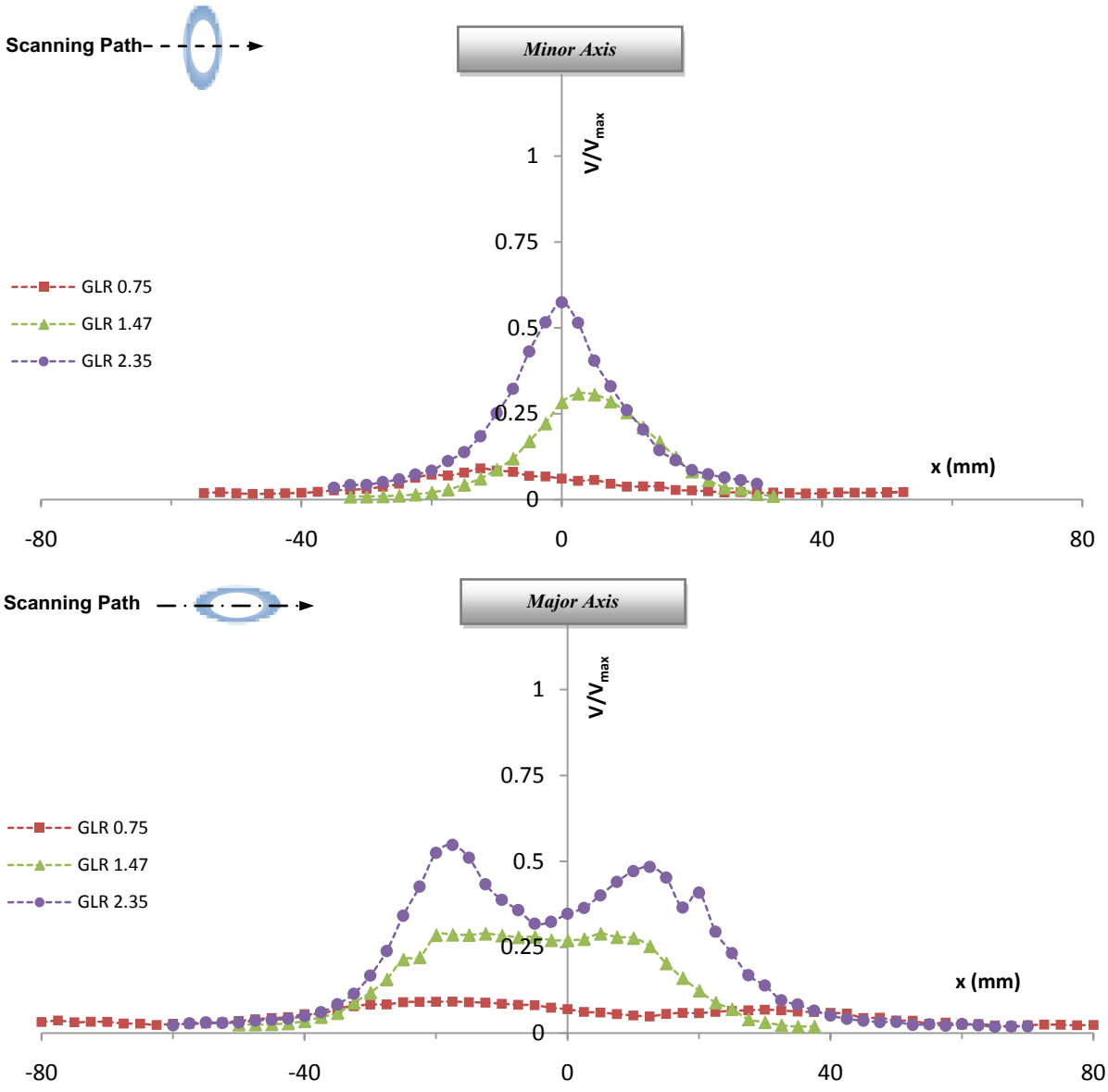

Figure 53: Elliptical velocity distribution taken at 76.2mm below exit

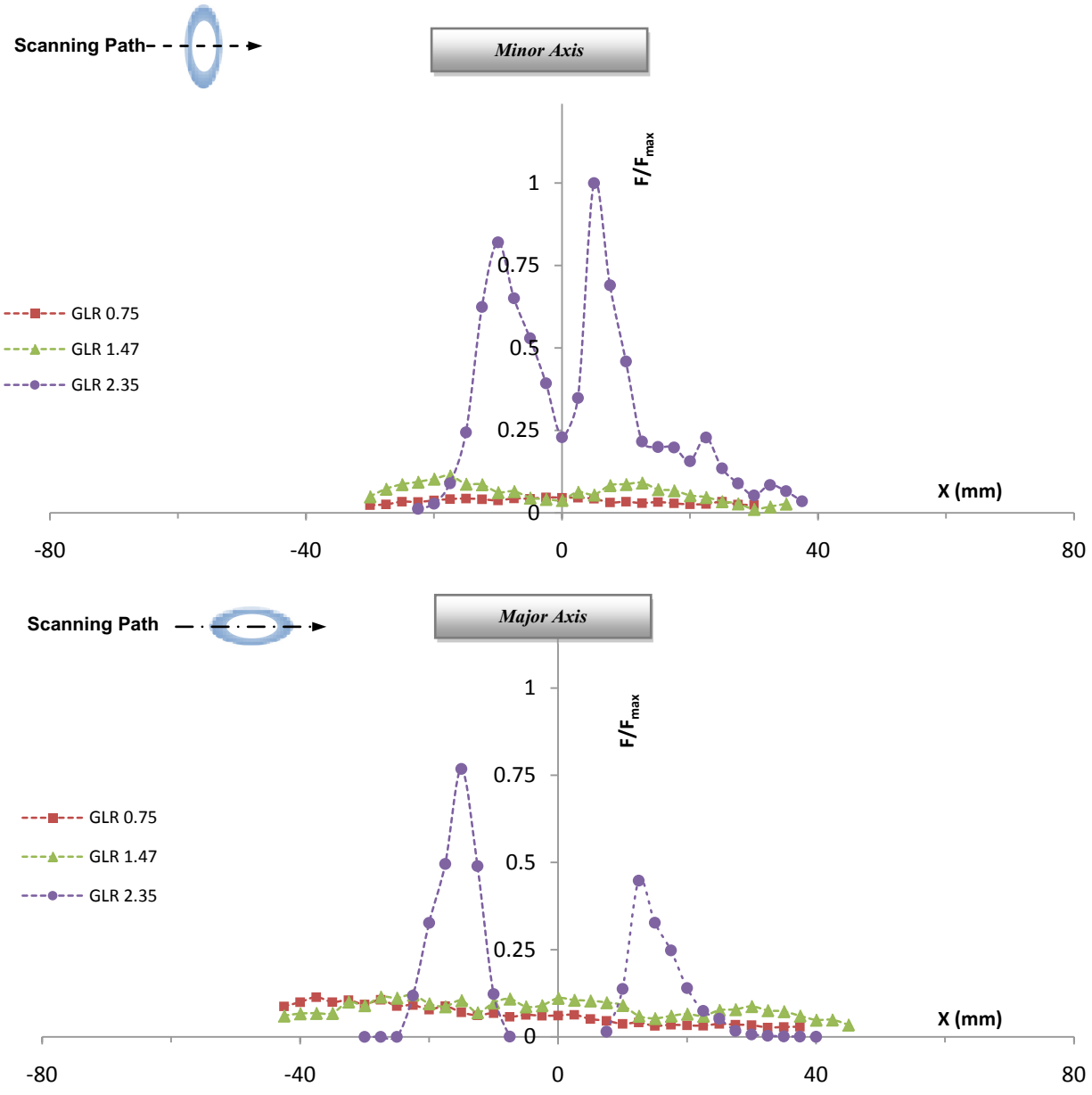

Figure 54: Elliptical volume flux taken at 12.7mm below exit

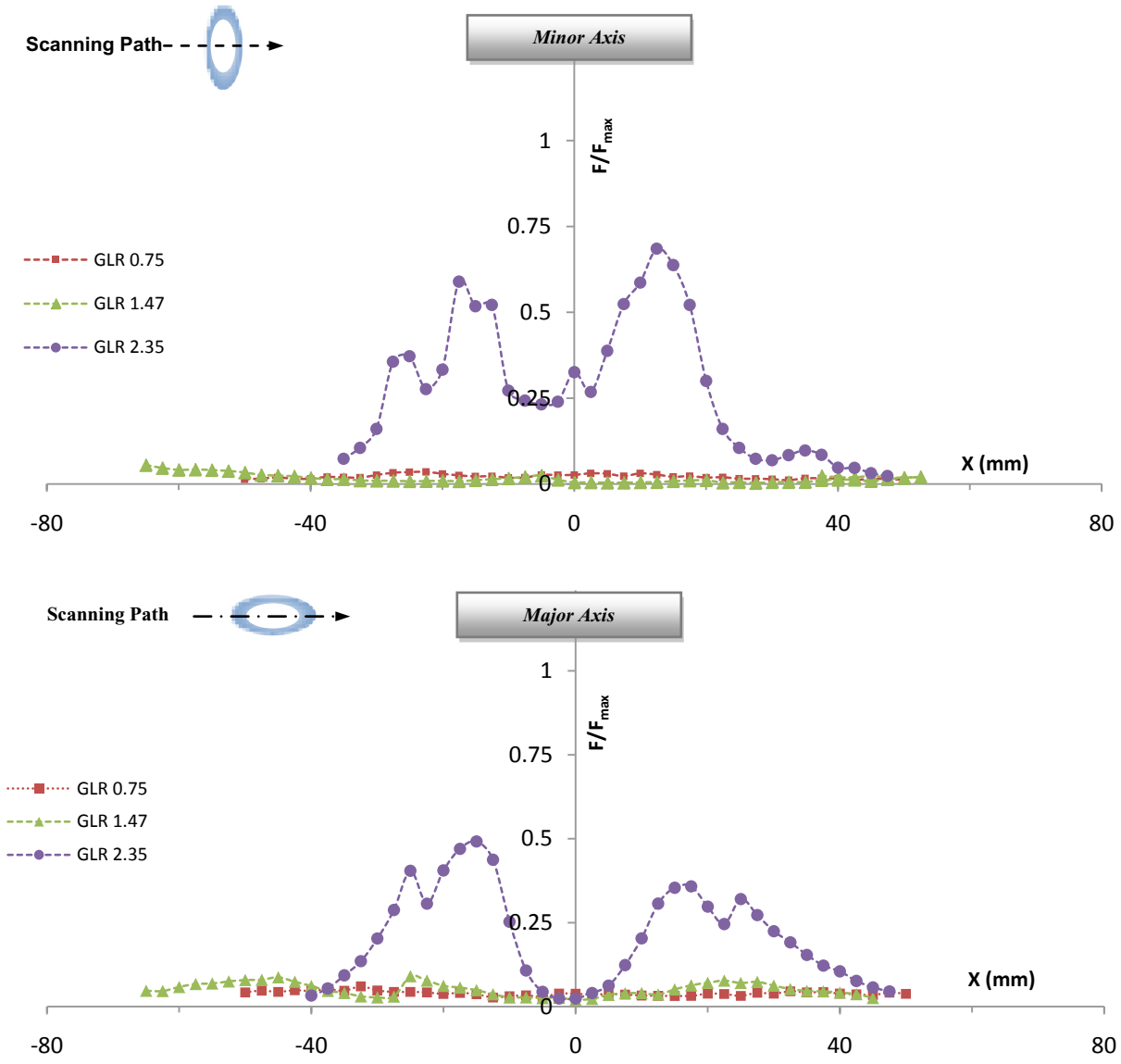

Figure 55: Elliptical volume flux taken at 38.1mm below exit

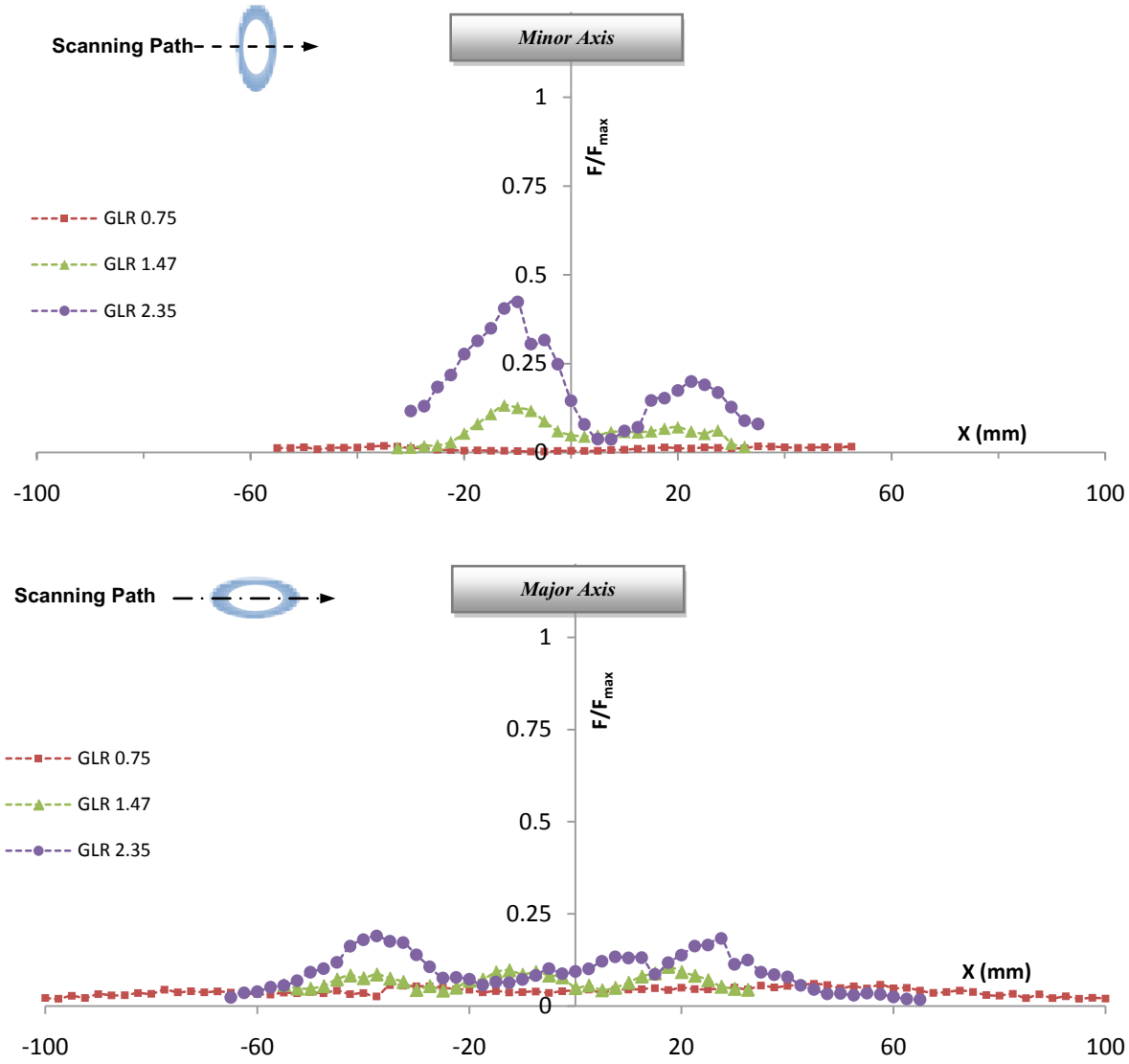

Figure 56: Elliptical volume flux taken at 76.2mm below exit

Finally, the swirl motion that was identified by the optical patternation leads to the consideration of the out of plane motion of some droplets (i.e. droplets entering and leaving the laser sheet). Other experimental works have shown that the out of plane motion of particles entering and leaving the laser sheet plane increases the overall error in PIV measurements (29) (30) (18). In this case, the swirl motion was not only picked by the patternation but PDPA velocity measurements of the nozzle's radial (horizontal) velocity also confirm the presence of high velocity magnitudes that would have left a thin laser sheet. Figure 57 and Figure 58 below show a plot of the radial velocity in the major and minor axis respectively. Notice that the major axis radial velocity shows strong indications of swirl motion since an axisymmetric velocity swirl of 10 m/s was captured. On the other hand, the radial velocity of the minor axis fluctuates and has a lower magnitude and is only 4m/s. Ideally in a circular spray both axis should show similar result; however, in this case the minor axis radial velocity is reduced owning to effect of the air profiler that disturbs the swirling effect causing the droplets to experience a downward motion and less radial motion. The last set of results looks into the volume flux measurements.

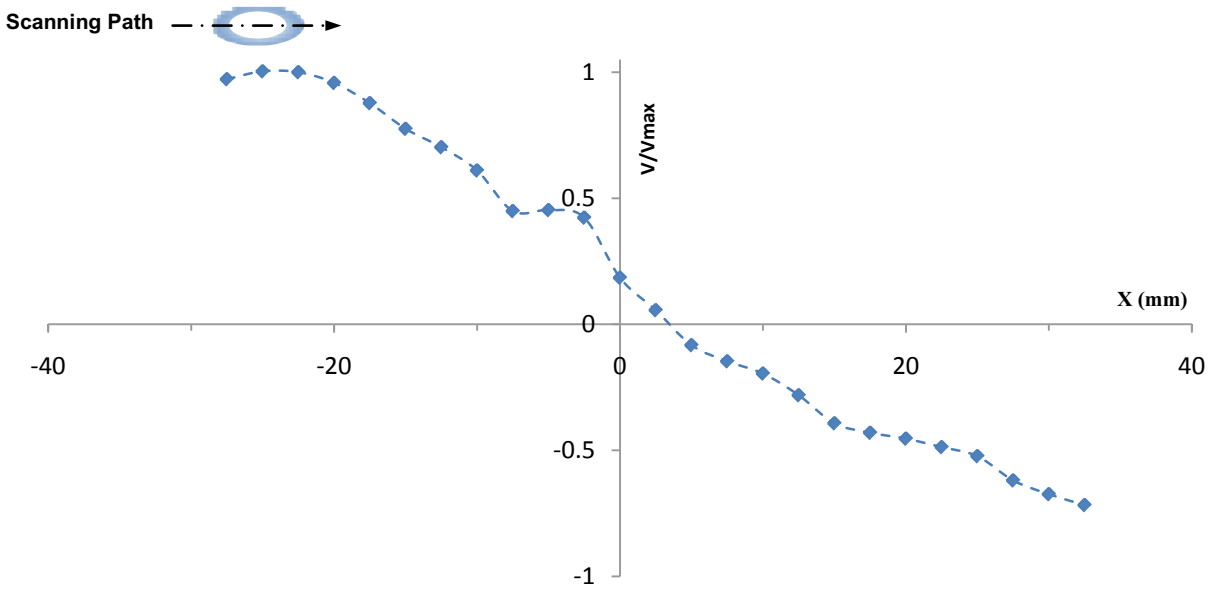

Figure 57: Radial velocity distribution of the elliptical spray in the major axis. The distribution shows signs that the droplets are swirling.

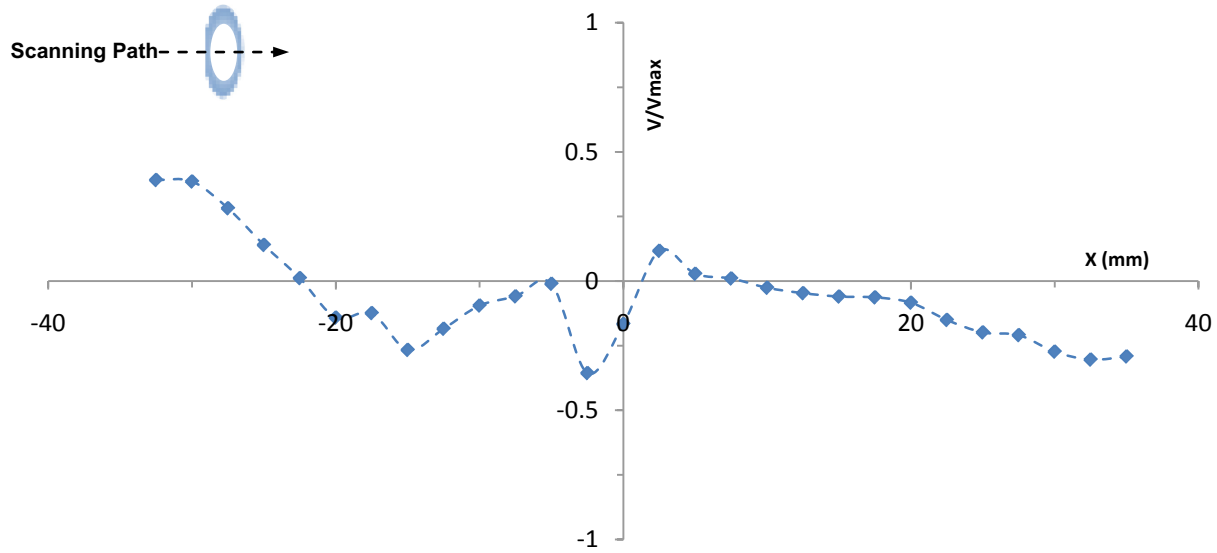

Figure 58: Radial velocity distribution of the elliptical spray in the minor axis. The magnitude of the distribution is less than its major axis counterpart due to the air profilers.

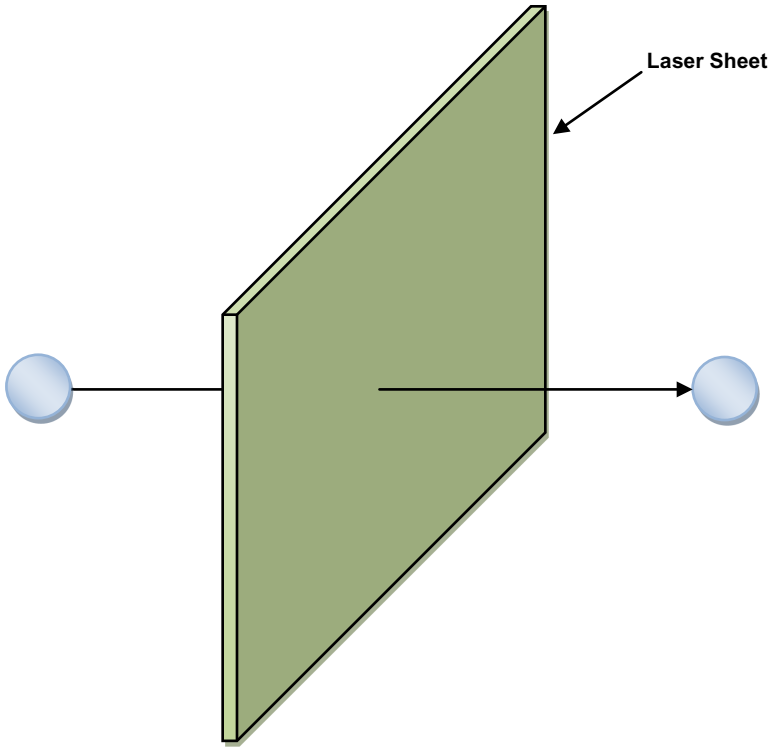

Figure 59: Example of how a droplet passing through the laser sheet may not be picked up by the PIV.

4.3. Comparing Nozzles

This final section of the results offers a direct comparison between the elliptical and conical spray using a select set of PDPA data. All data presented here where taken at the nozzles' nominal operating GLR of 2.35 and at a height of 38.1mm from the nozzle exit.

First, Figure 60 shows the SMD distribution of both nozzles resulted from the conical and elliptical spray. The major axis shows the smallest diameter to be 15μm; however that is within the deviation of ±5μm. It is also evident that the elliptical spray along both the major and minor axis has a wider distribution; whereas the conical is narrow and shows a steeper trend of droplet diameters increasing in size when moving away from the center.

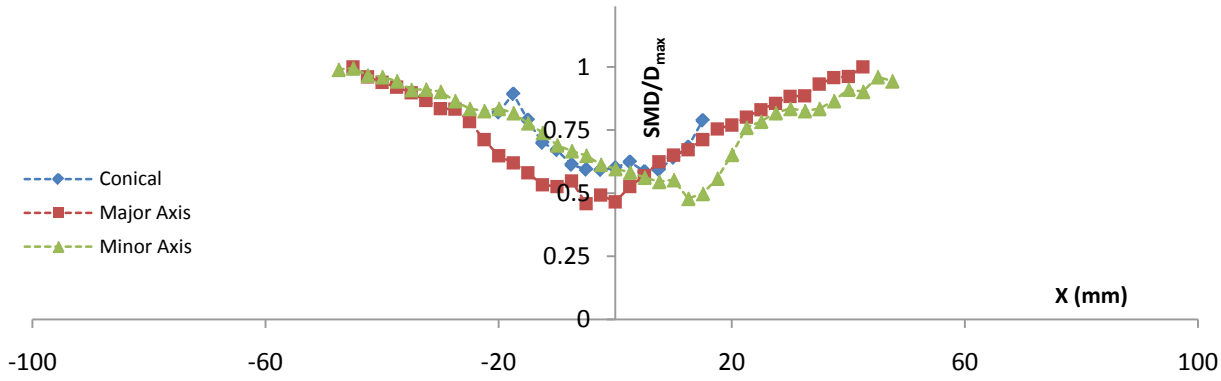

Figure 60: The SMD distribution for both nozzles shows little variation in droplet size; however wider a spread of droplets is achieved with the elliptical spray

Second, the velocity distribution in Figure 61 is where the differences are even greater. The conical spray clearly has the overall highest velocity magnitude where a maximum axial velocity magnitude of 36 m/s in the center of the spray was measured. This explains why the conical spray has higher penetration depths since the air velocity forces down droplets at a much higher rate than the elliptical spray in either axis.

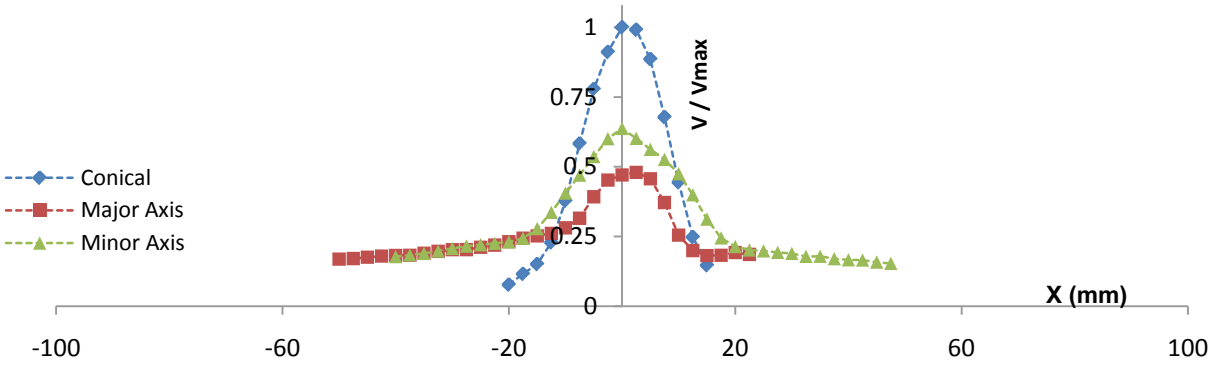

Figure 61: The axial velocity magnitude is highest with the conical where deeper penetration is expected

Third, the volume flux measurement in Figure 62 shows that the volume flux associated with the conical spray is highest at 0.1125 $cm^3/cm^2.s$ with a very narrow distribution. On the other hand, the elliptical spray's flux distribution is fairly low and wide spread along both axes.

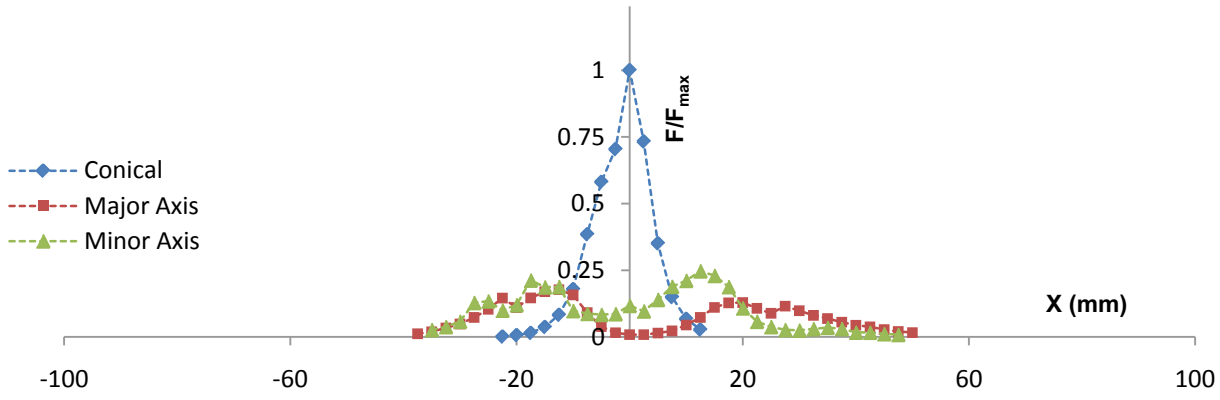

Figure 62: The volume flux distribution shows that the elliptical spray has a wider spread and the conical spray is narrow with deeper spray penetration

Therefore, the data presented show that both nozzles generate similar diameters in the center of the spray. However, the elliptical spray has a more uniform diameter distribution that spreads itself over a wider area. The velocity measurements showed evidence that the elliptical spray's droplets have slower axial velocities resulting in less penetration than the conical spray. Finally, the flux data has shown how the conical spray may have droplets similar in size to the elliptical, yet it has more droplets passing through the center of the spray than the elliptical because the conical spray forces the same volume of liquid within a more narrowly defined area.

5. Conclusions

5.1. Summary

The aim of this study was to experimentally analyze two types of air-blast spray atomizers. One atomizer was a standard circular hollow cone atomizer and the other was a novel hollow elliptical atomizer. The atomizers were run at various GLRs in order to compare their performance using non-intrusive laser diagnostic tools such as Shadowgraph, optical patternation, PIV, and PDPA. The results of this study have also shown that although each method has specific strong points that helped improve the understanding of how these atomizers performed. They did also show some weaknesses in other areas. Therefore, one can conclude that the individual experimental methods applied alone are not sufficient to establish a full scale understanding of spray atomizers; rather, it is the combination of all these experimental techniques that complement each other.

For the conical spray, the shadowgraph and patternation methods showed that increasing the GLR through an increase in air flow rates resulted in a contracting spray cone angle. The optical patternation also confirmed the contraction of the spray core evident from the reduction in cross-sectional spray pattern images. In addition, the patternation images showed that the conical spray initially showed a hollow circular spray pattern that shrunk in size. Further increases in air flow caused the conical spray to become solid instead of hollow. The shadowgraph images also showed signs of increasing penetration depth due to the high velocity gradients of air. Further confirmation what was seen in the images was validated using PIV and PDPA.

The PIV tests showed velocity profiles that not only increased with higher GLRs but that the spray profile also contracted. In particular, the velocity profile near the exit of the conical

spray showed low velocity magnitudes that eventually increased further downstream from the nozzle exit. The difference in magnitude indicated that droplets leaving the conical nozzle experienced a lag where the droplets accelerated further away from the exit once exposed to the aerodynamic forces of the high velocity air. The PDPA tests on the conical spray confirmed what was recorded by the PIV and provided spatially resolved information on the droplets. The droplet diameters measured by the PDPA showed that the smallest droplets occupy the central hollow region of the spray where little or no volume of liquid flows through. The largest droplets were detected in areas near the spray's periphery where primary breakup from the bulk liquid itself was occurring. The volume flux measured by the PDPA also coincided with previous experiments. Therefore, the increasing in GLR with the conical nozzle resulted in a spray that had a narrow liquid distribution but an increased penetration depth.

In the case of the elliptical spray, the shadowgraph images showed clear indications of a change in spray cone in different axes at low GLRs. The increase in GLR made it difficult to determine the exact angle due to the fine atomization quality. The optical patternation successfully captured the unique elliptical pattern at different GLRs and multiple locations from the nozzle exit. Furthermore, the optical patternation also showed signs of swirl motion in the cross-sectional spray pattern. It should be noted however that the pattern itself did not rotate in any of the patternation images. In addition, the pattern's major and minor axes remained aligned with the major and minor axes of the nozzle.

The PIV images of the elliptical spray showed different velocity profiles along the major and minor axes owning to the effect of the air profilers. There were also some difficulties encountered with PIV measurements using the elliptical spray. First, the velocity profile in

areas near the exit were oversaturated due to the presence of a large volume of droplets making it difficult for the PIV to determine valid velocity magnitudes. Second, the presence of swirl motion in the cross-sectional plane of the elliptical spray indicated a highly complex three dimensional flow that contributed to an increase in error of the PIV tests as there may have been droplets arriving and leaving the thin laser sheet of the PIV.

The PDPA tests showed that the elliptical spray has wider droplet distribution than the conical spray. In addition, the droplet diameters where distributed more uniformly compared to the conical spray, where differences in the smallest and largest diameters from the center of the spray to the edge were less substantial. Furthermore, the elliptical spray's axial velocity magnitude was significantly less and the volume flux was far more distributed.

5.2. Recommendations & Future Works

The work carried out during this study can be looked upon as a benchmark for future experimental works on other spray atomizers. There are several areas that can be extended to this work.

Future tests on the both the conical and elliptical spray could be done using liquids that have different surface tensions in order to see the effect it has on the breakup regime. This can be achieved using water with an additional surfactant such as a detergent which would reduce the water's surface tension allowing for a fluid that better resembles some of the fossil fuels used in gas turbine engines. In addition, liquids of varying viscosity should also be considered.

More importantly, the experiments showed the unique spray characteristics of the elliptical spray. Different velocity profiles where observed along two different axes of the elliptical

spray when using the PIV system. Furthermore PDPA results confirmed the evidence of the pattern that significant swirl motion resulted a in a highly three dimensional spray flow. Therefore, future PIV experiments can be realized using 3-D stereoscopic setups that will obtain all three velocity components (i.e. V_x, V_y, and V_z). In addition, post-processing of the data may be improved by implementing a multistep (i.e. recursive pass). These in turn would result in a more accurate velocity profile as well as enhancing the understanding of the elliptical spray's behavior.

Further improvements can be done to the PDPA system as well. The presented results showed that the laser probe may not have passed directly through the spray center line in some of the experiments which results in deviation from the actual major and minor axes. One way of improving the PDPA results could be done by conducting a cross sectional mapping of the spray profile. This would be similar to the scanning method used on the elliptical spray; however, it would cover the spray's entire cross-sectional pattern. This would not only improve droplet diameter and velocity measurements, it would also greatly enhance the accuracy of volume flux measurements that could be directly compared to the patternation images, as well as volume flow rate leaving the nozzle.

Bibliography

1. **G.G Nasr, A.J. Yule, L. Bending.** *Industrial Sprays and Atomization Design and Applications.* London : Springer, 2002.

2. [Online] [Cited: March 21, 2011.] http://delphi.com/manufacturers/cv/powertrain/injection-systems-and-components/diesel_fuel_injectors/.

3. **(ICAO), International Civil Aviation Organization.** [Online] [Cited: 03 08, 2011.] http://icaopressroom.wordpress.com/2010/02/.

4. —. [Online] [Cited: 03 08, 2011.] http://www.icao.int/CAAF2009/Docs/CAAF-09_IP008_en.pdf.

5. —. [Online] [Cited: 03 08, 2011.] http://www.icao.int/env/ClimateChange/PoA.htm.

6. Principles of Jet Engine Operation. [Online] [Cited: March 21, 2011.] http://www.leitemlane.com/jetoperation.htm.

7. **Lefevbre, A. H.** *Gas Turbine Combustion.* Washington, D.C. : Hemisphere Pub. Corp., 1999.

8. *Physics of Liiquid Jets.* **Jens Eggers, Emmanuel Villermaux.** 3, s.l. : Reports on Progress in Physics, 2008, Vol. 71.

9. *Drop and spray formation from liquid jet.* **Lin, S P and Ritz, R D.** 1998, Annu. Rev. Fluid Mech. , pp. 30 85-105.

10. **Lefebvre, Arthur H.** *Atomization and Sprays.* New York : Hemisphere Pub. Corp., 1983.

11. *On Spray Formation.* **P. Marmottant, E. Villermaux.** Marseille : J. Fluid Mechanics, 2004, Vol. 498. pp 73-111.

12. *Surface tension effects on two-dimensional two-phase Kelvin-Helholtz instabilities.* **Raoyang Zhang, Xiaoyi He, Gary Doolen, Shiyi Chen.** Los Alamos : Advances in Water Resources, 2001, Vol. 24. 461-478.

13. *Spray Patternation.* **Tate, R. W.** 10, s.l. : Ind. Eng. Chem., 1960, Vol. 52. 49-52.

14. *Spray characterization in high pressure environment using optical line patternator.* **Hyeonseok Koh, Dongjun Kim, Sanghee Shin,Youngbin Yoon.** Seoul : Measurement Science Technology, 2006, Vol. 17. 2159-2167.

15. **Dmdarevic, Fedja.** Optical Spray Pattern Analysis in a Domestic Oil Burner Flame. Queens : Queens University, 2002.

16. **Guy, Stephen Robert Dale.** OPTICAL PATTERNATION OF FUEL SPRAYS IN A GAS TURBINE. Ottawa : RMC, 2008.

17. *Advances in Optical Patternation for Sprays, With Applications.* **R.W. Sellens, G. Wang.** Pasadena : Eighth International Conference on Liquid Atomization and Spray System, 2000.

18. **M. Raffel, C. Willert, S.Wereley.** *Particle Image Velocimetry A Practical Guide.* s.l. : Springer. ISBN 978-3-540-72307-3.

19. *Comparisoon of Particle Image Velocimetry and Laser Doppler Anemometry Measurements in Turbulent Fluid Flow.* **M. P. Wernet, A. Subramanian, H. Mu, J. R. Kadambi.** s.l. : Annals of Biomedical Engineering, 2000, Vol. 28. 1393-1394.

20. *Development of a custom-designed echo particle image velocimetrey system for multi-component hemodynamic measurements: system characterization and initial experimental results.* **Lingli Liu, Hairong Zheng, Logan Williams, Fuxing Zhang, Rui Wang, et al.** 1397-1412, s.l. : Physics in Medicine and Biology, 2008, Vol. 53.

21. *Setting up a PDPA system for measurements in a Diesel spray.* **L. Araneo, V. Soare, R.Payri, J.Shakal.** s.l. : Journal of Physics, 2006, Vol. 45. 85-93.

22. **J.E. Seay, G.S. Smaulesen.** *Atomization and Dispersion of a Liquid Jet Into a Crossflow of Air.* Irvine : NASA, 1996. 198543.

23. *Liquid Atomization out of a Full Cone Pressure Swirl Nozzle.* **Nicolas Rimbert, Guillaume Castanet.** s.l. : Physics of Fluids, 2010.

24. *A new method for minimizing volumetric flux errors associated with PDPA measurements in the dilute region of full cone swirl atomizers.* **John D. Schwazkopf, Joseph S. Shakal, Courtney Bonuccelli.** Kyoto : ICLASS, 2006, Vol. 163.

25. *Digital Particle Image Velocimetry.* **Westerwheel, J.** Rotterdam : Delft University, 1993. ISBN 90-6275-881-9.

26. *Spray Charecteristcs of a liquid-liquid coaxial swilr atomizer at different mass flow rates.* **Soltani, M R, et al.** 2005, Aerospace Science and Technology, pp. 9 592-604.

27. *Droplet-size-classified stereoscopic PIV for spray charecterization.* **Virginia R Palero, Yuji Ikeda.** s.l. : Measurement Science and Technology, 2002, Vol. 13. 1050-1057.

28. *Spray Structure in Near-Injector Region of Areated Jet in Subsonic Crossflow.* **J. Lee, K. A. Sallam.** 2, s.l. : AIAA Journal of Propulsion and Power, 2009, Vol. 25.

29. *Evaluation of PIV Uncertainties using Multiple Configurations and Processing Techniques.* **Beresh, Steven J.** 6, s.l. : Experiments in Fluids, 2009, Vol. 47. 883-896.

30. *Measurement Uncertainty of Stereoscopic-PIV for Flow with Large Out-of-plane Motion.* **Doorne, C W H van, Westerweel, J and Nieuwstadt, F T M.**

31. *Particle Image Velocimetry: a reveiw.* **Grant, I.** 1997, Inst. Mech. Eng, pp. 211 55-76.

32. *Influence of the out-of-plane deformation and its elimination in white lite speckle photography.* **Jacquot, P and Rastogi, P K.** 1981, Opt. Laser Engr , pp. 2 33-55.

33. *Charecteristics of an acoustically modulated spray issued from circular and elliptical orifice nozzles.* **Messina, T. and Acbarya, S.** 2006, Atomization & Sprays, pp. 16 331-348.

34. *Analysis by droplet size classes of the liquid flow structure in a pressure swirl hollow cone spray.* **Santolaya, J L, et al.** 2010, Chemical Engineering Processing, pp. 49 125-131.

35. *Spray Diagnostics for the twenty first century.* **Bachalo, W D.** 2000, Atomization and Sprays, pp. 10 439-474.

36. *Experimental Study of Near-Field Flow Structure in Hollow Cone Pressure Swilr Sprays.* **Santolay, J L, et al.** 2007, AIAA Journal of Propulsion and Power, p. 23.

37. *Modelling of a hollow-cone spray at different ambient pressures.* **Takagi, M and Moriyoshi, Y.** 2004, Int. J. Engine Res, p. Vol 5.

38. *Comparison of PIV and PDA droplet velocity measurement techniques on two high-pressure water mist nozzles.* **PaulsenHusted, Bjarne, PerPetersson and oranHolmstedt, G¨.** 2009, Fire Safety Journal, pp. 44 1030–1045.

Appendix A

Flow Metering Devices

INTERCHANGEABLE

Designed for low flow rates, the ***Model P*** flow meter is a precision instrument embodying the inherent simplicity, versatility and economy of the classical rotameter. It is particularly suitable for metering carrier gases in chromatography, indicating and controlling gases in manufacturing processes, liquid and gas measurement in laboratories, pilot plants, flow and level indicating,etc.

Shipped completely assembled, flow meters include standard mounting fittings in a choice of materials, side plates, thick protective magnifying front shield and back plate, optional built-in control valve, and flow tubes selected from the Flow Capacities tables. Panel mounting style is convertible to bench mounting through the use of the optional acrylic tripod. The tripod has a built-in spirit leveler and leveling screws.

For multiple tube meters see pages 7 and 8.

design features

- ✓ Rib-guided or fluted metering tubes facilitate stable, accurate readings.
- ✓ Magnifier lens in front shield to enhance reading resolution.
- ✓ Interchangeability of flow tubes and floats.
- ✓ Ease of installation and exchange of flow tubes.
- ✓ "Non-rotating" adapter feature - glass flow tubes are prevented from turning during the tightening phase of the assembly procedure.
- ✓ OPTIGRAD™ scales minimize parallax and eye fatigue.
- ✓ Chemical compatibility.
- ✓ Simple means of panel mounting.

150 mm Meter with CV™ Valve

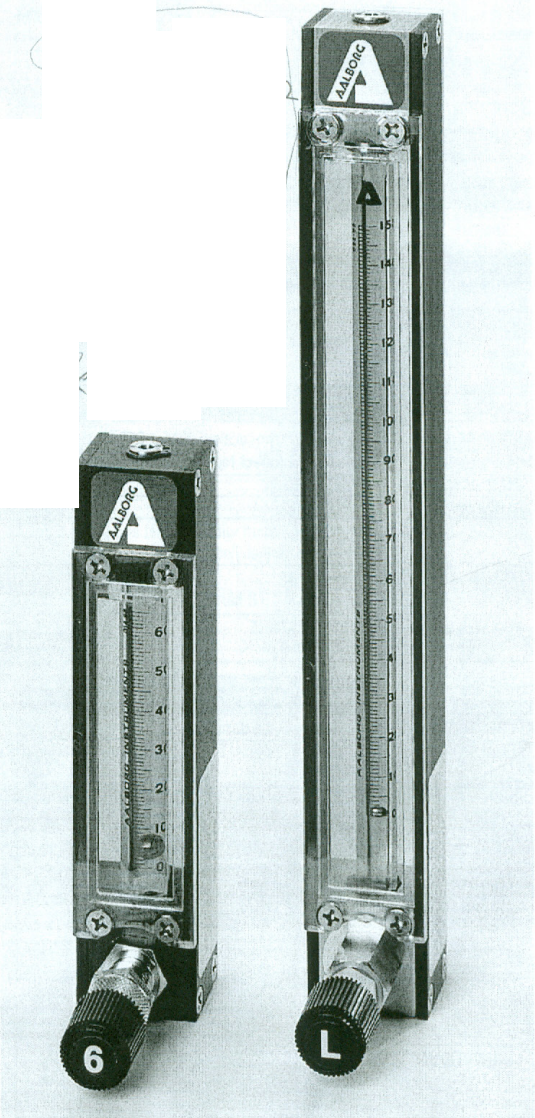

65 mm Meter with MFV™ Valve

BULLETIN EN(800)10 P

BUILT-IN VALVES

Meters are available with built-in needle valves (CV™), high precision metering valves (MFV™) with "non-rising stems", or with no valves. The higher cost of MFV™ valves is justified whenever high sensitivity control and resolution are desirable particularly in conjunction with metering tubes of very low flow rates.

Generally, for gas metering it is recommended that valves are positioned at inlets (bottom) for liquids valves may be positioned either at inlets or outlets (top). For vacuum services, valves must be mounted at outlets. If unspecified at the time of ordering, meters will be shipped with valves mounted at the inlets.

Panel mounting is convertible to bench mounting through the use of an optional acrylic tripod base with spirit leveler (catalog No. TP1).

SPECIFICATIONS	
STANDARD ACCURACY	±2% FS (mm scales) except 042 flow tubes. ±5% FS (direct reading scales) and 042 mm.
CALIBRATED ACCURACY	±1% FS.
REPEATABILITY	±0.25%.
USEFUL FLOW RANGE	10:1 minimum with one float and better than 20:1 with combination of two floats installed in meters.
MAXIMUM OPERATING PRESSURE	200 psig/13.8 bars.
MAXIMUM OPERATING TEMPERATURE	250 °F/ 121 °C.

**MATERIALS OF CONSTRUCTION	
FLOW TUBES	Heavy walled borosilicate glass.
FLOATS	Glass, Sapphire, 316 Stainless Steel, Carboloy® and Tantalum.
CHOICE OF MOUNTING FITTINGS IN CONTACT WITH FLUIDS	a) Aluminum, black anodized. b) Brass, chrome plated. c) 316 stainless steel.
SIDE PANELS	Aluminum, black anodized.
FRONT SHIELD	Lexan® with longitudinal magnifier lens for enhanced reading resolution.
BACK PLATE	1/8" thick white acrylics.
O-RINGS AND PACKING	Buna-N® o-rings in aluminum/ brass model. Viton® o-rings in stainless steel meters. ***OPTIONAL*** Viton® PTFE Kalrez® and EPR.
CONNECTIONS	1/8" NPT female inlet and outlet connections. ***OPTIONAL*** 1/4" FNPT, hose and compression fittings are available.

***The selection of materials of construction, is the responsibility of the customer. The company accepts no liability.*

Select flow tube consistent with requirements from flow capacity tables 6 to 23 (page 38 to 44).

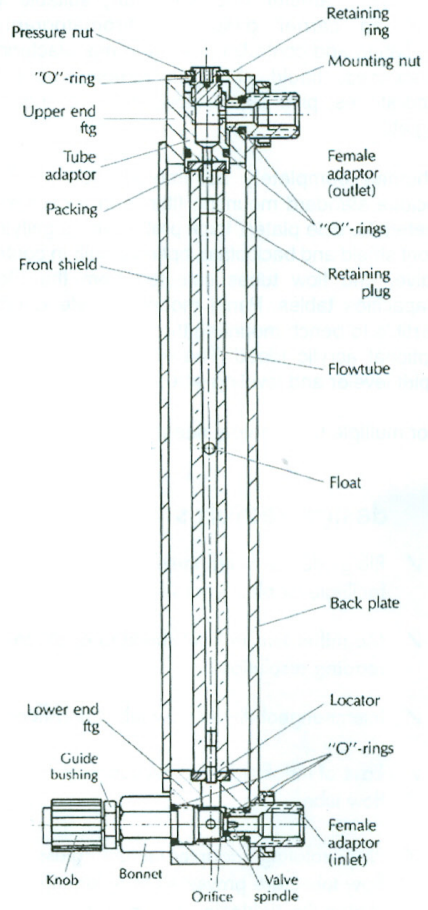

Assorted flow tubes may be used in conjunction with a single mounting frame, an apparent benefit in many laboratory applications.

Ordering information see page 9.
Dimensional information see page 8.

VFC Series Visi-Float® Flowmeter

Specifications - Installation and Operating Instructions

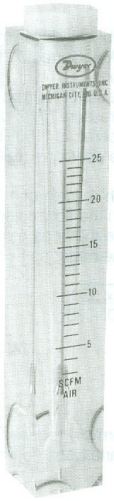

Back Connections

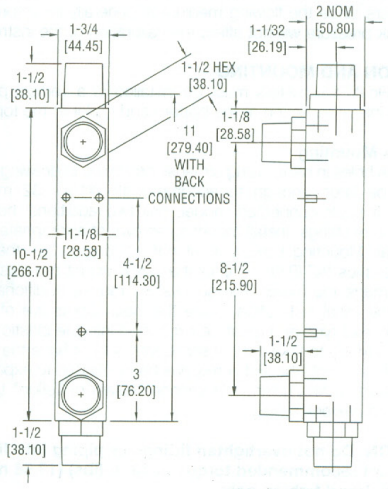

Dwyer Series VFC Visi-Float® flowmeters are available in two basic styles, either back or end connected with direct reading scales for air or water. Installation, operation, and maintenance are simple and require only a few common sense precautions to assure long, accurate, trouble-free service.

CALIBRATION

All Dwyer flowmeters are calibrated at the factory and normally will remain within their accuracy tolerance for the life of the device. If at any time you wish to re-check its calibration, do so only with instruments or equipment of certified accuracy. Do not attempt to check the Dwyer Visi-Float® flowmeter with a similar flowmeter as even minor variations in piping and back pressure can cause significant differences between the indicated and actual readings. If in doubt, your Dwyer flowmeter may be returned to the factory and checked for conformance at no charge.

LOCATION

Select a location where the flowmeter can be easily read and where the temperature will not exceed 120°F (49°C). The mounting surface and piping to the flowmeter should be free from vibration which could cause fatigue of fittings or mounting inserts. Piping must be carefully arranged and installed to avoid placing stress on fittings and/or flowmeter body. Avoid locations or applications with strong chlorine atmospheres or solvents such as benzene, acetone, carbon tetrachloride,etc. Damage due to contact with incompatible gases or liquids is not covered by warranty. Compatibility should be carefully determined before placing in service.

SPECIFICATIONS

Service: Compatible gases & liquids.

Wetted Materials:

Body: Acrylic plastic.
O-Ring: Buna-N (Viton® available).
Metal Parts: Stainless steel.
Float: Stainless steel.

Temperature & Pressure Limits: 100 psig (6.9 bar) @ 120°F (48°C).

Accuracy: 2% of full scale.

Process Connection: VFC: 1″ female NPT back connections. End connections optional. VFCII: 1″ male NPT back connections. End Connections optional.

Scale Length: 5″ typical length.

Mounting Orientation: Mount in vertical position.

Weight: 24-25 oz (.68-.71 kg).

PIPING

Inlet Piping:

It is good practice to approach the flowmeter inlet with as few elbows, restrictions and size changes as possible. Inlet piping should be as close to the flowmeter connection size as practical to avoid turbulence which can occur with drastic size changes. The length of inlet piping has little effect on normal pressure fed flowmeters.

For vacuum service, the inlet piping should be as short and open as possible to allow operation at or near atmospheric pressure and maintain the accuracy of the device. Note that for vacuum service, any flow control valve used must be installed on the discharge side of the flowmeter.

DWYER INSTRUMENTS, INC.
P.O. BOX 373 • MICHIGAN CITY, IN 46361 U.S.A.
Phone: 219/879-8000
Fax: 219/872-9057
www.dwyer-inst.com
e-mail: info@dwyer-inst.com

Discharge Piping
Piping on the discharge side should be at least as large as the flowmeter connection. For pressure fed flowmeters on air or gas service, the piping should be as short and open as possible. This allows operation at or near atmospheric pressure and assures the accuracy of the device. This is less important on water or liquid flowmeters since the flowing medium is generally incompressible and back pressure will not affect the calibration of the instrument.

POSITION AND MOUNTING
All Visi-Float® flowmeters must be installed in a vertical position with the inlet connection at the bottom and outlet at the top.

Surface Mounting
Drill three holes in panel using dimensions shown in drawing. Holes should be large enough to accommodate #10 - 32 machine screws. If back connected model, drill two additional holes for clearance of fittings. Install mounting screws of appropriate length from rear. Mounting screws must not be longer than the panel thickness plus 3/8" (9.66 mm), or the screw will hit the plastic and may damage the meter. The screws will require additional force during the initial installation, since the insert boots are of a collapsed thread type and must be expanded into the plastic for the knurled surface to take hold. Insert boots will not have the proper 10-32 threads until the first screw has been inserted to expand the boot. Attach piping using RTV silicone sealant or Teflon® tape on threads to prevent leakage.

CAUTION: Do not overtighten fittings or piping into fittings. Maximum recommended torque is 10 ft. (lbs) (13.56 newton (meter)). Hand tighten only.

In Line Mounting
Both end connected and back connected models may be installed in-line supported only by the piping. Be sure that flowmeter is in a vertical position and that piping does not create excess stress or loading on the flowmeter fittings.

OPERATION
Once all connections are complete, introduce flow as slowly as possible to avoid possible damage. With liquids, make sure all air has been purged before taking readings. Once the float has stabilized, read flow rate by sighting across the largest diameter of the float to the scale graduations on the face of the device.

The standard technique for reading a Variable Area Flowmeter is to locate the highest point of greatest diameter on the float, and then align that with the theoretical center of the scale graduation. In the event that the float is not aligned with a grad, an extrapolation of the float location must be made by the operator as to its location between the two closest grads. The following are some sample floats shown with reference to the proper location to read the float.

Variable Area Flowmeters used for gases are typically labeled with the prefix "S" or "N", which represents "Standard" for English units or "Normal" for metric units. Use of this prefix designates that the flowmeter is calibrated to operate at a specific set of conditions, and deviation from those standard conditions will require correction for the calibration to be valid. In practice, the reading taken from the flowmeter scale must be corrected back to standard conditions to be used with the scale units. The correct location to measure the actual pressure and temperature is at the exit of the flowmeter, except under vacuum applications where they should be measured at the flowmeter inlet. The equation to correct for nonstandard operating conditions is as follows:

$$Q_2 = Q_1 \times \sqrt{\frac{P_1 \times T_2}{P_2 \times T_1}}$$

Where: Q_1 = Actual or Observed Flowmeter Reading
Q_2 = Standard Flow Corrected for Pressure and Temperature
P_1 = Actual Pressure (14.7 psia + Gage Pressure)
P_2 = Standard Pressure (14.7 psia, which is 0 psig)
T_1 = Actual Temperature (460 R + Temp °F)
T_2 = Standard Temperature (530 R, which is 70°F)

Example: A flowmeter with a scale of 10-100 SCFH Air. The float is sitting at the 60 grad on the flowmeter scale. Actual Pressure is measured at the exit of the meter as 5 psig. Actual Temperature is measured at the exit of the meter as 85°F.

$$Q_2 = 60.0 \times \sqrt{\frac{(14.7 + 5) \times 530}{14.7 \times (460 + 85)}}$$

Q_2 = 68.5 SCFH Air

MAINTENANCE
The only maintenance normally required is occasional cleaning to assure proper operation and good float visibility.

Disassembly
The flowmeter can be completely disassembled by removing the connection fittings and top plug. When lifting out the float guide assembly, be careful not to lose the short pieces of plastic tubing on each end of the guide rod which serve as float stops.

Cleaning
The flowmeter body and all other parts can be cleaned by washing in a mild soap and water solution. A soft bristle bottle brush will simplify cleaning of the flow tube. Avoid benzene, acetone, carbon tetrachloride, gasoline, alkaline detergents, caustic soda, liquid soaps, (which may contain chlorinated solvents), etc., and avoid prolonged immersion.

Re-assembly
Install the lower fitting and then the float and float guide. Finally install the upper fitting and plug being certain that both ends of the float guide are properly engaged and the float is correctly oriented. A light coating of silicone stop cock grease or petroleum jelly on the "O" rings will help maintain a good seal as well as ease assembly.

ADDITIONAL INFORMATION
For additional flowmeter application information, conversion curves, correction factors and other data covering the entire line of Dwyer flowmeters, please request a dwyer full-line catalog.

Printed in U.S.A. 3/04 FR# 51-440448-00 Rev. 3

DWYER INSTRUMENTS, INC.
P.O. BOX 373 • MICHIGAN CITY, IN 46361 U.S.A.
Phone: 219/879-8000
Fax: 219/872-9057
www.dwyer-inst.com
e-mail: info@dwyer-inst.com

Appendix B

PIV Laser Specifications

Solo Specifications

The following tables show the Solo specifications for the different models available. Specifications are subject to change without notice.

Solo PIV Products

		Solo I-15	Solo II-15	Solo II-30	Solo III-15	Solo IV-50	Solo 120XT	Solo 200XT
Repetition Rate (Hz)		15	15	30	15	50	15	15
Energy[1] (mJ)	532 nm	15	30	30	50	50	120	200
	266 nm	NA	NA	NA	NA	NA	20	30
Energy Stability[2] (±%)	532 nm	4	4	4	4	6	4	4
	266 nm	NA	NA	NA	NA	NA	9	9
Beam Diameter (mm)		2.5	2.5	2.5	3.5	3.5	4.5	5.5
Pulse Width[3] (ns)		3-5	3-5	3-5	3-5	3-5	3-5	3-5
Divergence[4] (mrad)		< 3	<3	<3	<4	<5	<3	<3
Beam Pointing Stability (urad)		<100	<100	<100	<100	<200	<100	<100
Jitter (±ns)[5]		1	1	1	1	1	1	1

1. Optical losses due to optional attenuator will reduce maximum energy by 10%.
2. Pulse-to-pulse for 98% of shots after 30 minute warm up.
3. Full width half maximum.
4. Full angle for 86% of the energy, at $1/e^2$ point.
5. From Q-Switch synchout to light pulse for 98% of 1000 shots.

Physical Characteristics

	Laser Head*			Power Supply		
	Solo I, II, III	**Solo IV, 120**	**Solo 200 XT**	**Solo I, II, III**	**Solo IV, 200**	**Solo 120XT**
Length	13.775" / 350 mm	22.4"/569 mm	24.4"/620 mm	18.15" / 461 mm	22.0" / 559 mm	20.9"/531 mm
Width	7.0" / 178 mm	9.8"/249 mm	9.24"/235 mm	7.75" / 194 mm	10.8" / 275 mm	8.7"/221 mm
Height	3.187" / 81 mm	4.86"/123 mm	4.86"/123 mm	14.32" / 363 mm	15.8" / 402 mm	15.5"/394 mm
Weight	10 lbs. / 4.5 kg	32.5 lbs./14.8 kg	40 lbs./18.2 kg	48 lbs. / 22 kg	53 lbs. / 24 kg	50.7 lbs/23 kg
Length Umbilical	8 ft / 2.4 m	10 ft / 3 m	10 ft / 3 m			

* Width and Height include mounting plate

Operating Requirements

Table 2-1: Solo Performance Specifications

Temperature		50° – 86° ±10° F (10° – 30° ±5° C)
Relative Humidity		20—80% non-condensing
Voltage		100—240 V, 50/60 Hz
Power	Solo I, II, III	15 Hz-300 watts; 30 Hz-500 watts
	Solo 120XT	1000 watts
	Solo IV, 200XT	1500 watts